INFORMATION TO USERS

This manuscript has been reproduced from the microfilm master. UMI films the text directly from the original or copy submitted. Thus, some thesis and dissertation copies are in typewriter face, while others may be from any type of computer printer.

The quality of this reproduction is dependent upon the quality of the copy submitted. Broken or indistinct print, colored or poor quality illustrations and photographs, print bleedthrough, substandard margins, and improper alignment can adversely affect reproduction.

In the unlikely event that the author did not send UMI a complete manuscript and there are missing pages, these will be noted. Also, if unauthorized copyright material had to be removed, a note will indicate the deletion.

Oversize materials (e.g., maps, drawings, charts) are reproduced by sectioning the original, beginning at the upper left-hand corner and continuing from left to right in equal sections with small overlaps.

Photographs included in the original manuscript have been reproduced xerographically in this copy. Higher quality 6" x 9" black and white photographic prints are available for any photographs or illustrations appearing in this copy for an additional charge. Contact UMI directly to order.

Bell & Howell Information and Learning
300 North Zeeb Road, Ann Arbor, MI 48106-1346 USA
800-521-0600

UMI®

Heat Conduction in $YBa_2Cu_3O_{7-\delta}$: Effect of Anisotropy and Magnetic Field

Bojana Popić
Center for the Physics of Materials
Department of Physics, McGill University
Montréal, Québec, Canada
December 1998

A Thesis submitted to the
Faculty of Graduate Studies and Research
in partial fulfillment of the requirements for the degree of
Master of Science

To my mother, father, Zorana, Nemanja, and my grandparents.

CONTENTS

FIGURES AND TABLES

FIGURES

TABLES

RÉSUMÉ

Nous avons mesuré la conductivité thermique à basse température pour sonder les propriétés du supraconducteur non-conventionnel $YBa_2Cu_3O_{7-\delta}$ (YBCO). Deux aspects furent étudiés: 1) l'anisotropie dans le plan, afin de comprendre la contribution des chaînes CuO, et 2) l'effect d'un champ magnétique, pour étudier la contribution des lignes de vortex. Nos résultats sont en bon accord quantitatif avec la théorie des supraconducteurs "*d*-wave ". Nous avons trouvé une anisotropie très faible (voire négligeable), ce qui suggère qu'elle ne puisse simplement résulter de l'anisotropie du tenseur de masse ou de l'anisotropie de la fréquence de plasma. Les études en champ magnétique ont révélé une augmentation du terme linéaire (κ/T quand $T \rightarrow 0$) avec le champ, reflétant la contribution à la densité d'états des états électronique délocalisés à cause du décalage Doppler en présence de vortex. Nos résultats sont quantitativement en bon accord avec les prédictions théoriques.

ABSTRACT

We have used thermal conductivity measurements at low temperature to probe the behavior of the unconventional superconductor $YBa_2Cu_3O_{7-\delta}$ (YBCO). Two aspects were investigated: 1) the in-plane anisotropy, studied in order to gain insight into the contribution of CuO chains, and 2) the effect of a magnetic field, investigated in order to explore the contribution of vortices. Our results on the low temperature thermal conductivity are in good quantitative agreement with the theory for a *d*-wave superconductor. We have found a very weak (or even negligible) anisotropy suggesting that the anisotropy could not simply be explained by mass tensor anisotropy or the plasma frequency anisotropy. The magnetic field studies revealed an increase in the residual linear term (κ/T as $T \rightarrow 0$) with field, reflecting the contribution to the density of states from the extended quasiparticles due to their Doppler shift in the presence of vortices. These results are in good quantitative agreement with the theoretical predictions.

ACKNOWLEDGMENTS

I would like to express my genuine gratitude to my thesis advisor Professor Louis Taillefer for his guidance, valuable advice, patience, and kind support through all the phases of this research. His openness and willingness to help during the two years of research were a great motivation during my graduate studies.

My sincere appreciation to Mr. Heward Stikeman, O.C., L.L.D., Q.C. Stikeman, Elliot Barristers and Solicitors for the financial support through the two years of my graduate studies. Max Stern Recruitment Fellowship allowed me to pay all of my expense during the years as a graduate student at McGill University. Thanks to the Center for the Physics of Materials for their generous contributions to my financial well-being.

A very special thanks to all of my colleagues in the laboratory. May Chiao for teaching me a lot about the experimental physics and the data analysis. Thanks to Robert Gagnon for supplying me with the crystals, for helping me learn more about the contact making and for his valuable advice regarding the preparation of the new sample mount. Thanks to Dr. Rob Hill for his guidance during the experiments. Christian Lupien for providing me with the answers to my numerous computer related questions and for helping me with the experiments in the dilution refrigerator. Also Patrik Lambert and Stephane Legault for their support and help. Sincere thanks to Etienne Boaknin for his collaboration in editing. Without his generous help this report would not be the same. I would like to express a special thanks to Igor Herbut for the valuable discussion on high-T_c superconductors.

All my friends from around the world and ones that I have met in Montreal during these two years as well as the friends from the physics department, thank you for your love, constant encouragement and the fun times we had together.

Thanks to all the people of the machine shop for their assistance in machining different pieces of equipments such as the sample mounts.

Last, but certainly not least, my deepest appreciation to my family, and especially to my parents and my brother and sister, who have been so supportive and loving.

1

INTRODUCTION

Superconductivity was discovered in 1911 by Heike Kamerlingh Onnes. Researchers in his group noticed that the resistance of certain materials such as lead and mercury disappeared at low temperature. Since then, superconductivity has become a very widely researched topic. With the discovery of the high critical temperature superconductors by Bednorz and Müller in 1986, the physics of superconductivity has ceased to be only a low-temperature phenomenon. Nowadays, it is not uncommon that every academic and research institution has a at least one active group in the field of superconductivity.

One of the most striking features of the superconductors is the absence of the electrical resistance. But by no means is this the only fundamental property of superconducting materials. The anomalous behavior is present when the superconductor is placed in the external magnetic field. It is not only that the field does not penetrate completely inside the superconductor, but only a finite depth called penetration depth, but it is also that if material is cooled in the field below the critical temperature, the field will be expelled from the inside of the material as it becomes superconducting. The superconductors exhibit so called perfect diamagnetism. This is the famous Meissner Effect discovered by Meissner and Ochsenfeld in 1933. Furthermore, superconductors exhibit interesting behavior in specific heat and thermal properties.

Until high T_c superconducting materials were discovered, the standard BCS theory of superconductivity predicted that the highest critical temperature would be around 30 K; otherwise, the lattice would become too unstable and superconductivity would

be destroyed. These high T_c materials, mainly copper oxide crystals, have transitions to superconducting state at temperatures higher than the boiling point of liquid nitrogen (77 K). This makes them easily accessible: liquid nitrogen is readily available and it is quite inexpensive.

The possibility of transmitting an electrical current virtually without resistance bears a lot of important applications in itself. Prototype superconducting wires capable of transmitting current in very high magnetic fields are being developed. It is predicted that in next five to ten years, high-T_c cuprates will have significant impact on technology. Some of cuprate's technological applications include: SQUIDS, NMR coils, wireless communications subsystems, MRI coils, NMR microscopes, and digital instruments [1].

Some of the central predictions of the theory of unconventional superconductors are: the existence of a residual normal fluid (RNF) at zero energy, and universality in the transport properties in the zero temperature-limit. Here, we only focus on the high T_c cuprates. In order to fully understand these predictions, researchers have been undertaking various investigations. Our own investigations in the context of high T_c superconductors include:

1. effects of impurities (Zn and Ni doping) on transport properties.
2. anisotropy in transport in the basal plane.
3. effects of the magnetic fields; behavior in the vortex state.

The thermal conductivity of SC, as one of the transport properties, has been widely studied. It is one of the features of superconductors that differs from the normal metal behavior. All three effects mentioned above, can be studied via thermal conductivity measurements. Thermal conductivity can be used as a probe of the quasiparticle behavior especially at very low temperatures. It is a useful tool for the investigation of the gap anisotropy of unconventional superconductors as well as for examination of the effects of magnetic field.

The outline of my thesis is the following:

- Review of the superconductivity theory and heat transport.

- Experimental aspects and improvements.
- Effects of anisotropy and magnetic field on heat transport in $YBa_2Cu_3O_{6.9}$.
- Discussion of the results.
- Conclusion and the future prospects.

2

Review of Thermal Conductivity

In this chapter, a review of the basic aspects of thermal conductivity is given. But, prior to the discussion of heat transport, a short introduction to the theory of superconductivity is given. The reader is referred to the books by Tinkham [2], de Gennes [3], and Berman [4] for more extensive discussion of superconductivity and thermal transport in solids.

2.1 Introduction to the theory of superconductivity

2.1.1 A Brief Historical Overview

The era of superconductivity began with its discovery by Heike Kamerlingh Onnes and his research group in 1911. They noticed that the resistance of certain metals, such as lead and mercury, dropped abruptly to zero at a certain temperature, labeled T_c. The perfect conductivity, i. e. form of current without resistance, was discovered [5, 2].

In 1933, another discovery occurred which was to become known as the Meissner effect. When a magnetic field was applied to a superconductor, not only did the field not penetrate inside the material except in a thin region near the surface, but as the normal sample was cooled through T_c, the field was expelled from the interior. This was the discovery of perfect diamagnetism [5, 2].

Soon later in 1935, the London brothers proposed a phenomenological theory of the electromagnetic properties in which the wave functions were not modified considerably when the magnetic field was applied. In other words, they regarded the

superconducting state as being 'rigid'[5].

Pippard proposed a non-local modification of the London equations and introduced the concept of coherence length ξ_o which plays a role analogous to the mean free path ℓ in nonlocal electrodynamics of normal metals.

Pippard's coherence length is given by:

$$\xi_o = a\frac{\hbar v_f}{k_B T_c} \tag{2.1}$$

where a is a numerical constant of order unity. Pippard's proposition was analogous to Chambers's nonlocal generalization of Ohm's Law [5, 2, 6].

In 1950, Ginzburg and Landau put forward the general macroscopic phenomenological theory of phase transitions which was not as appreciated at the time of its appearance due to its phenomenological foundation. But the theory was a triumph of physical intuition [2].

Finally, in 1957, Bardeen, Copper and Schrieffer introduced the well known BCS theory of superconductivity, now labeled BCS Theory. The theory is based on the fermi liquid normal state; the essence of the theory is the attractive potential that can give rise to the Cooper pairing. The theory combines the electrons into the many body wave-function which is a coherent superposition of pairwise correlated states of band electrons. If superconductivity is to occur, an attractive interaction should dominate the repulsive short-range screened Coulomb interaction between the electrons.

BCS theory is based on the model, referred to as BCS model. The main simplifying assumptions of the BCS model are summarized here:

- the lattice is responsible for the positive attraction between the electrons via the exchange of virtual phonons,
- the potential is isotropic (s-wave); hence, the energy gap in the excitation spectrum is isotropic [7, 5].
- the weak coupling limit (weak interaction between electrons) was assumed; therefore, no k dependence is needed.

It seems by now that in the case of the cuprate superconductors, the mechanism responsible for superconductivity is something different than the electron - phonon

interaction. One of the signs of the unconventionality is the presence of nodes in the superconducting gap that lead to existence of the quasiparticles even at the zero temperature limit [8, 9]. The theory that would describe the unconventional superconductors has not yet been reached, but numerous aspects of the unconventional superconductors have been investigated.

In our lab, we use the thermal conductivity as a probe of the quasiparticle behavior in unconventional superconductors. Three of the main differences between a *s*-wave superconductor (conventional) and an unconventional, e.g. *d*-wave superconductor are:

1. effect of impurities
2. pronounced anisotropy
3. contribution of the vortices

All three features can be investigated using thermal conductivity. In my thesis, I will mainly focus on the second and the third feature.

2.1.2 BCS theory

BCS Theory, developed by Bardeen, Cooper and Schrieffer is a powerful and elegant microscopic theory that successfully predicts and explains the basic principles on which superconductivity rests as well as the features of superconducting materials. The theory rests on the idea that even a weak attraction can bind electrons into at bound state.

The wave function Ψ that describes the superconducting system is a many body coherent superposition of identical pair states. It can be written as:

$$\Psi_{\mathrm{BCS}} = \prod_{\vec{k}} \left(u_{\vec{k}} + v_{\vec{k}} c^{\dagger}_{\vec{k}\uparrow} c_{-\vec{k}\downarrow} \right) |0\rangle \tag{2.2}$$

where $\left|v_{\vec{k}}\right|^2$ is the probability of a pair state $\vec{k}$ being occupied, $\left|u_{\vec{k}}\right|^2$ is the probability of a pair state $\vec{k}$ being unoccupied and the $c^{\dagger}$'s are standard creation operators from second quantization.

It was shown by Cooper in 1956 that even a very weak attraction between two

electrons leads to the formation of a bound state, now called a Cooper pair. In the original model, the two electrons in a Cooper pair have opposite momenta and spins, $k \uparrow$ and $-k \downarrow$. The characteristic length scale of the correlation between two electrons in the Cooper pair is labeled by ξ. In conventional superconductors, the positive attraction between two electrons is the result of lattice polarization. Note the crucial role of the Pauli exclusion principle. The pairs can not be formed in isolation; it is necessary that there exists a Fermi sea.

We can visualize the mechanism for superconductivity in the following way. The first electron passes through point $\vec{r}$ and at time t and polarizes the lattice since the electron is negatively charged and it attracts the positively charged neighboring ions. The electron moves off fast at the Fermi velocity while the ions, who have much heavier masses than the electron, respond slower and relax from disturbance slower with a characteristic frequency of the order of Debye frequency. At later time t', there is still some positive charge on the lattice because it is still partially polarized due to the slow response. This can attract another electron. In such a way, the two electrons have interacted via a lattice vibration: a phonon. The two electrons are separated in time and space, and therefore the repulsive Coulomb interaction is reduced. The separation between the two electrons, as it has already been pointed out, is called the coherence length, ξ.

The pairs are created by the linear combination of the normal state electronic configurations with opposite spin and momenta whose energy is less than energy of the electrons in the normal state. In the ground state wave-function, the two states, $k \uparrow$ and $-k \downarrow$ are either both occupied or both unoccupied. In order to create an excitation, quasiparticles, there is a certain minimum energy that needs to be supplied and that energy is given by the superconducting energy gap. Therefore, the energy gap plays the role of the minimum excitation energy [2]. As shown by Valatin and Bogoloyubov, excited states can simply be treated as quasiparticle excitations that obey Fermi-Dirac statistics.

The quasiparticle energy is given by:

$$E_k = (\epsilon_k{}^2 + |\Delta_k|^2)^{1/2} \tag{2.3}$$

where ϵ_k is the unperturbed plane-wave (or band) energy measured from the Fermi energy, $\epsilon_k = \xi_k - E_f$, and ξ_k is the unperturbed plane-wave (band) energy. It is evident that Δ plays the role of the energy gap since at the Fermi surface where $\epsilon_k = 0$, the energy of excitation

$$E_k = |\Delta_k| \tag{2.4}$$

meaning that the energy is finite and greater than zero [2].

At very low temperatures, the system is not excited much, the mean free path for scattering the quasiparticle by the other quasiparticle is large and it is sound to treat the excitations as independent of each other. These quasiparticles correspond to the normal electrons in the two fluid model [10].

Bardeen et al. [5] arrived at a self-consistent equation for the energy gap that directly relates the k dependence of energy gap Δ_k to the symmetry of the pairing potential V_{kl}.

$$\Delta_k = -\frac{1}{2}\sum_l \frac{\Delta}{(\Delta_l^2 + \epsilon_l^2)^{1/2}} V_{kl} \tag{2.5}$$

[2, 7].

Because of the BCS assumptions that the potential was isotropic and non-zero only in a thin shell around the Fermi surface, the BCS gap has no k dependence. But the symmetries other than s-wave can lead to anisotropic gap such as d-wave gap. The anisotropic potential V_k will lead to the gap Δ_k that is not isotropic. Therefore, one can study Δ_k in order to reveal information about V_k.

The temperature dependence of the BCS gap is given by:

$$\frac{1}{N(0)V} = \int_0^{\hbar\omega_c} \frac{tanh\frac{1}{2}\beta(\epsilon^2 + \Delta^2)^{1/2}}{(\epsilon^2 + \Delta^2)^{1/2}} d\epsilon. \tag{2.6}$$

From this expression, Δ can be calculated numerically [2].

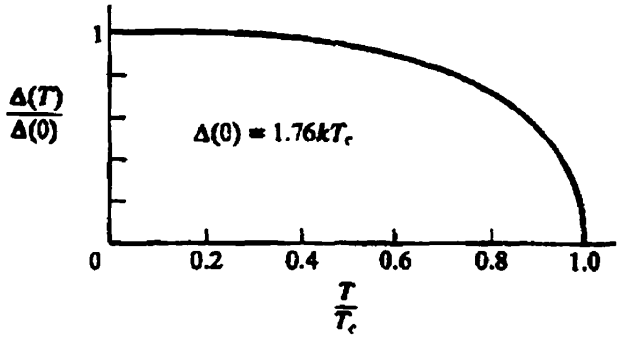

Figure 2.1: The temperature dependence of the BCS energy gap after [2].

The temperature dependence of the gap Δ arises from the many body interaction. The variation of Δ with the square root of $(T_c - T)$ is characteristic of all mean-field theories. Figure 2.1 shows the energy gap as a function of temperature in BCS theory. Near T_c, the gap behaves as $\frac{\Delta(T)}{\Delta(0)} \propto (T_c - T)^{1/2}$ with $\Delta(0) = 1.76 k_B T_c$ as a zero temperature value of the gap. It was calculated using the weak coupling limit, although it is a good approximation for most other cases. Near $T = 0$, the temperature variation of the gap is exponentially slow. Below about $T/T_c \approx 0.4$, the gap becomes essentially constant because at these temperatures not many quasiparticles are thermally excited.

Several measurements reveal the existence of a gap; for example the specific heat as a function of temperature at low temperatures. In the normal metal, at low temperatures, the specific heat is given by:

$$C(T) = AT + BT^3 \tag{2.7}$$

where the first term is attributed to electrons and the second to phonons. The specific heat of a superconducting sample shows a jump in the specific heat as a result of the discontinuity in the density of states at T_c. The specific heat, just below critical temperature, jumps to some higher value than the one in the normal state and continues to decrease but in an exponential manner falling well below the normal state value as $T \rightarrow 0$. The value of C(T) in the superconducting state at low temperatures is much smaller than the value in the normal state. The electronic term is not linear any more but it exhibits an exponential behavior of the form $e^{-\Delta/k_B T}$, where Δ is

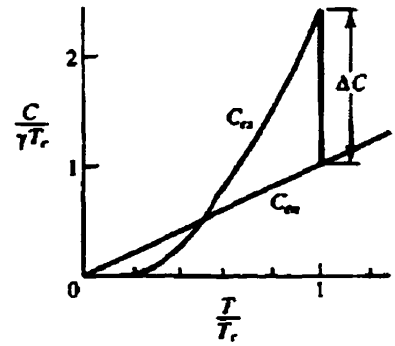

Figure 2.2: Temperature dependence of the specific heat in both normal and superconducting states after [2].

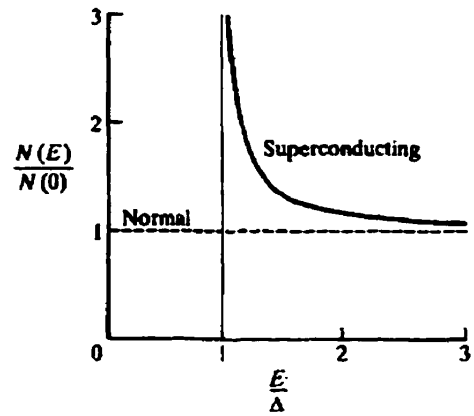

Figure 2.3: The density of states in normal and superconducting states as function of temperature after [2].

the value of the gap. This exponentially activated behavior in the thermal properties is typical of the systems in which the ground state is gapped from the excited state [11]. All of this is seen on the figure 2.2.

A fundamental quantity in calculations of the quasiparticle properties is the density of states, DOS. In the isotropic case, i.e. s-wave the density of states is zero below the gap energy and it diverges just above the point where the energy is equal to the gap energy, meaning where the temperature is equal to the critical temperature. All k states whose energies fall in the gap in the normal metal are raised in the energy above the gap in the superconducting state.

Figure 2.3 shows the density of states in the superconducting and normal states. Since it is well established by now that the quasiparticles can be treated simply as

fermions, it is sound to evaluate the superconducting density of states by equating:

$$N_s(E)dE = N_n(\epsilon)d\epsilon \tag{2.8}$$

Since we are interested in the energies that are just a few meV away from the Fermi Energy, we can take

$$N_n(\epsilon) = N(0) \tag{2.9}$$

Using this assumption, along with the expression for the energy of a quasiparticle ($E_k = \Delta^2 + \epsilon^2$), we arrive at the following expression for the density of states:

$$N_s(E)/N(0) = d\epsilon/dE = E/(E^2 - \Delta^2)^{1/2} \text{ if } (E > \Delta) \tag{2.10}$$

and

$$N_s(E)/N(0) = 0 \text{ if } (E < 0) \tag{2.11}$$

We expect a divergent density of states right above energy equal to Δ. The total number of states is conserved [2].

The BCS theory is very successful in explaining conventional superconductivity, where the mechanism responsible for the superconductivity is the electron phonon interaction. On the other hand, the unconventional superconductivity, where the gap function has nodes, can not be described by the phonon mechanism. In unconventional superconductors, such as the high-T_c cuprates, pairing is not likely to be electron-phonon. But the BCS theory, in its general from, is still valid in the case of unconventional gap symmetry. BCS model can be relaxed in order to describe such systems.

The problem of the non-phonon mechanism is intimately related to that of the critical temperature. This is because the critical temperature is expressed though the parameters of the pairing interaction. For example, in the conventional superconductors T_c is given by $T_c = 1.14\hbar\Omega e^{1/\lambda}$ where $\Omega \simeq \Omega_D$ and λ is the coupling constant [12].

Even long before the BCS theory, there was a hope for high temperature superconductivity. In the early 1960's after the development of BCS theory, it was erroneously believed, because the theory implied it, that high temperature superconductivity was not attainable. It was believed then that the superconductivity was just a low temperature phenomena. The coupling constant λ was predicted to have a highest value of 0.5; otherwise, the lattice would become to unstable. This limit on the coupling constant set the limit on the T_c. According to the BCS formula, the critical temperature was expected to be order of magnitude smaller than the Debye temperature. It follows then that the critical temperature could not be high. But, in 1964 the hope was revived by a paper by Little in which he proposes the model for non phononic mechanism of superconductivity that would allow high critical temperatures. Little's work played a crucial role in the further development of superconductivity. Not only because it proposed the non phonon mechanism, but it revived the old dream of high temperatures superconductivity [12].

Several different mechanisms were proposed but the consensus has not yet been reached on what is the mechanism involved in the unconventional superconductivity.

2.2 *Review of thermal and electrical conductivity in solids*

The heat current in a sample is given by the following formula:

$$j_h = -\kappa \nabla T \tag{2.12}$$

where j_h is the heat current, κ is the thermal conductivity, and ∇T is the temperature gradient.

When in equilibrium, there is no net heat flow, and the thermal current is zero. If there is a disturbance, such as a temperature gradient, the heat current will flow.

Generally in the solid, heat conduction is due to different excitations such as lattice vibrations, electrons, magnons etc. Therefore, the total thermal conductivity can be written very generally as:

$$\kappa_{tot} = \kappa_e + \kappa_{ph} + \kappa_m + ... \tag{2.13}$$

In the case of the YBCO crystals, we do not expect any appreciable magnon contribution to the thermal conductivity because either there are no magnons present as in $YBa_2Cu_3O_{6.9}$ which is non-magnetic, or because the spin wave gap in AFM insulating $YBa_2Cu_3O_{6.0}$ is at the order of 100 K; the effects of magnons are negligible and can be safely excluded from the analysis at low temperatures [8].

The thermal conductivity of a metal in the superconducting state is in general very different from the thermal conductivity in the normal state. This was first pointed out by earlier works of Mendelssohn [13] and Olsen and Rosenberg [14]. The heat current in superconductors is carried only by quasiparticle (the 'normal fluid') and by phonons. Because Cooper pairs do not carry any entropy, they are not effective carriers of heat.

Now, as the temperature decreases below T_c, the number of quasiparticles decreases as electrons condense into a Cooper pairs. So, we expect $\kappa(T)$ due to electrons to decrease with temperature faster than in the normal state. And indeed in a conventional superconductor, the electronic thermal conductivity decreases exponentially as the temperature decreases. For unconventional superconductors, the situation is more complicated, as we shell see.

Cooper pairs are also not effective as scatterers of phonons and electrons. As T is reduced, there are less electrons off which phonons are scattered and the phonon mean free path increases. Hence, $\kappa(T)$ due to phonons can be much larger than in the normal state [12]. If the phononic (lattice) contribution to the thermal conductivity is negligible in the normal state, then as electrons condense, the thermal conductivity in the superconducting state becomes lower than the thermal conductivity in the normal state.

The microscopic theory of Bardeen, Rickayzen and Tewordt [10] gave a clearer picture of the thermal conductivity in the superconducting state. This will be discussed in more detail later on, but let just mention that they were able to calculate the magnitude and temperature dependence of the lattice and electronic thermal conductivities in the superconducting state [15, 10].

2.2.1 *Electrons*

The Drude theory for metallic conduction developed at the turn of the century is based on classical physics where electrons are treated as a gas-like particles. Although it fails to explain some experimental details that require extensive quantum-mechanical approach, it is still widely used for rough estimates of the transport properties in metals [11]. The Drude model assumes that electrons are accelerated by the electric field for the average distance ℓ (mean free path) before they lose the extra velocity acquired. The acceleration process is stopped by the electron's collision with the atom. Then, the electrical conductivity as carried by electrons is given by:

$$\sigma = \frac{n_e e^2 \tau}{m_e} \tag{2.14}$$

where n_e is the number of free electrons per unit volume, m_e and e are electron mass and electron charge respectively, and τ is the scattering (relaxation) time.

Thermal conductivity is treated in a similar manner. In the presence of the temperature gradient, electrons travel a distance ℓ (mean free path) before colliding with atoms and transferring their excess thermal energy. The heat conduction is given by the following formula:

$$\kappa = \frac{1}{3} C_e v_f^2 \tau \tag{2.15}$$

where C_e is the specific heat of electrons.

If we take the ratio of the thermal and electrical conductivities as given by the above expressions using the appropriate substitutions, we arrive at the following :

$$\frac{\kappa}{\sigma} = \frac{\pi^2}{3}\left(\frac{k_B}{e}\right)^2 T \tag{2.16}$$

This is just a Wiedemann-Franz Law stating that the ratio of the two conductivities is proportional to the temperature [4, 11]. The constant in the above expression is the Lorenz number, L_s, whose value, now labeled the Sommerfeld value of the Lorenz number, is equal to $2.44 \times 10^{-8}\ W\Omega/K^2$.

At high temperatures, the mechanism that mostly limits the electronic mean free path is scattering of electrons by the lattice. At these temperatures, effectiveness of the lattice in scattering off electrons is proportional to the vibrational energy of lattice which (lattice energy) is in turn proportional to the temperature. It follows then that the mean free path of the electrons is proportional to $1/T$. Hence, the electrical conductivity is expected to vary as $1/T$. At lower temperatures, the lattice is less effective in the scattering electrons and limiting their passage; it follows that the electrical conductivity increases faster than the $1/T$ law.

We will be interested in the low temperatures where the electrons are mostly scattered not by the lattice but by the imperfections in the lattice (impurities, interstitial atoms, defects...). Here, the mean free path of electrons becomes constant independent of temperature. Therefore, the electrical conductivity is constant at low temperatures as well. At low temperatures, the phonon mean free path is mostly limited by the crystalline boundaries as we shell see in the next section.

One can utilize the Wiedemann-Franz law along with the known behavior of the electrical conductivity, discussed above, to extract information about the expected behavior of thermal conductivity in metals. The general results of such naive analysis are in pretty good agreement with what has been observed because in most metals thermal conductivity is almost entirely due to electrons; but the details are incorrect because we can not generally assume that the mean free path in expression for the thermal conductivity is the same as the mean free path in the expression for σ.

If the heat transport at low temperatures is dominated by electron - impurities scattering which is an elastic process, the Wiedemann Franz law should be obeyed. On the other hand, if the predominant mechanism for scattering is inelastic electron - electron scattering, we do not expect W-F to hold. In inelastic scattering, there is loss of the heat from the system to the surrounding, and the heat transport by electrons will be degraded. One can think of this scenario as being equivalent to charge transport. We think of the electron's charge as being responsible for the transport of the electric current. Due to the electric charge being fixed, the only way

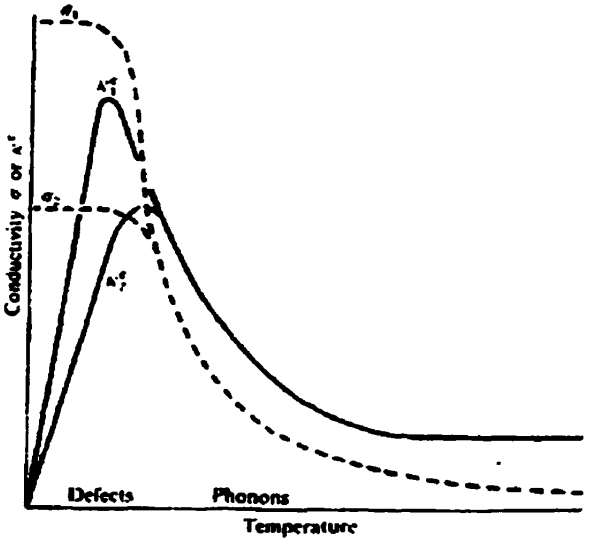

Figure 2.4: Thermal κ and electrical σ conductivity in metal as function of temperature after [4].

of degrading the electrical current is by changing the momentum of the electron. In the case of thermal conductivity, one can think of the 'charge' on the electron as being simply the energy carried by it. Depending on the nature of the scattering process, the thermal conductivity will be affected differently; hence, the ratio of thermal to electrical conductivity will either stay the same, meaning W-F will hold; or it will not stay constant and W-F will fail [7].

At low temperatures, electrons are mainly scattered by impurities. This is an elastic process and we expect W-F law to hold. For example, aluminum is the system in which electrons dominate transport at all temperatures, and we expect W-F law to be obeyed at low temperatures.

The results illustrated in figure 2.4 are the following. The thermal conductivity at high temperatures is constant. At low temperatures it is proportional to the temperature. This is easily realized if σ (whose temperature dependence we know) is plugged into the expression for the Wiedemann-Franz Law. In the temperature range between the two extremes, the variation of the thermal conductivity is not as rapid as the Wiedemann-Franz Law would predict [4].

However, in YBCO, such a simple picture is not valid. In these systems, electron-

electron interaction is strong. An example of a such an interaction would be the interaction via exchange of virtual spin fluctuations. The thermal conductivity at low temperatures will be discussed later on in section 2.4.

2.2.2 *Phonons*

In non-metallic crystals, the only carriers of heat are phonons. Here, we can not speak of electric conductivity simply because there are no itinerant electrons present. Phonons are quanta of energy of lattice vibration in each vibrational mode. Their mean free path is nowadays commonly defined as a measure of rate at which the energy is exchanged between different vibrational (phonons) modes. If the vibrational energy of some part of the crystal is increased, meaning that the temperature in that region of crystal is increased, the temperature gradient will be established such that heat flows from the region of higher temperature to the region of lower temperature.

Debye investigated heat transport by lattice vibrations, and he viewed it as being equivalent to the wave motion. He defined the phononic mean free path as the distance the wave travels before its intensity reduces (by scattering) to $1/e$ of its original intensity. As in the case of electrons, the thermal conductivity due to phonons can be written as:

$$\kappa = \frac{1}{3} C v l \tag{2.17}$$

where C is the heat capacity of the lattice and v is the mean phonon velocity [4].

Let us now look at the mean free path and its behavior in different temperature regimes. We will use that knowledge later to deduce information about the expected behavior of phonon thermal conductivity. At high temperatures, the mean free path of phonons is determined almost solely by the interaction of the phonons between themselves. Then, as in the case of electrons, the mean free path of phonons is proportional to $1/T$. As the temperature decreases, the interactions among phonons are less effective in limiting the phonon mean free path, and mean free path increases more rapidly than $1/T$. At low temperatures, the interactions among phonons them-

selves reduce, and the mean free path becomes constant of the order of the crystal dimensions (dependent on the size and the shape of the crystal and limited by the external boundaries of the crystal).

If we regard the mean phononic velocity as being independent of temperature, we can extract the behavior of the thermal conductivity due to phonons by taking into account the mean free path, as discussed earlier, and the temperature dependence of the specific heat. At high temperatures, where ℓ is inversely proportional to temperature, the specific heat is almost constant leading to the thermal conductivity being proportional to $1/T$. As the temperature decreases, specific heat C also starts to decrease and ultimately to vary as T^3. This is just a well-known Debye result for low temperature specific heat, $C_v \propto (T/\theta_D)^3$, where θ_D is Debye temperature; but, the exponential dependence of the mean free path is the dominant factor and thermal conductivity essentially follows the exponential variation in temperature. At low temperatures, where mean free path is virtually constant, C is still cubic in temperature, and thermal conductivity varies as T^3 [4].

It is useful to compare the mean free paths in metals and non-metals at low temperatures where both ℓ_e and ℓ_{ph} become constant. At low temperatures, constant electron mean free path is determined by the lattice defects while the mean free path of phonons is limited by the size of the crystal. Generally, the thermal conductivity due to phonons is also influenced by the defect in the lattice but this effect diminishes considerably at low temperatures. As the temperature decreases, only long wavelength lattice waves are important, and they reach $\sim$ 100 atomic spacing at 1 Kelvin for the average crystal (here, average refers to crystals whose Debye temperatures are between 200 and 300 K). Long wavelengths are almost unaffected by the lattice disorder at the atomic scale but are strongly affected by the scattering off the external boundaries of the crystal. As for the ordinary metals, the energies of electrons that are responsible for the heat conduction are little dependent on the temperature. Since the de Broglie wavelengths of these electrons in most metals (such as for example in copper), are of the order of the interatomic spacings, electrons are

strongly scattered by the imperfections in the crystal [4].

As stated by Ashcroft and Mermin in *Solid State Physics*, the famous Boltzmann equation lies at the heart of the theory of transport in solids [11]. It is the starting point for derivation of various transport properties. In our case, we use it in order to arrive at the expressions for thermal conductivity in solids. Berman's book *Thermal Conduction in Solids*[4] extensively treats the thermal conductivity due to phonons. Here we will highlight the basic steps of the derivation.

Boltzmann equation has the following form:

$$\left(\frac{\partial f}{\partial t}\right) + F \cdot \frac{1}{\hbar}\vec{\nabla}_k f + v \cdot \vec{\nabla}_r f = \left(\frac{\partial f}{\partial t}\right)_{coll.} \tag{2.18}$$

where f is distribution function, $F = eE$, and E is electrical field. Here, the terms on the left hand side are usually referred to as *drift terms*, while terms on the right hand side are commonly known as *collision terms* [11].

In practice, it is quite difficult to solve the Boltzmann equation; but if some approximation tools such as the relaxation-time approximation are used, one can arrive at the quite satisfactory expressions for the transport properties. According to relaxation-time approximation, we can write:

$$\left(\frac{\partial f}{\partial t}\right)_{scatt.} = -\frac{f(\vec{k}) - f_o(\vec{k})}{\tau(\vec{k})} \tag{2.19}$$

The approximation is exact for the isotropic fermi surface, isotropic elastic scattering and spatially homogeneous disturbance. When heat flows in the system, the system is disturbed from its equilibrium state, given by the equilibrium distribution function $f_o(\vec{k})$. In the case of phonons, $f_o(\vec{k})$ is just given by the Bose-Einstein distribution function:

$$f_o = \frac{1}{exp(\epsilon - \mu)/k_B T - 1} \tag{2.20}$$

The presence of a temperature gradient also implies that the spatial gradient term $\vec{\nabla}_r f$ in 2.18 is non-zero.

In a steady state conditions and without the electromagnetic force, the first and second terms on the left hand side in equation 2.18 are zero. Then, the Boltzmann

equation becomes:

$$\left(\frac{\partial f}{\partial t}\right)_{coll.} = v \cdot \vec{\nabla}_r f \tag{2.21}$$

The next step is to linearize the Boltzmann equation. To the first order, under the relaxation-time approximation assumption that the distribution at the presence of temperature gradient is not much different from the equilibrium distribution $f_o(\vec{k})$, we can write:

$$\vec{v} \cdot \vec{\nabla}_r f = \vec{v} \cdot \vec{\nabla}_r f_o = \vec{v} \vec{\nabla} T \frac{\partial f_o}{\partial T} \tag{2.22}$$

Making use of the fact that $\frac{\partial f_o}{\partial T} = -\frac{\epsilon_k}{T}\frac{\partial f_o(\vec{k})}{\partial \epsilon_k}$ we arrive at the linearized Boltzmann equation in the relaxation-time approximation:

$$f(\vec{k}) - f_o(\vec{k}) = -\tau(\vec{k})\epsilon_k \vec{v_k} \cdot \frac{\vec{\nabla} T}{T}\frac{\partial f_o(\vec{k})}{\partial \epsilon_k}. \tag{2.23}$$

The heat current j_h due to the phonon with wavevector $\vec{k}$ is the product of the thermal energy in that mode and the group velocity of propagation.

$$j_h = 2\sum_k |f_k - f_o|\epsilon_k \vec{v_k} = -2\sum_k \epsilon_k^2 \vec{v_k^2}\frac{\vec{\nabla} T}{T}\frac{\partial f_o}{\partial \epsilon_k}\tau_k. \tag{2.24}$$

Since $j_h = -\kappa \nabla T$, it follows that the thermal conductivity can be written as:

$$\kappa_{ii} = \frac{2}{T}\sum_k \mu_i^2 \epsilon_k^2 \vec{v_k^2}\frac{\partial f_o}{\partial \epsilon_k}\tau_k \tag{2.25}$$

where μ is a directional cosine, $\cos\theta$, and θ is the angle with respect to the temperature gradient axis. Changing the summation over momenta k into an integration over energy and using the appropriate substitutions along with some simplified approximations of Debye theory, we arrive at:

$$\kappa = \frac{k_B}{2\pi^2 v_{ph}}\left(\frac{k_B}{\hbar}\right)^3 T^3 \int_0^{\theta/T} \tau(x)\frac{x^4 e^x}{(e^x - 1)^2}dx. \tag{2.26}$$

Here, θ is the Debye temperature, v_{ph} is the average phonon velocity, and $x = \hbar\omega/k_B T$. Using the expression for phononic heat capacity in Debye approximation, thermal conductivity can also be written as:

$$\kappa = \frac{1}{3} v^2 \int_0^{\theta/T} \tau(x) C(x) dx. \tag{2.27}$$

In terms of mean free path, one can write $\tau(x) = l(x)/v$ and therefore, $\kappa = \frac{1}{3} v \int l(x) C(x) dx$. This is just the extension of the simple kinetic expression for thermal conductivity from the beginning of this chapter.

It is clearly seen that the phononic thermal conductivity depends on the specific heat and on mean free path. At very low temperatures, the specific heat of phonons is cubic in temperature (just a Debye result, $C \propto T^3$), and ℓ becomes independent of temperature and limited by the crystalline dimensions (boundaries). Therefore, thermal conductivity of phonons at low temperatures varies as T^3.

In a lot of metals, which are regarded as good heat conductors, the heat is predominantly carried by electrons. For example, in metals such as silver and coper, the electronic heat conduction is so dominant that it is a good approximation to regard the conduction to be due to electrons in the whole temperature range up to the melting temperature. On the other hand in some other metals, such as antimony and bismuth and many alloys, lattice conductivity is comparable to the conductivity due to electrons and even exceeds it in some temperature ranges.

One can arrive at the expression for the thermal conductivity due to electrons in metals following a procedure analogous to the one employed for the phonon thermal conductivity. If we start with the Boltzmann equation, as it is done in the case of phonons, we will arrive at the expression for the normal state electron thermal conductivity in metals. The same can be done for the electrical conductivity σ_e. In this case, the electron distribution function, which is the central quantity in the Boltzmann equation, is given by Fermi-Dirac statistics since electrons are fermions. Therefore, the average population of the electron state with energy ϵ and with a particular spin orientation can be written as:

$$F(E_i) = \frac{1}{exp(\epsilon - \mu)/k_B T + 1} \tag{2.28}$$

where μ is a chemical potential [4].

Again, as in the case of phonons, τ designates the rate at which non-equilibrium electron distribution tends to return to the equilibrium as a result of the scattering processes. If τ is the same for all electrons over the Fermi surface, then upon manipulation of the Boltzmann equation, one arrives at the following expressions for the electrical and thermal conductivities:

$$\sigma_e = \frac{n_e e^2 \tau}{m_e} \tag{2.29}$$

and

$$\kappa = \frac{1}{3} c_e v_e^2 \tau. \tag{2.30}$$

where $v_e = v_f$ [4, 7].

2.3 Conventional Superconductors

The extensive theoretical study of the thermal conductivity in the conventional superconductors has been done in the theoretical paper *Thermal Conductivity of Superconductors* by Bardeen, Rickayzen, and Tewordt that appeared in 1959. We summarize their findings as they have set the cornerstone for the treatment of the heat conduction in conventional superconductors. For more thorough explanation, the reader is referred to the original paper [10] and reference therein.

In general, as in the case of any solid material that contains both electrons and phonons, the heat current in superconductors can be carried both by electrons and phonons. It is not uncommon that at a certain temperature range lattice conductivity completely dominates the electron conductivity, and vice versa.

2.3.1 Electrons

The main finding by Bardeen et al. was that the mean free path of the excitations was the same in the normal state as in the superconducting state:

$$\ell_s = \ell_n. \tag{2.31}$$

In the superconducting state, the relaxation time τ_s can be written as:

$$\tau_s = \left|\frac{E}{\epsilon}\right| \tau_n \tag{2.32}$$

where τ_n is the relaxation time in the normal state [10]. The group velocity of the quasiparticles in the superconducting state is given by:

$$v_k = \frac{1}{\hbar}\nabla_k E_k = \frac{1}{E_k}\left(|\epsilon_k|\frac{1}{\hbar}\nabla_k \epsilon_k + |\Delta_k|\frac{1}{\hbar}\nabla_k \Delta_k\right) \tag{2.33}$$

The last term on the right hand side can be shown to be small, and therefore the velocity can be written as:

$$v_k = \left|\frac{\epsilon_k}{E_k}\right| v_F = \frac{N(0)}{N_s(E)} v_F \tag{2.34}$$

where $N(0)$ is the density of states at the Fermi level in the normal state, $N_s(E)$ is the quasiparticle density of states, and v_F is the fermi velocity [7]. Therefore, by taking the product of v_k and τ_s we see that the temperature dependence cancels out leaving us with:

$$\ell_s = v_k \tau_s = v_F \tau_n = \ell_n \tag{2.35}$$

Therefore, the mean free path in the superconducting state is the same as in the normal state, assuming an s-wave scattering, namely $\tau_k \rightarrow \tau_s$ [10, 7].

The expression for the thermal conductivity due to electrons when predominant scatterers are impurities (elastic scattering) was given by:

$$\kappa_{es} = -\frac{2N(0)v_o\ell}{3T}\int_{\Delta(T)}^{+\infty} dE E^2 \frac{\partial f}{\partial E}. \tag{2.36}$$

The expression for the normal state κ_{en} was obtained from the above expression, letting $\Delta \rightarrow 0$. Dividing the two conductivities, Bardeen et al. have arrived at:

$$\frac{\kappa_{es}}{\kappa_{en}} = \int_{\Delta(T)}^{+\infty} dE E^2 \frac{\partial f}{\partial E} / \int_0^{+\infty} d\epsilon \epsilon^2 \frac{\partial f}{\partial \epsilon}. \tag{2.37}$$

For $T \ll T_c$, the expression was reduced to:

$$\frac{\kappa_{es}}{\kappa_{en}} \propto \left(\frac{\Delta}{k_B T}\right)^2 e^{\frac{-\Delta}{k_B T}}. \tag{2.38}$$

[10], [7]. Therefore, in conventional superconductors, at low temperature, κ_{es} shows an exponentially activated behavior which is characteristic of the transport properties in conventional superconductor.

2.3.2 *Phonons*

According to Bardeen et al., thermal conductivity of the lattice in the superconducting state should scale as T^2. The T^2 dependence is also true for the normal state. Therefore, the form of the thermal conductivity due to lattice stays the same when the superconducting state is entered from the normal state. Again, they start with the Boltzmann equation and using the appropriate substitutions they arrive at the following expression for $\kappa(T)$ in the superconducting state:

$$\kappa_{ph-s} = D\left(\frac{T}{\Theta}\right)^2 \int_0^{+\infty} \frac{u^3 du}{(e^u - 1)(1 - e^u) g(u)} \tag{2.39}$$

where D is a constant independent of temperature and $g(u)$ is a lengthy function that is given in terms of the energies: E, E', ϵ and ϵ_o [10].

After we have presented the theoretical expressions for the thermal conductivity in conventional superconductors, let us briefly touch upon some experimental results. Aluminum, whose T_c is around 1.1 K, is a conventional superconductor that serves as a excellent example of the superconducting system where electrons dominate the transport of heat throughout the whole temperature range. Since the Debye temperature for aluminum ($\theta_D = 394K$ [11]) is much bigger than the critical temperature for superconducting transition ($T_c = 1.1K$), we expect that the transport at all temperatures, and specifically at very low temperatures, will be dominated by electrons. One expects that measurements of the thermal conductivity of the aluminum in the superconducting state agree with the BRT calculation for the case of electronic thermal

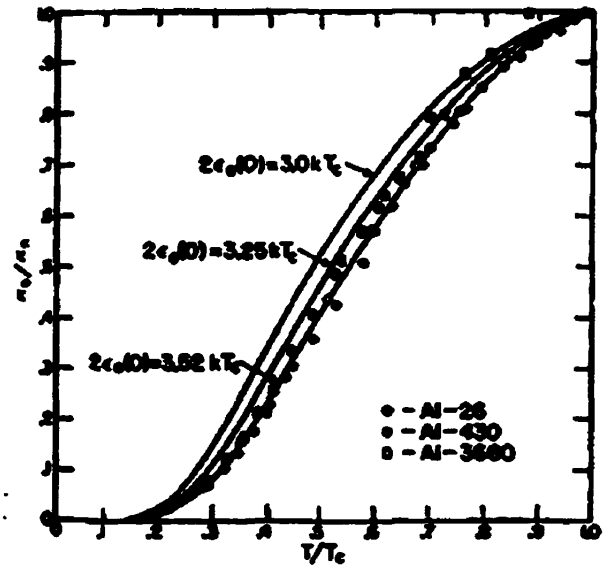

Figure 2.5: The theoretical BRT curve along with the Satterthwaite's results for three Al samples with different impurity concentration after [16].

conductivity when elastic scattering dominates, given in section 2.3.1. The informative study on aluminum was done by Satterthwaite [16]. He measured the thermal conductivity of normal and superconducting aluminum for three different levels of impurities. Therefore, he examined the system with different mean free paths, depending on the level of dirtiness of the aluminum. The measured data κ_s/κ_n was plotted against reduced temperature T/T_c along with the theoretical BRT curves for three closely spaced BCS values of the energy gap at the absolute zero, $2\Delta_o = 3.0kT_c$, $2\Delta_o = 3.25kT_c$, $2\Delta_o = 3.52kT_c$. This is shown on the figure 2.5.

He found that, for all three specimens, the measured thermal conductivity was in agreement with BRT predictions for the expression of κ_e with dominant elastic scattering. His data fitted the BRT curve with value of the energy gap $2\Delta_o = 3.52kT_c$ as good as any other of the two choices. Therefore, Satterthwaite concluded that κ was not sensitive enough function of the energy gap, and that his data was not accurate enough to claim the disagreement with other measured values for the energy gap that ranged from $3.25kT_c$ to $3.37kT_c$. For more explanation the reader is referred to the original paper [16] and references therein.

All three specimens showed linear temperature dependence of the normal state thermal conductivity in agreement with the theory of transport in metals. The superconducting κ was closely approximated by exponential law $\kappa_s \propto e^{-bT_c/T}$, as proposed by Zavaritskii [17]. But the author pointed out that although his findings agreed qualitatively with Zavaritskii's, there was no detailed agreement between his findings and Zavaritskii's proposition for the expression for κ.

He also noticed that the variation of the mean free path by as much as a factor of 140 did not appreciably change κ_s/κ_e ratio as a function of the reduced temperature. The transition temperature T_c varied only slightly with mean free path; and therefore, the same κ_s/κ_n ratio for specimens with different mean free paths would indicate slightly different energy gaps. He found that the difference was consistent with Anderson's theory of dirty superconductors.

We have also measured the thermal conductivity of normal and superconducting states of pure Aluminum (99.99% purity); the results will be discussed in chapter 3. Let us just mention that we also found good agreement with standard BRT curve.

But unlike aluminum where electrons dominate transport at all temperatures, there are other systems, such as niobium, where phonon transport complicates the situation at low temperatures. Kes et al. [18] have measured thermal conductivity of niobium. Their findings are shown in the figure 2.6.

In this system according to BRT [7], the electronic contribution to thermal conductivity is negligible for $T < 2K$. Therefore, as the temperature decreases, the phonon contribution increases since there are less electrons to serve as scatterers and κ_{ph} may even dominate the heat conduction at low temperatures. The phonon mean free path ℓ_{ph} also increases until limited by the sample boundaries, and κ_{ph} increases; but at the same time, the number of phonons decreases. Kes et al. have noticed a pronounced peak at low temperatures arising from the competition between increasing phonon mean free path and decreasing number of phonons at low temperatures [18, 7].

Unlike in aluminum, where the predominant heat carriers at all temperatures are electrons, in the unconventional superconductor YBCO the scenario is more similar

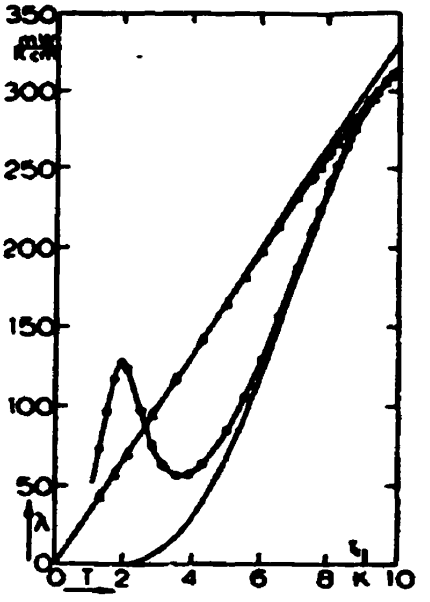

Figure 2.6: The thermal conductivity of niobium in superconducting state after [18].

to niobium. This is because phonons in YBCO are also important. The critical temperature of YBCO is around 93 K and the Debye temperature is $\theta \simeq 400$ K [19]. Therefore, we do expect appreciable phonon contribution to the thermal conductivity at low temperatures.

2.4 *Unconventional Superconductors*

Since all our experiments are done at low temperatures, here is the outline of the theoretical findings for the thermal and electrical conductivity in unconventional superconductors in the low temperature limit.

In unconventional superconductors, thermal conductivity differs significantly from that of normal superconductors. In cuprates, the relative importance of κ_e and κ_{ph} depends on the temperature. At very low temperatures, the two contributions to the thermal conductivity are comparable; but at T< 1 K the interesting physics lies in κ_e. Using thermal conductivity as a probe of a quasiparticle behavior and by going well below 150 mK, one has a reliable way of extracting the phononic contribution to the total thermal conductivity and separating electronic and phononic contributions

to the total thermal conductivity.

Another aspect of unconventional superconductors is that both the finite temperature correction to $\kappa(T)$ in zero field and the finite field corrections to $\kappa(T)$ at $T = 0$ K, give us information about the scattering phase shift δ_o. But since the finite temperature corrections are quite small (0.1% effect below 1 K), finite H corrections to κ at $T = 0$ are more promising for the study of δ_o.

2.4.1 *Electrons*

One should ask in what way is an unconventional superconductor different from a conventional superconductor? The main three differences are:

- effect of impurities
- pronounced anisotropy in transport properties
- contribution of vortices.

The low temperature κ in d-wave superconductor is dominated by nodes; therefore, in the superconductors with a gap that has nodes along certain crystalline directions, one observes anisotropy in the transport properties as well as pronounced effect of impurities. The unconventional superconductor with a gap that has linear line nodes, has linear density of state in excitation energy, $N(\epsilon) \sim N_f \frac{\epsilon}{\Delta_o}$ [20, 21]. But in the presence of impurities, the energy is altered by the random distribution of impurities. Impurities are always present in the crystals and are the source of the scattering. The disorder in d-wave systems gives rise to a finite density of states at zero energy [9] and to a broadening of the gap node. A new energy scale develops, labeled γ below which the density of states is constant and non-zero at zero energy ($T = 0$)[22]. In such a system, novel features are predicted to occur such as zero energy quasiparticles. The existence of this so called residual normal fluid (RNF) is a direct and novel consequence of impurity scattering.

We talk of two regimes:

- gapless regime ($\epsilon < \gamma$), where DOS is finite and non-zero

and

- clean (diagnostic) regime ($\epsilon > \gamma$), where $N(\epsilon) \sim \epsilon$.

Both γ, the impurity bandwidth, and $N(0)$, the density of impurity bound states at zero energy are finite for any finite concentration of impurities $n_{imp.}$; furthermore, both are dependent of Γ, the scattering rate, and δ_o, the scattering phase shift [22] γ, which is the crossover energy scale that separates universal behavior from non-universal, is (for the given impurity concentration) largest in the limit of unitarity scattering, and for $d_{x^2-y^2}$ pairing is given by: $\gamma \sim \sqrt{\pi\Delta_o\Gamma_u/2}$. In the Born limit, $\gamma \sim 4\Delta_o exp(-\pi\Delta_o/2\Gamma_u)$ where $\Gamma_u = \frac{n_{imp}}{(\pi N_f)}$ is the scattering rate.

It has been predicted by Patrick Lee in 1993 [9] that in unconventional superconductors with a certain gap topology at low temperature (i.e. a linear line node such as 2D unconventional superconductors with $d_{x^2-y^2}$ symmetry), transport in the $T \rightarrow 0$ limit should be universal, independent of the concentration of impurities and of scattering phase shift. This is the result of the perfect compensation between the growth in the residual normal fluid density with increasing impurity concentration and the concomitant reduction in the mean free path of the carriers as T $\rightarrow$ 0.

In 2D, the electrical conductivity (per plane) as found by Lee [9], in the universal limit is given by:

$$\sigma(\omega \rightarrow 0) \equiv \sigma_{oo} = \left(\frac{\epsilon^2}{2\pi\hbar}\right)\frac{2}{\pi}\frac{v_f}{v_2} \tag{2.40}$$

where v_f is Fermi velocity and v_2 is velocity along the direction parallel to the Fermi surface ($\hat{k_2}$). In the two dimensional coordinate system $\hat{k_1}$ is normal to the Fermi surface and at 45 degrees with respect to the a axis, and $\hat{k_2}$ is parallel to the Fermi surface. The two velocities, v_1 and v_2, completely define the quasiparticle spectrum at low energy (near the nodes): $E = \hbar\sqrt{v_f^2k_1^2 + v_2^2k_2^2}$. The ratio of two velocities is a measure of the slope of the gap since $\Delta_k \sim \hbar v_2 k_2$ near the node. Electrical conductivity is independent on both impurity concentration and the scattering rate [9].

In the other language, in terms of the density of states, Graf et al. [22] have derived the theoretical expressions for the thermal and electrical conductivity due to electrons at zero temperature limit. They have also calculated the leading temperature correc-

tions to the thermal conductivity at higher temperatures [22]. Their main finding was that κ was also universal in the limit of T $\rightarrow$ 0. Furthermore, the Wiedemann-Franz law was found to be obeyed in the limit $k_B T \ll \gamma$. But, the significant temperature dependence of the Lorenz ratio was found for $T < T_c$. The quasiclassical calculations by Graf et al. reproduce Lee's result for the isotropic systems, $\vec{p_f} = p_f(cos\phi, sin\phi)$ and for the standard model for d-wave pairing, i.e. $\Delta(\vec{p_f}) = \Delta_o cos(2\phi)$.

The result for the low temperature limit of thermal conductivity with d-wave pairing is universal but depends on the slope parameter.

$$\frac{\kappa_{||}}{T} \equiv \frac{\kappa_{oo}}{T} \simeq \frac{\pi^2}{3} N_f v_f^2 \frac{2}{\pi \mu \Delta_o} \tag{2.41}$$

where $\mu = \frac{1}{\Delta_o} |\frac{d\Delta(\phi)}{d\phi}|_{\phi_{node}}$; it measures the slope of the gap at the node. The dependence of the universal value of $\kappa(T)$ on μ reflects the importance of a low-energy continuum states with $\epsilon \ll \Delta_o$ in formation of zero-energy impurity bound states [22, 8].

Similarly, the universal value of σ in the plane given by the language of Graf et al. [22] is in agreement with Lee's finding with $\mu = 2$.

$$Re\sigma_{||}(T, \omega \rightarrow 0) \simeq 2e^2 N_f v_f^2 / (\pi \mu \Delta_o) \tag{2.42}$$

The leading order finite temperature corrections to the transport coefficients were obtained by Graf et al. via Sommerfeld expansions of previously calculated expressions for thermal and electrical conductivity. For the $d_{x^2-y^2}$ pairing, these are:

$$\frac{\kappa_{||}(T)}{T} \simeq \frac{\kappa_{oo}}{T} \left(1 + \frac{7\pi^2}{15} \frac{a^2 T^2}{\gamma^2}\right). \tag{2.43}$$

to a leading order in aT/γ. The coefficient a is strongly dependent on the phase shift; therefore, the finite temperature corrections in zero field give us information about the scattering phase shift δ_o. For resonant (strong) scattering $a = 1/2$, independent of the specific pairing state. In the Born limit (weak scattering), for $d_{x^2-y^2}$ pairing, $a = \pi \mu \Delta_o \tau_o / 2$. It is important to point out that the finite temperature cor-

rections are in general small, and at $T < 1$ K they are only at the order of 0.1 %, unlike the finite field zero temperature corrections to κ which can be much bigger.

Finally, the third main difference between conventional and unconventional superconductors is given through their behavior when an external magnetic field is applied. The vortex contribution to $\kappa(T)$ is discussed later on, but let's just point out that the finite field corrections are potentially a great tool for investigation of δ_o. These corrections in the clean limit when the field is applied in the direction perpendicular to the heat current, $H \perp j_Q$ are given by:

$$\frac{\kappa(0;H)}{T} = \frac{\kappa_o}{T} \frac{\rho^2}{\rho\sqrt{1+\rho^2} - sinh^{-1}\rho} \tag{2.44}$$

where $\rho^2 = \frac{8\hbar\Gamma H_{c2}}{\pi^2 a^2 \Delta_o H}$, κ_o/T is the zero temperature and zero field universal value of thermal conductivity, and a is a constant of the order unity [23].

2.4.2 *Phonons*

In this section, the temperature dependence of the thermal conductivity due to phonons in cuprates is discussed. In the low temperature limit $T \to 0$, the thermal conductivity due to phonons approaches the well-known Debye T^3 asymptotic behavior given by equation 2.27 [8]. It stems from the cubic temperature dependence of the low-temperature phonon specific heat C_{ph}, combined with the fact that at these temperatures ($T < 150$ mK) ℓ_{ph} achieves its maximum, boundary-limited value, independent of temperature.

Then, the thermal conductivity due to phonons can be written as:

$$\kappa_{ph} = \frac{1}{3}\beta < v_{ph} > \Lambda_o T^3. \tag{2.45}$$

Here, β is the specific heat coefficient, Λ_o is the temperature-independent, maximum phonon mean free path, and $< v_{ph} >$ is a suitable average of the acoustic sound velocities. In high quality crystals $\Lambda_o = 2\overline{w}/\sqrt{\pi}$, where $\overline{w}$ is the mean geometric width of a rectangular sample [8, 24].

Early work on κ in high-T_c superconductors showed that $\kappa \propto T^2$. This was well

accepted as a correct temperature dependence [25]. Such a temperature dependence was an indication that thermal carriers in these systems were phonons since, after all, that was the temperature dependence of κ_{ph} in the superconducting state derived early on by Bardeen, Rickayzen and Tewordt [10]. But recently it has been shown in our lab [7, 8] that it is only by going quite low in temperature (namely to $T < 150$ mK), that one can reach the correct asymptotic T^3 dependence due to phonons and can extract the correct phononic term. The validity of such a dependence is verified by comparing the theoretical Debye prediction using the known values for the various parameters in the above Debye expression and the values obtained from the linear fit of the data. It has been shown by Taillefer et al. that our data agrees quite well with the theoretical values [8].

In summary, the total thermal conductivity at low temperatures in high-T_c superconductors (cuprates) can be written in the following form:

$$\kappa_{tot.} = aT + bT^3 \tag{2.46}$$

where the first, linear term is attributed to electrons and the second, cubic term to phonons.

3

EXPERIMENTAL SETUP

3.1 *Experimental setup for thermal conductivity measurements*

The thermal conductivity measurement is a powerful bulk probe of superconducting properties. It is also a directional probe that allows us to examine the gap anisotropy in unconventional superconductors. Some of the other advantages of this measurements are are the following. It does not require extra input, extra assumptions or complex analysis. Reasonably high precision can be achieved (relative 2-3%, absolute 10%). Very low temperatures are accessible ($T < 0.1K$). Lastly, the thermal conductivity measurement is a fairly straight-forward measurement.

3.1.1 Steady state method

In our laboratory, we have employed a standard one heater two thermometers steady state method for measuring $\kappa(T)$. The heat is supplied at one end of the parallepiped shaped crystal (sample) and removed at the other end. The two thermometers mounted along the crystal are used to monitor the temperature across the sample. Depending on the orientation of the crystal, one can measured thermal conductivity along different crystalline directions. The thermometer that is closer to the heat source is labeled T_{hot}, and the one closer to the heat sink is labeled T_{cold}. The copper block on the sample mount is used as a heat sink. The simple diagram of our setup is given in figure 3.1.

Then, the thermal conductivity is related to the rate P at which heat is supplied

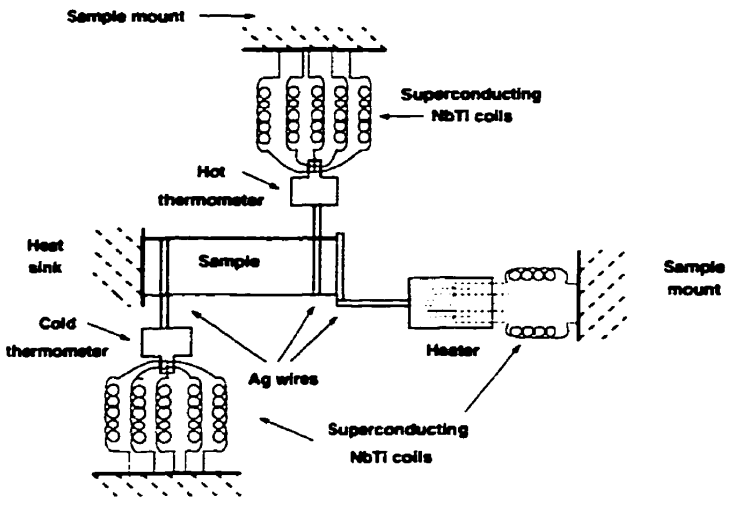

Figure 3.1: The schematic of the experimental setup for the thermal conductivity measurement using the standard one-heater two-thermometers steady state method.

by the following simple formula:

$$\kappa = \frac{P}{\Delta T \alpha} \tag{3.1}$$

where ΔT is the temperature gradient across the sample equal to $(T_{hot} - T_{cold})$ and α is just a geometric factor that tells us about the size of the sample (the distance between the two contacts on the sample divided by the cross sectional area of the sample).

Generally, there are two methods of obtaining the geometric factor. One method uses SEM (Scanning Electron Microscope) to look at the crystal's dimensions, while the other is based on the resistivity curves. We use the same contacts to measure resistivity as those used to measure thermal conductivity. Assuming that we have good contacts on our samples (meaning that we eliminate/minimize the heat losses through the contacts), we can obtain the geometric factors for the different samples by forcing the resistivity curves for the crystals to be parallel based on reasonable assumption that the only difference between samples is in the elastic, temperature-independent term. The elastic term just sets the size of the intercept on the resistivity versus the temperature curve.

3.1.2 Contacts and the connecting leads

The contacts are made using superconducting/nonsuperconducting solder. Flux is used to aid in making contacts. It is used as the agent which helps soldering to be confined to the particular shape and not smear around. The thermometers on the sample mount are connected to the sample via silver wires. The electrical contacts on the sample are also made with silver wire using silver epoxy annealed at 500°C for 1 hour and quenched at room temperature. It is made sure that the thermal resistivity of the contacts is comparable to the thermal resistivity of the samples such that no heat is lost in the contacts. This is the criteria for good contacts. The heater is connected to the sample via Ag wires and to the ground via NbTi coils (15 cm in length prior to coiling).

3.1.3 Electronic equipment

All measurements were done using LR700 resistance bridge from Linear Research and the temperature controller AVS - 46 resistance bridge from RV Elektronikka OY. The two lock-in amplifiers were used to monitor the voltage output across the two thermometers as a function of the time.

The data that is recorded comprises the following quantities:

- Stabilization temperature monitored by the germanium thermometer,
- current across the heater,
- resistances of the two thermometers with and without the heat on,
- voltages across the two thermometers with and without the heat on.

All data is collected by the computer that is interfaced with the electronic devices. The electronic equipment is placed inside the cage to shield radio frequencies. Since our lab is close to the Mount Royal where radio station's antennas are nested, one has to be careful and screen the possible interferences from occurring. These antennas produce high frequency signals (100 MHz). Therefore, all of the electrical devices were placed inside a Faraday cage to prevent these frequencies from coupling to the signal we measured. The base of the cage is a wooden frame on which two layers of

the copper mesh are placed. In April 1998, a new Faraday cage was set up in our lab such that both the fridge and the electrical devices are enclosed in it. However, none of my measurements discussed here were performed inside this new cage.

All measurements, except for the normal state Al thermal conductivity (which was measured in the dipstick), were conducted using the Oxford Kelvinox 300 dilution refrigerator equipped with a 15 tesla superconducting magnet that is situated at the bottom of the cryostat. The dilution refrigerator has been in our lab since 1992. All of the work of setting it up and wiring it were done before my arrival at McGill by Ph.D student Benoit Lussier and post-doctoral fellow Brett Ellmann. The basic procedure for measurements of low temperature thermal conductivity in superconductors (high T_c) was developed prior to my arrival to the lab, as well. The improvements to the set up for measuring thermal conductivity, namely, the design of a new sample mount for samples with high thermal resistance, were done by myself. This is discussed later in this chapter.

One of the problems that one encounters when dealing with the low temperature measurements is the self heating of the thermometers that are used to monitor the temperature. At very low temperatures, the thermometers are to stay 'isolated' from the outside world, and the only way they can dissipate the heat is through the sample itself. One has to be careful to avoid the self heating of the thermometers; otherwise, the data points collected will not be a measure of the desired situation. One way to avoid self heating is to use the lowest possible excitation that is inputed into the system in order to develop the temperature gradient across the sample. One downfall of this is that we will reduce the sensitivity since as excitation voltage is decreased, the ratio of signal to noise decreases as well. An other possibility is to use limiting resistor of the higher resistance. For all measurements we used a 2.2 $M\Omega$ resistor, except for the one on the aluminum where we used a 5 $M\Omega$ limiting resistor. The role of the limiting resistor is to convert the input voltage signal from the lock-in amplifier into the current.

3.1.4 Thermometry

The Germanium thermometer, which is placed at the bottom of the mixing chamber in a field-compensated region of the magnet, was used to measure the reference temperature. It was obtained from and calibrated by the Lakeshore in the 50 mK to 5 K range.

The thermometers used to monitor the temperature gradient across the sample were RuO_2 thick film resistors obtained from Orsay. These sensitive 2.2 $k\Omega$ resistors already had contacts when we obtained them. The bottom part of them was glued to the thin copper plate. We just needed to shorten the contacts slightly and to wound them one time along the bottom of the copper plate and glue them some more with GE varnish in order to insure a good thermal contact. All of the thermometers were tested for their performance prior to mounting them on the sample mount. We have simply measured their resistance at low temperatures ($T < 1K$) in one of the dilution fridge runs in our lab. The thermometers were connected to the sample mount via five superconducting Niobium Titanium wires (25 μm in diameter) for the four probe electrical measurements (V+, V-, I+, I-). In order to preserve the space, I made a superconducting coils out of these wires by wounding 15 cm of the wires into the coils. They were copper plated at the ends in order to make contacts to the copper pads on the mount via superconducting solder.

The measurements of the temperatures of the hot (T+) and the cold (T-) thermometers were done using the two lock-in amplifiers SR 850 from Stanford Research Systems. During the run, we monitored the voltages across the two thermometers as a function of time on the lock-in amplifier's display windows. It was a good visual aid in monitoring the noise on the thermometers, and it allowed us to determine the necessary time for stabilization of our signal. As mentioned earlier, the limiting resistor was used to convert the voltage input signal into the current.

The heater used in our set up was a strain gauge. It was connected to the sample via a silver wire (100 μm in diameter). The electrical contacts from the copper plate to the heater were made via two superconducting Niobium Titanium wires coiled

just like the thermometers' connections. They were attached to the heater with superconducting solder. The resistance of our heater was constant below 1 Kelvin. Its value was recorded with a two probe measurement using a digital multimeter right before starting the thermal conductivity run when the system has already achieved the base temperature.

3.2 *Improved sample mount*

The new improved sample mount was designed for measuring the thermal conductivity of samples with high thermal resistance. That means that one aims at a design which minimizes, as much as possible, the heat losses through the leads enabling us to measure the thermal conductivity of such samples.

The improvements include: the removal of the vespel posts that used to support the thermometers, the replacement of non-superconducting manganine wires that connect the thermometers to the copper pads (ground) with superconducting Niobium Titanium wires, and the reduction of the amount of copper used.

In the case of samples with high thermal resistance, it is crucial to insure that all of the heat supplied to the one (hot) end of the sample travels to the other (cold) end of the sample. The best way to do this is to make the thermal path from the thermometers to the heat sink very highly thermally resistive. The best choice of material for such a path is a superconducting wire because superconductor is a poor conductor of heat.

Figure 3.2 shows a simple schematic of the new sample mount. The new mount was designed such that the coils that are used to make contacts between the copper pads and the thermometers are superconducting (but without the insulation) NbTi coils as opposed to the previously used non-superconducting Manganine coils [7]). It is desirable that the length of the wires that connect the thermometers to the copper pads is increased as to decrease possible heat losses through the wires. The longer the wire the higher the resistance leading to a minimization of the heat losses. Since the length of the Niobium Titanium wire before winding was approximately 15

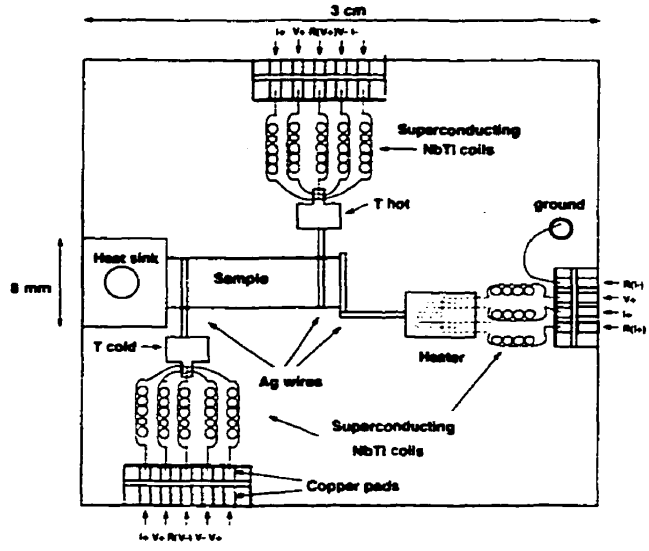

Figure 3.2: The simple schematic of the new sample mount with its parts.

cm, we were not particularly worried about some of the winds in the coils touching each other. We were sure that even if two adjacent winds on the coils touched, we had enough winded length to compensate for such a minute short. Furthermore, as the coils were soldered to the mount and connected to the thermometers, they were stretched enough such as to minimize the possible shorts if adjacent winds would touch.

Firstly, the copper plate, dimensions 3 *cm* by 3 *cm* by 1.5 *mm* (thickness) was machined in the machine shop at the McGill University. In the middle portion of the upper end of the plate, the copper part in the shape of a cube (area 8 *mm* by 8 *mm*) was placed to serve as a heat sink. It was made such as to have a hole for the screw.

In order to make the contact pads, the cleaned copper plate was covered with epoxy on its four corners. Then, small pads of tissue paper (a good thermal insulators) were placed over the spots covered with the epoxy and glued to the four corners of the plate. The top portion of the four rectangular shaped paper pads were then covered with the approximately 1 *mm* of the epoxy paste in which small rectangular copper pads were nested. These were to serve as contact pads. They were very well insulated from each other by the epoxy paste that surrounded them and kept them from touching. These pads were used to make contacts from the mount to the thermometers needed

for the four probe electrical measurements. Unlike in the previous sample mount, the thermometers on the new sample mount were not placed on the vespel posts. They were smaller and lighter and were able to be supported only by the five coils. They also had much less copper underneath them than the previously used thermometers.

For the magnetic studies, we used the old sample mount because a new one was not suitable for in field measurements since the superconducting coils would be affected by the magnetic field. The non-insulated superconducting coils tended to move and tangle in a manner to create a short in a circuit. From the previous experience, it was noticed that copper parts on the mount (copper plate underneath the thermometers and copper pads used for the electrical contacts) took a long time to thermalize in field due to large thermal capacity of Cu. Therefore, we removed the copper parts on our sample mount and replaced them with silver ones hoping that the time constants for the thermometers to stabilize in field would be greatly reduced.

3.3 *Principles of dilution fridge operation*

When one talks about the refrigeration, one is mostly concerned with two thermodynamics laws. The second law states that the entropy of the system always increases. The third law says that the heat capacity of any metal goes to zero as $T \rightarrow 0$. The object of a good refrigeration system is twofold: to minimize the increase in entropy, or in other words, to do the least work that is required to remove the certain amount of heat from the system, and to optimize the overall efficiency of the system even though the cold end of the system (due to Third Law) suffers from the low efficiency.

The principle of all refrigerators is basically the same: some amount of work is inputed at the warm end in order to remove an amount of heat Q at the cold end. This process leads to the net increase in total heat but that heat is released to the surroundings at the warm end. It is important to bare in mind that the efficiency, as a measure of the irreversibility of the process, drops as the temperature decreases [26].

The Kelvinox dilution fridge is a unit that allows very low temperature measure-

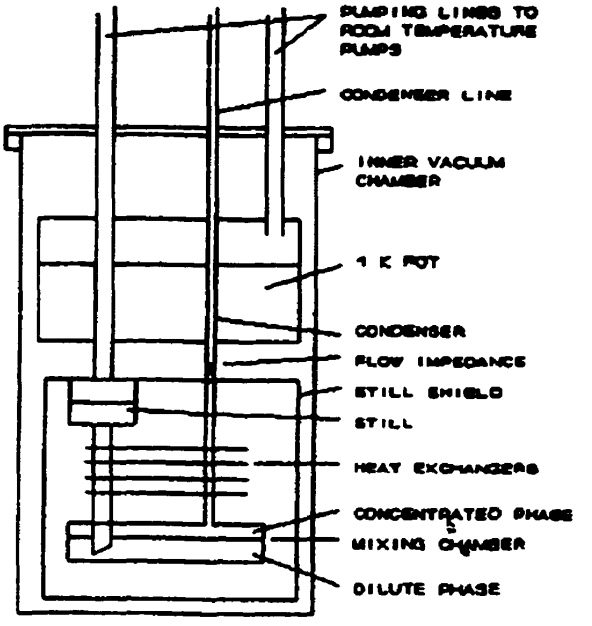

Figure 3.3: The schematic diagram of the dilution refrigerator with its main parts after [27].

ment to be conducted. In our lab, we are able to measure the thermal conductivity down to 50 mK using the germanium thermometer to monitor the stabilization temperature. The resistance of the germanium rapidly increases as the temperature is decreased. In practice, our dilution fridge is capable of measuring temperatures down to 8 mK using a nuclear orientation thermometer.

The dilution fridge consists of the following important parts:

- The 1 K pot that is used to condense the $^3He/^4He$ mixture into the dilution unit. It will cool the mixture of helium isotopes down to 1.2 K but not low enough for the phase separation to take place.

- Still

- Coil heat exchangers

- Silver heat exchangers

- Mixing chamber

The schematic presentation of the dilution refrigerator is shown on figure 3.3. The top of the refrigeration unit has ports that give access to all of the lines inside the

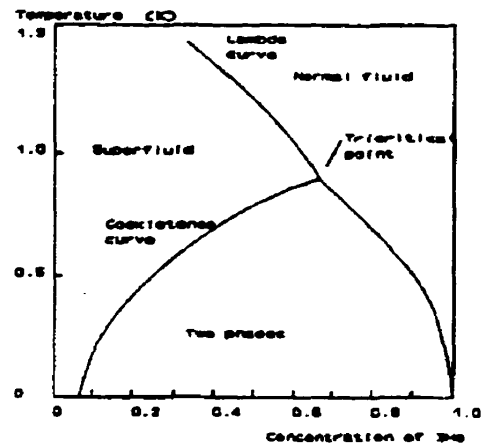

Figure 3.4: Phase diagram of ^{3}He/^{4}He mixture used for cooling to the base temperature of 50 mK, after [27].

refrigerator as well as the refrigerator's parts to which those lines lead. There are some additional ports, such as magnet connections, relief valves and ports for the liquid helium and liquid nitrogen transfers but that will not be discussed in any great detail except listing them here.

The principles of the dilution fridge operation are thoroughly discussed in books by Pobell [28], and Lounasmaa [29]. Therefore, we will present a short summary and refer the reader to the books for a more extensive description of the dilution fridge operation.

When the fridge reaches the temperature of liquid helium, 1 K pot is used to condense the ^{3}He/^{4}He mixture into the dilution unit. At this point, the mixture is not cooled down to the temperature of phase separation but only to 1.2 K. To reach the temperature close to the one for the phase separation (0.87 K) the still is used; in fact, the still is the first part of the fridge to cool below 1.2 K. The incoming ^{3}He is cooled by the still before it enters the heat exchangers and the mixing chamber. Gradually, the rest of the dilution unit is cooled to the temperature of the phase separation [27].

When the mixture of the two stable helium isotopes (^{3}He and ^{4}He) is cooled below 0.87 K, the phase separation takes place. The phase diagram of the ^{3}He/^{4}He mixture is represented on figure 3.4. The phase boundary is inside the mixing chamber, while

the liquid surface is positioned in the still. The ^{3}He phase is a concentrated phase and consists of almost pure ^{3}He liquid. It floats on the top of the dilute phase that consists of superfluid ^{4}He with approximately 6% ^{3}He . ^{3}He is a fermion and therefore unlike ^{4}He which is a boson, it is active and behaves as an ideal gas. ^{4}He on the other hand, is inert due to its superfluid properties and zero nuclear spin. Therefore, ^{3}He will move through the ^{4}He phase without interacting with it. The process of cooling takes place in the dilution unit of the refrigerator, more specifically in the mixing chamber. In a continuously operating system, ^{3}He must be extracted from the dilute phase and returned to the concentrated phase keeping the system in a dynamic equilibrium. ^{3}He is pumped out of the lower dilute phase with a powerful roots pump (it is pumped away from the liquid surface in the still). The concentration of ^{3}He in the still therefore becomes lower than it is in the mixing chamber. The result of the pumping is to produce the osmotic pressure between the two phases since the equilibrium concentration is disturbed. ^{3}He atoms from the concentrated phase migrate across the phase boundary to the dilute phase. This process of cooling is equivalent to the process of evaporation of the liquid into a gas phase, resulting in an effective cooling of the system. The process continues to work even at the lowest temperatures because the equilibrium concentration of ^{3}He in the dilute phase is still finite even as $T \rightarrow 0$. For the continuous operation, the ^{3}He that has been pumped out needs to be reinjected into the mixing chamber. But before it is reinjected, it needs to be liquefied by putting it in thermal contact with the main helium bath and precooled by series of heat exchangers. This is done to avoid excessive heat loads [7, 27].

The cooling procedure to the base temperature of 50 mK is done in several steps which involve in addition to achieving the low temperatures, the electrical check-up and the leak testing procedures. In order to reach low temperatures, it is necessary to provide a very good vacuum; the system should be as clean as possible. Therefore, it is crucial to detect any possible leak at all stages as they will destroy the vacuum of the system and prevent us from reaching very low temperature. The system is

first brought from room temperature to liquid nitrogen temperature (77 K) and then cooled further to liquid helium temperature (4.2 K). The final cooling is done via the dilution fridge that utilizes the cooling power 'stored' in the stable mixture of the two helium isotopes (as discussed previously).

3.3.1 *The room temperature procedure*

Our thermal conductivity set up allows us to measure the thermal conductivity of up to three different samples. Upon mounting the samples on the sample mounts, they are placed on the end of the mount holder. It has the shape of a copper rod of approximately 30 cm in length with a broadened rectangular region at the end where the three sample mounts are placed. It is easily screwed at one end to the bottom of the mixing chamber. Once it is placed, a quick electrical check is done to insure that all connections are in good working order. The inner and outer shields are placed over the dilution refrigerator. In the mean time, the Outer Vacuum Chamber (OVC) is pumped preferably for a couple of days, first with the mechanical and then with the dilution pump.

Upon successful electrical check, the whole refrigeration unit is inserted into the cryostat. The necessary lines are connected, and the leak test on the lines (still line, condenser line, 1K pot) and on the OVC and the IVC (Inner Vacuum Chamber) can be done using the leak detector that is equipped with a dilution pump. At this time, we also pump on the still and condenser line. Since the insert is safely placed into the cryostat, the final electrical check can be done.

3.3.2 *Cooling to 77 K:*

As it takes some time for the system to pre-cool to 77 K and to come into equilibrium, it is preferable to perform the liquid nitrogen transfer at the end of the day and allow the fridge to cool over night. Prior to the transfer, two bellows of nitrogen gas are placed into the inner vacuum chamber (IVC) to serve as an exchange gas in cooling and to isolate the IVC. The nitrogen liquid is then transferred into the main bath. The transfer lasts approximately three hours. The leak test is done to insure the

proper working order at 77 K. Two probe and four probe electrical checks are done when liquid nitrogen temperature is achieved. The next step, after the equilibrium is achieved, is to start pumping on the exchange gas and blow out the liquid nitrogen from the main bath into the jacket using the slight overpressure of the nitrogen bath (200 milli bar). The main bath is pumped to insure that all liquid nitrogen is removed. When this is done, the leak testing can be performed. The ^{3}He and ^{4}He mixture is cleaned before proceeding to the next step of cooling to 4.2 K. The liquid nitrogen through put test shows if there are any blockages in our system.

3.3.3 *Cooling to 4.2 K:*

Again, the exchange gas is inputed into the IVC; this time we use helium gas (250 milli bar). The main bath is then filled with the helium liquid by transferring helium into it through the siphon port on the cryostat; the process takes several hours. Upon filling the main bath with liquid helium, and when the germanium thermometer shows a stable 4.2 K temperature, we perform the electrical check; the helium gas is removed from the IVC by the pump. Leak tests are also done at this point. Since the system is only at 4.2 K, in order to lower the temperature, one has to start the condensing process. In order to further reduce the temperature to about 1.2 K, the 1 K pot is pumped on. But this temperature is not low enough for the phase separation to take place. Some power from the still is inputed into the system for it to cool down below 1 K. When the mixture of the two helium isotopes is cooled below 0.87 K, the phase separation takes place. This process of cooling via the power stored in the mixture was described earlier in the section 3.3.

3.4 *Heat losses and Aluminum test*

3.4.1 *Heat losses*

The heat losses associated with the measurement of heat conduction can be categorized in the following three groups:

- Heat lost due to the measuring leads.

- Heat lost due to gas conduction.
- Heat lost due to radiation (important only at $T > 100K$).

All of the three losses should be minimized to ensure proper measurement that will yield reliable data. Since the heat losses due to radiation become significant only at higher temperatures, $T > 100K$ (see reference [7]), they will not be discussed here. All our measurements were done at much lower temperatures, below 1 K where these losses are negligible.

In order to prevent the heat losses due to gas conduction, it should be insured that the experiment is performed in a good vacuum. Therefore, it is necessary, at the various stages of the cooling, to perform the leak testing procedure. In the case of our experimental set-up, the only gas left at temperatures less than 1 K is some helium exchange gas because all other substances in our set-up become solid at these temperatures. Helium gas can liquefy and cause thermal shorts in our set up. To prevent this from occurring, it is made sure that the helium exchange gas is pumped well at 4 K. But usually, this is not a problem.

The heat loss we are most concerned of in our experimental setup is the heat loss due to measuring electrical leads and supports. One wants to insure that the whole heat supplied to one end of the sample travels to the other end of the sample; or in other words, that the temperature gradient applied across the sample be fully developed.

There are two main conditions that will, if employed, lead to a minimization of heat losses: firstly, good contacts on the sample, i.e. ones with a thermal resistance comparable to thermal resistance of the sample in the normal state, $W_{sample} \cong W_{contacts}$. Secondly, the thermal resistance of the leads should be made much bigger than the thermal resistance of the sample plus contacts, $W_{leads} \gg W_{sample} + W_{contacts}$. The schematic descriptions of the thermal paths in our thermal conductivity circuit is shown on figure 3.5.

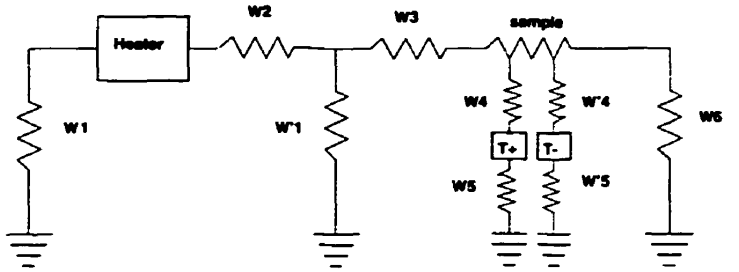

Figure 3.5: The schematic representation of the thermal paths in our thermal conductivity circuit.

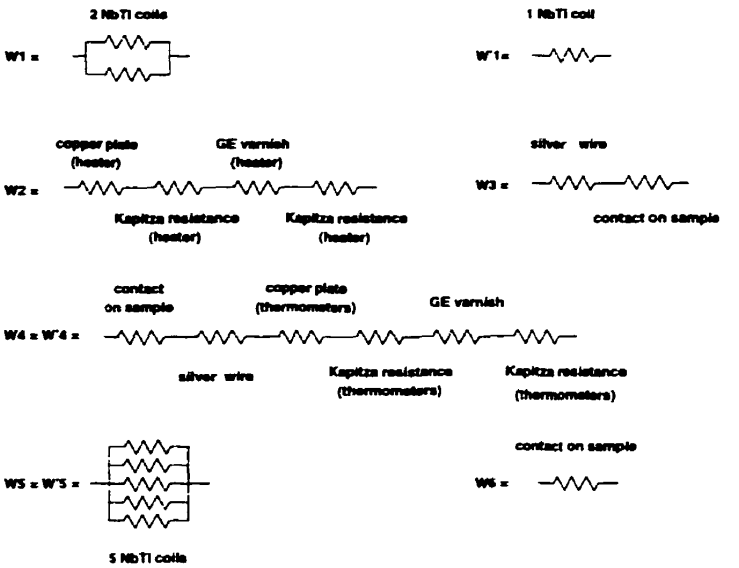

Figure 3.6: The detailed schematic representation of the various thermal resistances used in estimation of the heat losses.

3.4.2 *Estimation of the heat losses due to measuring leads*

The detailed schematic description of the various thermal resistances used in the estimation of the heat losses is shown on figure 3.6.

The Kapitza resistance used in tables 3.1 and 3.2 was calculated using the expression given in Pobell's book (and references therein [28]). The thermal resistance for a boundary between copper and glues is given by:

$$AR_kT^3 = 0.007\ \frac{cm^2K^4}{mW} \tag{3.2}$$

where $A = 5.5 \times 10^{-2}(3.1 \times 10^{-2})\ cm^2$ is the area of the contact between the copper plate and the glue for the heater (thermometers), R_k is the Kapitza (boundary) resistance, and T is the temperature.

We assumed that the thermal resistance of the contact on the sample was the same as the thermal resistance of the aluminium sample in the normal state. Then, $W_{contact}$ can be calculated in the following manner. We estimated that the length of the sample was approximately equal to the length between the contacts; therefore, the resistance of the sample in the normal state at 4.2 K was equal to the resistance $R_{4.2K} = 505\ \mu\Omega$ (which was constant below 4.2 K) as measured in the fridge run. Wiedemann-Franz law for the normal state of Al was used to obtain the values for the normal state thermal conductivity of aluminum at 0.1 K and 1 K and thus the thermal resistance of the contacts on the sample (since the two were assumed to be equal):

$$W_{contact}T = \frac{R_{4.2K}}{L_o} \tag{3.3}$$

where $W_{contact} = 1/\kappa_{contact}$ is the thermal resistance of the contact at 4.2 K and L_o is Summerfeld value of the Lorenz number equal to $2.44 \times 10^{-8}\ W\Omega/K^2$.

The value for the thermal resistance of the aluminium sample at 0.1 K and 1 K was obtained in the following manner: The normal state thermal conductivity of Al at 0.1 K and 1 K was obtained in the manner discussed above. Then, utilizing the BRT standard theoretical curve, it was estimated that at 0.1 K ratio of κ_s/κ_n was 0.0008, and at 1K approximately 0.92. From these values, $W_{sample} = W_6 = 1/\kappa_{sample}$ was calculated and recorded in tables.

In order for heat losses from the heater to be negligible, the thermal path from the heater through the sample to the heat sink ($W_2 + W_3 + W_{sample} + W_6$) should be much less resistive than the direct path from the heater to the heat sink (W_1 or $W_2 + W_1'$).

In order for the heat losses from the thermometers to the sample to be negligible, the path between them should be much less resistive than the path from the thermometers to the heat sink. Therefore, one requires that $W_4(W_4') \ll W_5(W_5')$.

Using the data from the tables 3.1 and 3.2 for the heat loss along the heater path,

Table 3.1: Thermal conductivity and the geometry of the various components used in thermal conductivity setup. † This quantity could not be measured and thus was estimated

Compound name	Length cm	Area cm^2	$\kappa(0.1K)$ $\frac{mW}{cmK}$	$\kappa(1K)$ $\frac{mW}{cmK}$
NbTi wire	15	4.9×10^{-6}	1.5×10^{-3}	1.5×10^{-1}
GE varnish (heater)	1.0×10^{-2}†	5.5×10^{-2}	4×10^{-4}	3×10^{-2}
GE varnish (thermometers)	1.0×10^{-2}†	3.1×10^{-2}	4×10^{-4}	3×10^{-2}
Copper plate (heater)	1.5×10^{-2}	5.5×10^{-2}	4×10^{1}	4×10^{2}
Copper plate (thermometers)	5×10^{-2}	3.1×10^{-2}	4×10^{1}	4×10^{2}
Silver wire	1×10^{0}	7.9×10^{-5}	1×10^{1}	1.1×10^{2}

Table 3.2: Thermal resistivity of the various components used in thermal conductivity setup.

Compound name	W(0.1K) $\frac{K}{mW}$	W(1K) $\frac{K}{mW}$
NbTi wire	2.04×10^{9}	2.04×10^{7}
GE varnish (heater)	4.5×10^{2}	6.1×10^{0}
GE varnish (thermometers)	8.1×10^{2}	1.1×10^{1}
Copper plate (heater)	6.8×10^{-3}	6.8×10^{-4}
Copper plate (thermometers)	4.0×10^{-2}	4.0×10^{-3}
Silver wire	1.3×10^{3}	1.2×10^{2}
Kapitza resistance (heater)	1.3×10^{2}	1.3×10^{-1}
Kapitza resistance (thermometers)	2.3×10^{2}	2.3×10^{-1}
Sample	2.6×10^{5}	2.3×10^{1}
Contact on sample	2.1×10^{2}	2.1×10^{1}

we get:

$$\frac{W_2 + W_3 + W_{sample} + W_6}{W_1} = 3 \times 10^{-2}\ (2 \times 10^{-3})\ \% \tag{3.4}$$

and

$$\frac{W_2 + W_3 + W_{sample} + W_6}{W_1' + W_2} = 1.3 \times 10^{-2}\ (1 \times 10^{-3})\ \% \tag{3.5}$$

for temperature, T = 0.1 K (1 K)

For the heat losses associated with the thermometers' path we have:

$$\frac{W_4}{W_5} = \frac{W_4'}{W_5'} = 7 \times 10^{-4}\ (4.0 \times 10^{-3})\ \% \tag{3.6}$$

We performed the test on aluminum (see next section) in order to test for the heat losses of the new sample mount. It is clear, from the above calculations, that the heat losses due to electrical leads and supports in the thermal conductivity measurements performed in our lab can be safely neglected over the whole temperature range.

3.4.3 *Test on aluminium wire*

In order to test the new improved sample mount for heat losses and general performance, we performed a test on a wire of aluminum. We measured the thermal conductivity of 99.999 % purity aluminum wire [30] in the superconducting state from 170 mK up to 900 mK using the dilution fridge. The length of the wire was chosen such that the thermal resistance of aluminum in its superconducting state was comparable to the thermal resistance of our most resistive sample, deoxygenated $YBa_2Cu_3O_{6.0}$, $W_{deox} \sim 5.6 \times 10^4\ K/mW$ at 0.1 K. The normal state thermal conductivity of aluminum was measured in the dipstick above 1.5 K, and it gave a perfectly linear κ_n below $\sim$ 5 K: $\kappa_n/T = 5094\ mW/cmK$. It verified that the Wiedemann-Franz law held and that the normal state thermal conductivity of aluminium could be written as: $\kappa_n = \sigma L_o T = L_o T/R_o$. The critical temperature could not be measured because neither the refrigerator nor the dipstick are capable to operate around 1.1 K. The refrigerator has an upper limit of 1 K, and dipstick lower limit of 1.5 K. Therefore, we were only probing the superconducting state in the dilution fridge measurements. We assumed that the critical temperature of our sample (with $RRR = 513$) was

1.178 K which was justified by the previous measurements on aluminum where T_c for aluminum with $RRR = 430$ was found to be 1.178 K [16].

Aluminum is often used for testing. It is a well-behaved conventional superconductor that follows the standard (BRT) thermal conductivity curve in the superconducting state. The critical temperature is around 1 K and the critical magnetic field needed to kill superconductivity is only at the order of couple hundred Gauss. Since the Debye temperature for aluminum is much larger than the superconducting critical temperature ($\theta_D = 394\ K \gg T_c$ [11]), we expect the heat transport at all temperatures and even at very low temperatures to be dominated by electrons (in high purity samples).

If there are heat losses, then the experimentally measured thermal conductivity will turn out to be higher than the standard BRT curve. The reason for this is that if heat is lost, we will not acquire the temperature gradient that we aimed for; this will lead to overestimation of $\kappa(T)$ because $\kappa(T)$ is inversely proportional to the temperature gradient.

The thermal conductivity of the aluminum wire was measured in the dilution fridge from 170 mK up to 900 mK using the standard one heater two thermometers steady state method described at the beginning of this chapter . The characteristics of the sample were the following. The length of the wire in between the contacts was calculated to be 1.918 cm from the ratio of the quoted room temperature resistivity in Alfa AESAR [30] $\rho = 2.655\ \mu\Omega cm$ and value of the resistance at room temperature $R_{297K} = 259.4\ m\Omega$. The resistance at liquid helium temperature (4.2 K), recorded during the LHe temperature electrical check in the fridge was $R_{4.2K} = 505\ \mu\Omega$ and remained constant below 4.2 K. Using the above values of resistances, we got the residual resistivity ratio, the ratio of the resistance at room temperature to one at liquid helium temperature, to be $RRR = 513$. It is a measure of the purity of the sample, which was seen to be high.

We have plotted the thermal conductivity of aluminium divided by temperature as a function of the temperature from 170 to approximately 900 mK, as measured in

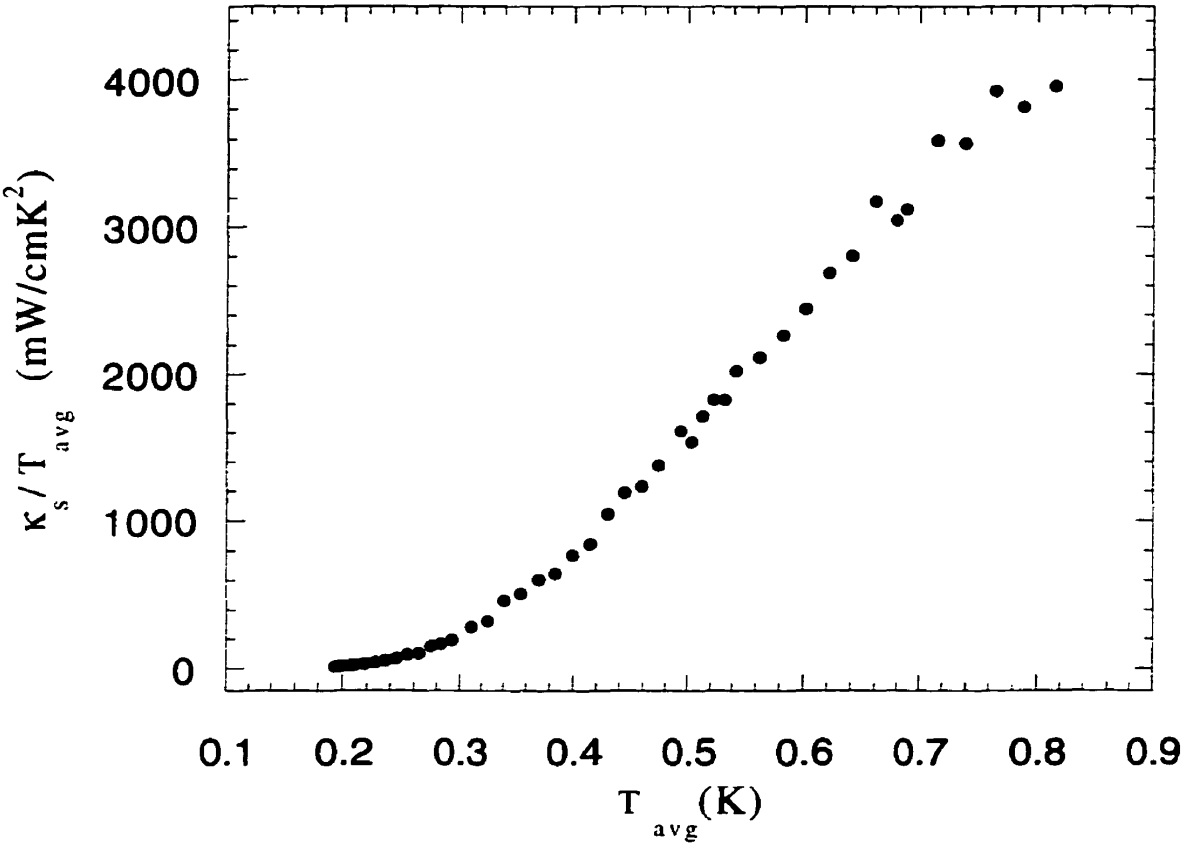

Figure 3.7: The thermal conductivity of aluminium in the superconducting state divided by temperature versus the temperature.

the dilution fridge. Our results are shown on figure 3.7.

In order to compare our results with the standard (BRT) curve, we needed to obtain the ratio of the superconducting to normal state thermal conductivity. Assuming Wiedemann-Franz law (as justified by the measurement on the normal state thermal conductivity of Al in the dipstick where κ_n was found to be perfectly linear), the thermal conductivity in normal state κ_n' without the geometric factor can be written as:

$$\kappa_n' = \frac{L_o T}{R_o} \tag{3.7}$$

The superconducting state κ_s, again without the geometric factor, is given by:

$$\kappa_s' = \frac{P}{\Delta T} \tag{3.8}$$

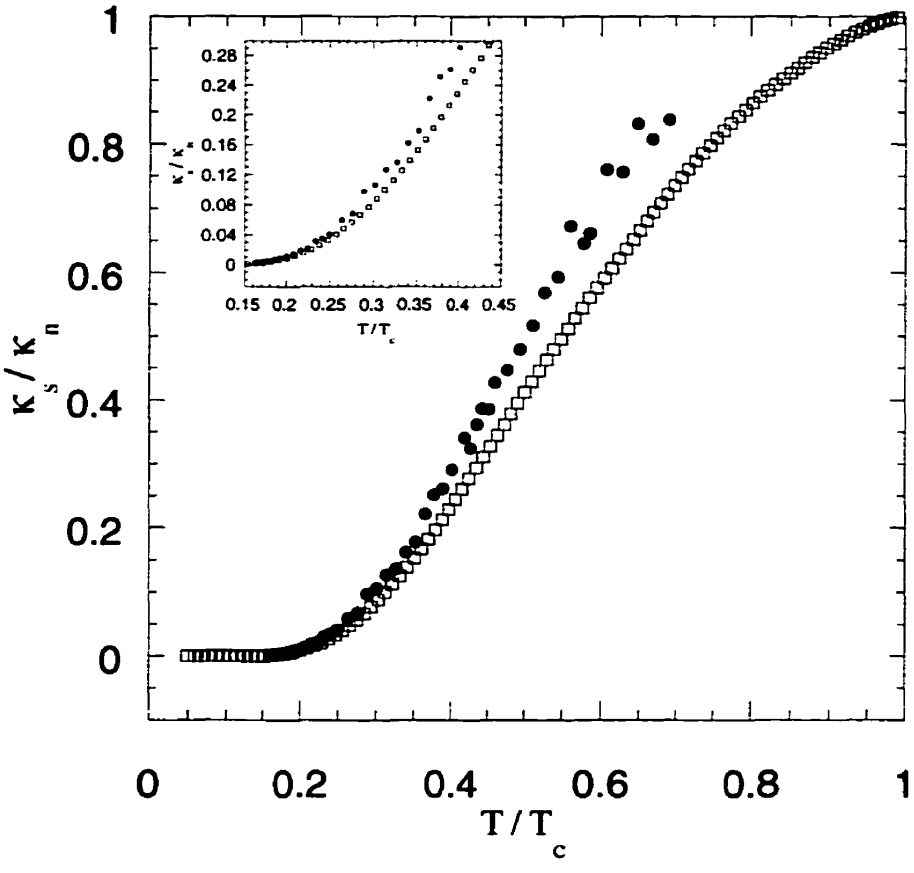

Figure 3.8: Ratio of the thermal conductivity of aluminum in superconducting state to thermal conductivity in normal state (solid circles) against the reduced temperature (where T_c was taken to be 1.178 K), along with the standard BRT curve (open squares).

where P is the power through the heater and ΔT is the temperature gradient across the sample. Then the ratio of the two conductivities is simply:

$$\frac{\kappa_s'}{\kappa_n'} = \frac{\kappa_s}{\kappa_n} = \frac{PR_o}{L_o \Delta T\ T} = \frac{P \times 5.05 \times 10^{-4}\Omega}{2.44 \times 10^{-8}\ W\Omega/K^2 \Delta T\ T} = \frac{P \times 20700\ K^2/W}{\Delta T\ T} \tag{3.9}$$

where κ_s and κ_n are the superconducting and normal state thermal conductiv-

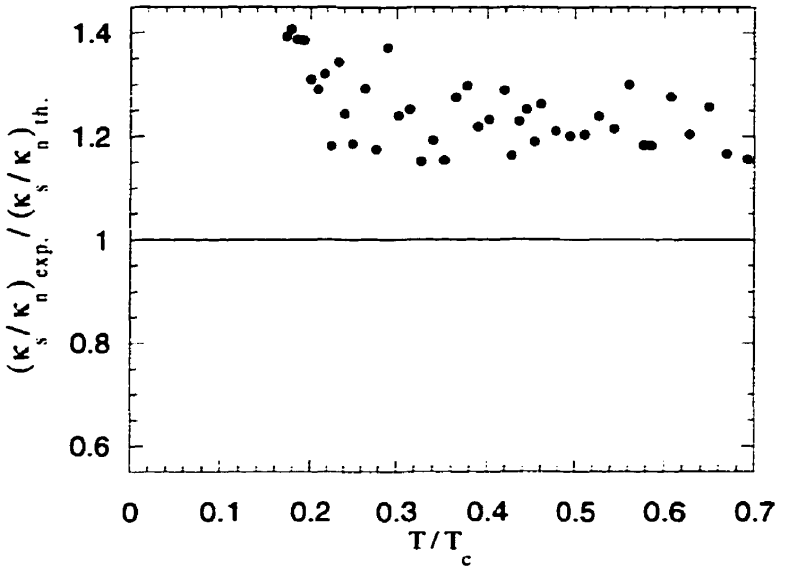

Figure 3.9: The ratio of the experimentally determined $(\kappa_s/\kappa_n)_{exp.}$ to the theoretically determined $(\kappa_s/\kappa_n)_{th.}$ versus the reduced temperature T/T_c, where T_c is taken to be 1.178 K.

ity with the geometric factor included. The ratios with and without the geometric factor are equal because the geometric factor cancels out. This way, we eliminate the uncertainty in the geometric factor. Our data on aluminum shows very good agreement with the predicted theory. Figure 3.8 shows the theoretically calculated ratio of the superconducting to the normal state thermal conductivity as a function of the reduced temperature for aluminum [10] and our results plotted on the same graph. The inset shows the low temperatures results. We are particularly interested in the low temperature limit because that is the limit where heat losses are most intensified. At the higher temperatures, our values are somewhat higher which can be attributed to the scattering of data at higher temperatures. This might a problem with the fitting of the data. The voltage and current readings are collected using two thermometers mounted on the sample mount (T_{hot} and T_{cold}). These thermometers, which monitor the temperature gradient in the dilution fridge experiments, need to be fitted so that the temperature in Kelvin can be obtained. Since in our analysis we used a power law to fit the thermometers, it is possible that at the end points of the fit we have curve fitting problem. The frequency of the data points at higher temperatures is less than at the low temperatures which gives us somewhat less data

points from which to extract the curve fit.

Figure 3.9 shows the ratio of the experimentally determined $(\kappa_s/\kappa_n)_{exp.}$ to the theoretically calculated $(\kappa_s/\kappa_n)_{th.}$ versus the reduced temperature T/T_c. From the plot it is evident that the heat losses through the whole temperature range are approximately of the same magnitude ranging from 15 % to a maximum value of 40 %. The experimentally determined ratio of the superconducting to normal state κ is at most 40 % higher than the theoretically predicted one. We believe that by normalizing the results by forcing the ratio to go to 1 at $T/T_c = 1$ (by definition) the relative magnitude on the percent heat losses would be reduced. But, since the experimental data could not be collected in the dilution fridge at the temperature as high as 1.1 K, we do not have a way of determining the exact normalization factor. Although at first it appears that the heat losses are high, we are able to justify them through the uncertainty on the value of the T_c. The position of the experimentally determined κ_s/κ_n in relation to standard BRT curve is sensitive to the value of T_c. By just changing the value of the T_c by few percent, the experimental curve is shifted. Therefore, it is possible that the experimental curve is underestimated as a result of an underestimation of the T_c. This would affect the ratio of the experimentally determined $(\kappa_s/\kappa_n)_{exp.}$ to the theoretically determined $(\kappa_s/\kappa_n)_{th.}$. Since we could not measure the T_c, we made a reasonable assumption that it was close to 1.178 K as given for the aluminium with the similar purity [16]. Furthermore, some uncertainty is buried in the normal state thermal conductivity since we did not measured it directly in the dilution refrigerator.

We conclude this section by pointing out that the heat losses through the whole temperature range were of approximately the same magnitude and were less than 40 %. Through the whole temperature range, the heat losses varied not more than (40 - 15) % = 25 %. But this seemingly high value is probably due to the uncertainty in T_c and κ_n and could possibly be re-normalized if the proper normalization factor could be obtained.

4

THE HIGH-T_c SUPERCONDUCTOR $YBa_2Cu_3O_{7-\delta}$

In this section, we summarize some of the basic features of the high-T_c superconductor $YBa_2Cu_3O_{7-\delta}$.

4.1 Crystal structure

The high T_c cuprates have a highly anisotropic structure that belongs to a wide class of perovskites. Some of the materials in this class are: $La_{2-x}Sr_xCuO_4$ (T_c = 38 K), $YBa_2Cu_3O_7$ (T_c = 93 K), $Bi_2Ca_2Sr_2Cu_3O_{10}$ (T_c = 110 K). $Tl_2Ca_2Ba_3Cu_3O_{10}$ (T_c = 125 K). $YBa_2Cu_3O_{7-\delta}$ which is the focus of my thesis and is the most thoroughly studied of the high-T_c's, was discovered in 1987 [7].

The general structural characteristics of these class of compounds are as follows:

1) highly two dimensional CuO_2 planes positioned in the *ab* plane and responsible for superconductivity.

2) metal-oxygen insulation planes which serve as a charge reservoirs and separate sets of adjacent CuO_2 planes. Here, the metal atoms are La, Ba, Tl or Bi.

The crystal structure of $YBa_2Cu_3O_{7-\delta}$ consists of double CuO_2 layers stacked on top of each other along the *c* axis and one dimensional CuO chains positioned along the *b* axis. The lattice parameters for $YBa_2Cu_3O_{6.9}$ are: a = 3.88 Å, b = 3.84 Å and c = 11.63 Å [7]. There are two CuO_2 planes per 11.63 Å. In addition, there are metal-oxygen isolation planes which act as a charge reservoirs and separate one layer of the CuO_2 planes from the other layer. In the case of $YBa_2Cu_3O_{7-\delta}$ the metal atoms are Ba atoms (for example in LaSrCuO, these atoms are La atoms). The two adjacent copper oxygen planes which form a layer are separated from each

other by Yttrium atoms; the Yttrium atom simply servers as a spacer between CuO_2 planes. The presence of the double CuO_2 layers is the key feature of the unit cell of $YBa_2Cu_3O_{7-\delta}$ [7, 26].

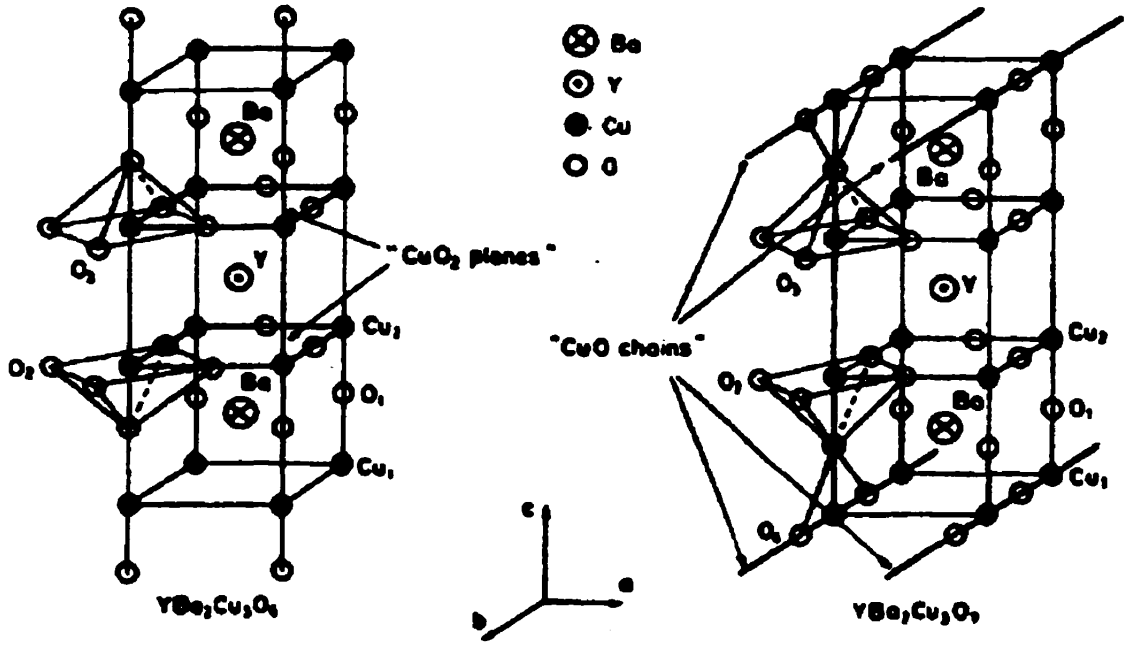

Figure 4.1: The crystal structure of YBCO, after [7, 31].

Figure 4.1 shows the crystal structure of $YBa_2Cu_3O_{7-\delta}$. This structure gives this class of superconductors prominent quasi-two-dimensional character which results in many anisotropic properties.

Clearly, since there are planes and chains in the structure, there are two channels of electronic conduction in $YBa_2Cu_3O_{6.9}$. Therefore, it is not surprising that one finds anisotropy in transport properties, such as the normal state resistivity, the temperature dependent penetration depth, and the in-plane thermal conductivity of $YBa_2Cu_3O_{6.9}$. We are interested in:

1. general behavior of CuO_2 planes

and

2. behavior of CuO chains.

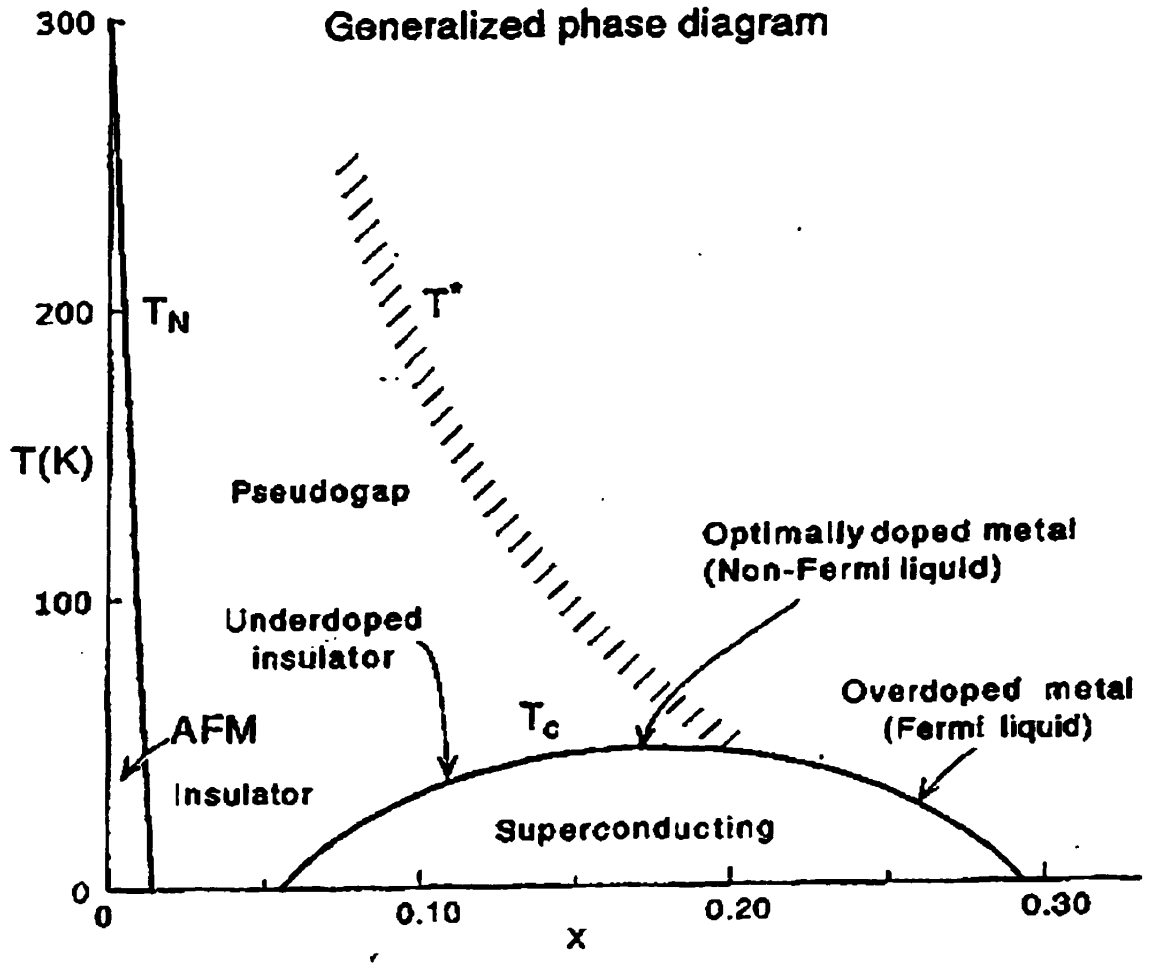

Figure 4.2: Generic phase diagram of the temperature versus the dopant concentration x in cuprates. The solid lines labeled T_N and T_c set the borders for the antiferromagnetic (AFM) and superconducting regions respectively (after [1]).

4.2 *Oxygen doping*

One can profoundly alter the properties of $YBa_2Cu_3O_{7-\delta}$ by changing the oxygen content. When it is reduced, oxygen is removed from the chains. When complete deoxygenation is achieved, $\delta = 1$, $YBa_2Cu_3O_{7-\delta}$ becomes $YBa_2Cu_3O_{6.0}$ and the crystal is tetragonal and a (non-superconducting) insulator [26]. By adding oxygen, eventually the crystal becomes metallic with $\delta \simeq 0.1$. At this point, the $YBa_2Cu_3O_{6.9}$ is optimally doped and the maximal T_c is achieved. When $\delta = 0.0$, the crystal $YBa_2Cu_3O_7$ is fully doped.

The generic phase diagram for the cuprates is presented in figure 4.2. One can observe the change in phase of $YBa_2Cu_3O_{7-\delta}$ as a function of the oxygen doping. $YBa_2Cu_3O_{6.0}$ is an insulating antiferromagnet. As oxygen content is increased, the Neel temperature reduces and finally vanishes when $\delta = 0.64$. Upon further increase in oxygen content, from $\delta = 0.36$ to $\delta = 0$, the crystal becomes metallic, nonmagnetic, and superconducting. The maximum T_c is achieved for $\delta = 0.05$ (called optimal).

The proximity of the antiferromagnetic and superconducting phases has attracted a lot of interest. Some new theories have emerged recently in order to explain this phenomenon. One of them is the Unified theory of antiferromagnetism and superconductivity proposed by Zhang et al. [32], commonly known as SO(5) theory. It postulates that the two phases (antiferromagnetism and superconductivity) have the same origin and can be unified into a single theory, just like the phenomena of electricity and magnetism are unified in the electromagnetic theory. No conclusion has yet been reached on this issue, and more research is needed.

4.3 Crystal preparation

All crystals used in the measurements presented in this thesis were grown by Robert Gagnon, a research associate in our lab. They were grown by the self-decanting flux method [33, 34]. One starts with powders of Y_2O_3 (99.9999%), $BaCO_3$ (99.9999%), and CuO (99.9999 %) mixed in a molar ratio Y:Ba:Cu of 1:18:45. YSZ (yttria-stabilized zirconia) crucibles were used as they are known not to contaminate YBCO significantly [33, 34]. The crystals are oxygenated for 6 to 10 days at 500° C in flowing O_2 gas and quenched at room temperature. The oxygen content is then expected to be $6.9 < 7 - \delta < 6.92$, based on existing oxygen diffusion studies [35, 36]. In the air above 800°C, $YBa_2Cu_3O_{7-\delta}$ has tetragonal crystal symmetry. As the crystal is cooled, oxygen enters the chains and the crystal becomes orthorhombic which results in an asymmetry between a and b axes. We say that the sample becomes twinned with small domains. Since the a and b dimensions of the crystal are comparable, it is quite easy for a and b axes to become reversed when the unit cell is repeated

again and again to form the grain. Then, there is a slight change in direction of the orientation but not enough change for it to be considered a new grain [26]. The crystals are detwinned by applying a uniaxial pressure of approximately 50 MPa at 550°C in air for 30 minutes or less. Then, the detwinned crystals are reoxygenated for 1 day at 550° C in O_2.

Electrical contacts on the crystals are made with silver wire using silver epoxy annealed at 500° C in O_2 for 1 hour and quenched at room temperature. The typical diameter of the contacts is 40μm and the typical resistance of the contacts is $< 0.1\Omega$ at room temperature. The resistive transitions are typically narrow ($\sim$ 0.2 K) and $T_c \sim$ 93 to 94 K. The extent of detwinning can be measured by a polarized light microscope. The dimension of the crystals and the separation between the contacts are measured by scanning electron microscope [37].

4.4 *Normal state resistivity*

It is well established by now that the normal state properties of high T_c superconductors are unusual. The first anomalous normal state properties of this class of superconductors to be identified were the electrical resistivity and the Hall effect [1].

For optimally hole doped systems of high-T_c superconductors, the in plane resistivity $\rho_{ab}(T)$ a has linear temperature dependence between T_c and high temperatures ($\sim$ 1000 K). The extrapolated residual resistivity is very small, $\rho_{ab}(0) \approx 0$. The total normal state resistivity can be written as:

$$\rho_{ab}(T) \approx \rho_{ab}(0) + cT. \tag{4.1}$$

[1, 39]

The linear dependence of the resistivity was observed for the most optimally doped compounds [39]. But there are some previous studies in YBCO that showed that ρ in a-b plane was not linear. The distinct upturn in $\rho(T)$ has been observed in powders [40] and in thin films [41] as well as in crystals [42, 43, 33, 34]. The upturn was attributed to the chains although the detailed description of the separate conducting

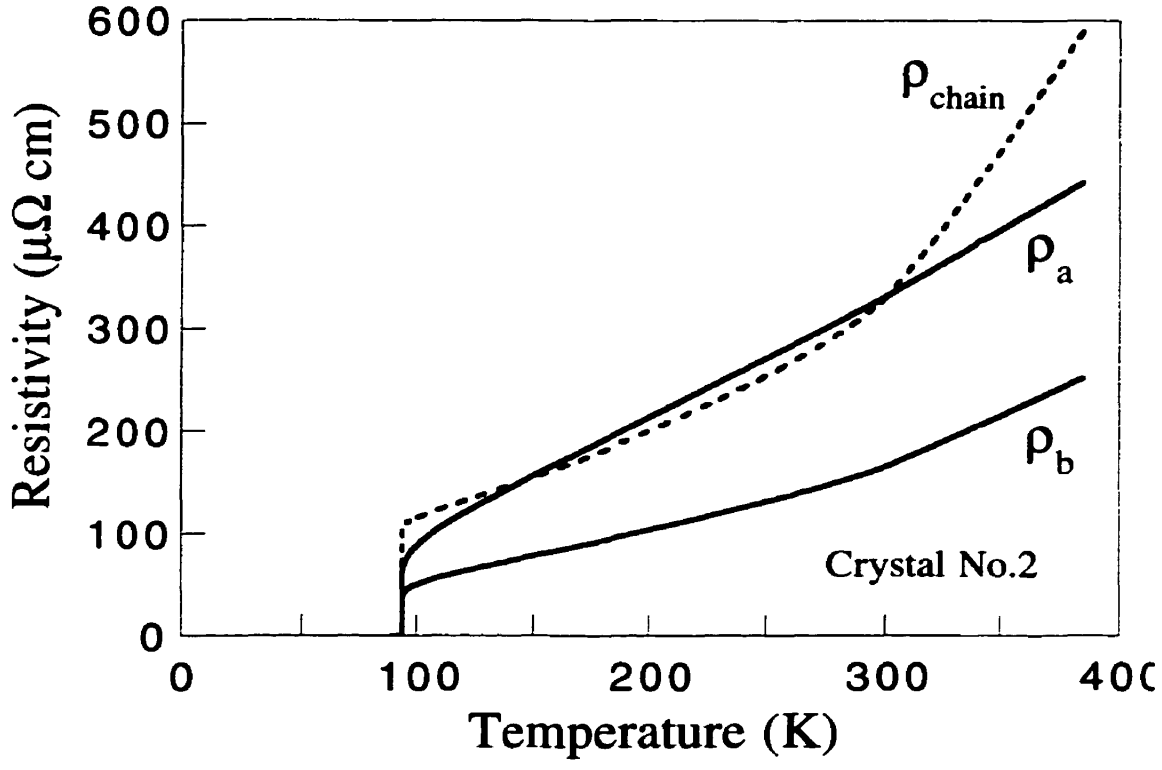

Figure 4.3: Temperature dependence of the resistivity along a and b directions for $YBa_2Cu_3O_{6.9}$[38].

planes and chains was missing. Clearly, the chain and the plane resistivities are different. Furthermore, the anisotropy here is not constant, in particular as $T \to 0$. Therefore, the anisotropy is not describable simply by mass tensor anisotropy (see chapter 5). Then, it is natural to ask what role in the superconductivity is played by the chains?

The normal electrical resistivity of $YBa_2Cu_3O_{7-\delta}$ has been measured by Gagnon et. al [38]. They were able to characterize the resistivity curves by treating the resistivity along the b axis as the sum of the resistivities of plains and chains. For more details on their study, the reader is referred the the later discussion and to the original paper [38]. Gagnon et al. showed that conduction in Cu-O chains was very different to that of the CuO_2 planes.

Friedemann et al. [43] were the first to use detwinned crystals and measure the

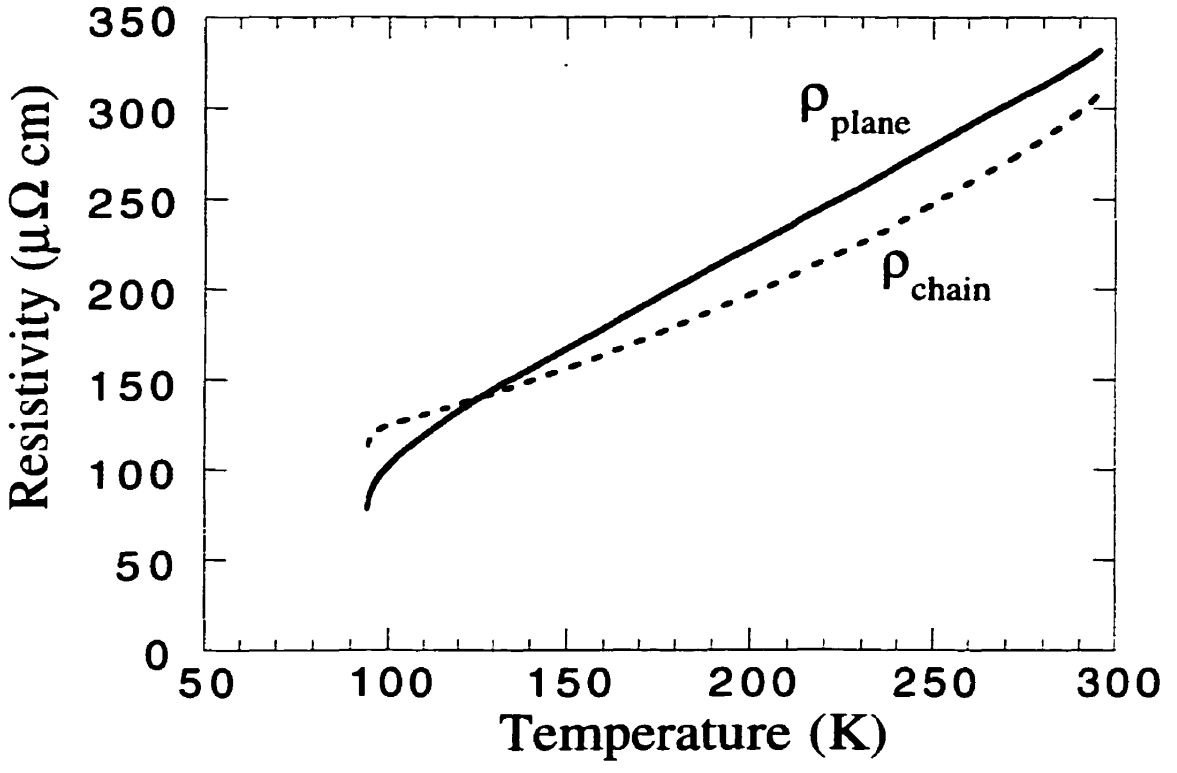

Figure 4.4: Temperature dependence of the chain and plane resistivity for the detwinned $YBa_2Cu_3O_{6.9}$ crystal. The chain resistivity was obtained using the simple model of two parallel conduction channels for the b axis after [38].

resistivity along the a and b axes separately. Their crystals were grown in YSZ crucibles, known not to contaminate the crystals significantly. They were the first to report separate temperature dependence of ρ_a and ρ_b. Their findings were: an anisotropy ratio of $\rho_a/\rho_b = 2.2 \pm 0.2$ for temperatures between 150 and 275 K; both ρ_a and ρ_b were reported to be linear in temperature. But although only one of their crystals showed a slight upward curvature in both ρ_a and ρ_b above 240 K, the authors didn't attempt to explain that feature.

It is known that the anisotropy is reduced by:

1. reducing the oxygen level,

2. by putting the impurities into the chains.

Welp et al. [44] found lower anisotropy ratio that ranged from $\rho_a/\rho_b = 1.2$ to 1.85 and was sample dependent. But their crystals were grown in gold crucibles that are known to contaminate the samples and introduce up to several percent

gold impurities into the crystals that preferentially go into the Cu-O chains. They attributed the lower anisotropy to a high sensitivity of the chains resistance to oxygen disorder. But it appears that the more suitable explanation for their findings would be that the introduction of the gold impurities into the chains increased the chain resistivity. The contamination by gold, therefore, could cause lower anisotropy ratio since ρ_b incorporates chain resistivity in itself; as ρ_b increases, ρ_a/ρ_b must decrease. The chain carriers were scattered more by the impurities; ρ_{chain} increased and the intrinsic behavior of chains was masked by increased scattering. Like Friedemann et al.[43], Welp et al. [44] have also found both ρ_a and ρ_b to be linear in temperature from $T \sim T_c$ up to 300 K. They didn't detect any deviation from linearity.

Gagnon et al. [38] performed systematic study of resistivity along a and b directions in detwinned $YBa_2Cu_3O_{7-\delta}$ crystals. They obtained an anisotropy ratio $\rho_a/\rho_b = 2.12 \pm 0.05$ at T = 250 K in agreement with previous studies mentioned earlier by Friedemann et al. [43]. But unlike the previously mentioned studies, their study was able to recognize qualitatively the differences between $\rho_a(T)$ and $\rho_b(T)$. Above the superconducting fluctuation regime ($T_c < T < 130K$), ρ_a was found to be perfectly linear in temperature up to T = 300 K.

$$\rho_a = \rho_a^o + A_a T \tag{4.2}$$

The residual resistivity along a was very small, even negative $\rho_a^o = -14\mu\Omega cm$; the coefficient of a linear temperature term was $A_a = 0.94\ \mu\Omega cm K^{-1}$. On the other hand ρ_b had a distinct upward curvature as a result of the contribution from the chains. Above 150 K, Gagnon et al. found that ρ_{chain} roughly obeyed the following equation:

$$\rho_{chain} = \rho_{chain}^o + A_{chain} T^2 \tag{4.3}$$

[38].

Their results of the temperature dependence of the resistivities along the a and b directions are shown on figure 4.3. To understand the observed temperature dependence of the chain resistivity, Gagnon et al. applied a simple model to the b-axis

conductivity: the model of parallel conduction channels. According to this model, one can view the b axis conductivity as the sum of the separate conductivities in CuO_2 planes and along Cu-O chains, or in mathematical form: $1/\rho_b = 1/\rho_a + 1/\rho_{chain}$. In light of this model, one obtains the following expression for ρ_{chain}:

$$\rho_{chain}(T) = \frac{\rho_a \rho_b}{(\rho_a - \rho_b)} \tag{4.4}$$

where it is assumed that resistivity in the plane was isotropic and $\rho_{plane} = \rho_a$.

Gagnon et al. plotted ρ_{plane} and ρ_{chains} versus temperature. From the plot on figure 4.4 it was evident that:

1. $\rho_{plane}(T)$ and $\rho_{chain}(T)$ were about the same magnitude.

2. an obvious difference existed between the temperature dependence of the two resistivities:

ρ_{plane} was linear in T, while ρ_{chain} was quadratic.

CONCLUSION:

The in-plane resistivity (resistivity in the basal plane) of the high quality $YBa_2Cu_cO_{6.9}$ can be summarized as follows: Below 300 K, ρ_{chain} obeys T^2 law in temperature with large extrapolated residual resistivity ($\sim 100\mu\Omega cm$) while the ρ of the planes is perfectly linear with negligible residual resistivity ρ_o. Above 300 K, the chain resistivity increases steeply. This is possibly due to the onset of an additional scattering mechanism probably related to the enhancement of the oxygen mobility [38].

5

EFFECT OF ANISOTROPY: RESULTS AND DISCUSSION

Here, we present our results on the effect of anisotropy on the heat transport along with a review of previous findings. We compare our results with the present theory.

One of the interesting features of $YBa_2Cu_3O_{7-\delta}$ that comes out of unconventional gap pairing is the anisotropy in the transport properties. As it was mentioned earlier in chapter 3, the thermal conductivity is a directional probe that allows us to examine properties along different axes in the crystal.

In our lab, we have measured thermal conductivity of $YBa_2Cu_3O_{6.9}$ along high symmetry directions in the basal plane at both gapless and clean regimes. In order to resolve the anisotropy in the basal plane, the thermal conductivity along the a and b axes was measured separately on five detwinned, high purity crystals. Three of the samples had the heat current directed along the a axis while two of them had the current along the b axis. We extracted the residual linear term at $T \rightarrow 0$. We have found very weak anisotropy in the zero temperature limit of $\kappa(T)$ which is in contrast to the quoted 2.2 ± 0.2 anisotropy in the square of the london penetration depth or plasma frequency. Our results will be explained and discussed later on in this chapter (see section 5.2).

5.1 Motivation for anisotropy studies

Lets us first motivate the anisotropy study by simply looking at the crystal structure of $YBa_2Cu_3O_{6.9}$. The lattice consists of:

- roughly tetragonal CuO_2 planes positioned in the a-b plane and stacked in pairs on top of each other along the c axis, thus forming CuO_2 bilayers,

and

• one dimensional CuO chains that run along the b axis between bilayers.

(See figure 4.1 for the structure of $YBa_2Cu_3O_{7-\delta}$.)

Clearly, two channels (namely planes and chains) of electronic conduction are supported by the crystal structure of $YBa_2Cu_3O_{6.9}$. The charge conduction along the b axis is higher than along the a axis. Therefore, one expects some anisotropy in the transport properties along the two directions.

It has been agreed generally that the most important element in the high temperature $YBa_2Cu_3O_{7-\delta}$ superconductors are two dimensional copper-oxygen planes believed to be responsible for the superconductivity. But although the origin of the superconductivity is attributed to these planes, there are other elements in the unit cell that need to be examined in order to fully understand these systems. Various theoretical investigations of the CuO chains and their role in the gap structure of $YBa_2Cu_3O_{7-\delta}$ have been driven by two experimental results namely, tunneling experiments that give results inconsistent with $d_{x^2-y^2}$ symmetry [45], and measurements of the penetration depth along the a and b directions indicating that superfluid densities along a and b differ only in magnitude and have the same functional form [46]. Some previous experimental work on anisotropy in transport properties in YBCO includes the resistivity measurements along the a and b axes, high temperature thermal conductivity along the a and b directions, the microwave conductivity measurements along the two axes, and the penetration depth along two axes. These findings will be discussed in the following few sections. But still, there is no general agreement on the magnitude nor the origin of the anisotropy in the different transport properties.

5.1.1 London penetration depth

Zhang et al. [46] used cavity perturbation technique to measure the real and imaginary part of the surface impedance. The real part of the surface impedance, called surface resistance R_s, gives information about the real part of the conductivity, σ_1. The real part of conductivity, in turn, is sensitive to the density of states of quasiparticles and scattering rate of thermally excited quasiparticles. On the other hand, the

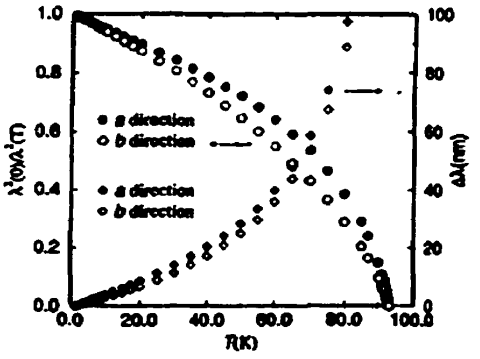

Figure 5.1: The change of penetration depth from 1.3 K, $\Delta\lambda(T) = \lambda(T) - \lambda(1.3K)$ and $\lambda^2(0)/\lambda^2(T)$ in the a and b directions versus the temperature. $\lambda_a(0)$ is taken to be 1600 $\AA$ and $\lambda_b(0)$ was 1030 $\AA$ from infrared data (after [46]).

imaginary part of surface impedance, called surface reactance, is directly related to the penetration depth λ. The temperature dependence of λ, labeled $\Delta\lambda(T)$, in turn, reflects the quasiparticle density of state available for thermal excitations. Therefore, $\Delta\lambda(T)$ probes the gap structure of the superconducting state. Below 25 K, $\Delta\lambda(T)$ is linear in T for high quality YBCO single crystals [47] which suggests a pairing state with nodes in the gap [46].

Zhang et al. found both $\Delta\lambda_a$ and $\Delta\lambda_b$ to be linear in temperature at $T < 15$ K, and the slopes for $\Delta\lambda_a$ and $\Delta\lambda_b$ were $4.7\AA/K$ and $3.6\AA/K$ respectively. Their main finding was that the penetration depth along the a and b directions did not differ much in the form but only in the magnitude. This is clearly seen on figure 5.1 taken from the original paper by Zhang et al. [46].

Basov et al. [48] studied the penetration depth anisotropy using the infrared spectroscopy technique. The far infrared reflectance measurement has an advantage over other techniques used to probe superfluid (such as μSR, dc magnetization or microwave techniques) since it gives the absolute values of each of the diagonal components of the london penetration depth while other techniques give usually the average of at least two components. The superconducting penetration depth can be found from reflectance measurements using Kramers-Kronig (KK) analysis of $R(\omega)$. It gives us a real and imaginary part of the complex conductivity $\sigma(\omega)$.

$$\sigma(\omega) = \sigma_1(\omega) + i\sigma_2(\omega). \tag{5.1}$$

The imaginary part of the conductivity $\sigma_2(\omega)$ is directly related to the square of the frequency dependent london penetration depth λ_L^2 and the square of the plasma frequency of the condensate ω_p^2.

$$\frac{c^2}{\lambda_L^2} = \omega_p^2 = 4\pi\omega\sigma_2(\omega) \tag{5.2}$$

where ω_p^2 is given by $4\pi n_s e^2/m^*$ (n_s is density of the condensate and m^* is the effective mass of the carriers)

Basov et al. [48] found that the superconducting penetration depth in untwinned crystals was smaller in the chain direction than in the direction normal to the chains. They concluded that a large portion of the spectral weight attributed to the chains in the normal state condensed below T_c. The superconductivity in the crystals was not confined only to the planes but extended to the chains as well. They found that the anisotropy in the normal state microwave conductivity and in the penetration depth was close to 2.2 and accounted for these results by the anisotropy in the squared plasma frequency $\omega_{Db}^2/\omega_{Da}^2 = 2.2 \pm 0.2$ (the anisotropy in the n/m^* ratio, the ratio of the carrier density to the effective mass).

Their results showed that the penetration depth along the b direction λ_b, was much smaller compared to the penetration depth along the a direction λ_a. The values they obtained for the crystals were the following. For $YBa_2Cu_4O_8$: $\lambda_b = 800$ $\AA$ and $\lambda_a = 2000$ $\AA$. For the two $YBa_2Cu_3O_{7-\delta}$ crystals, labeled sample 1 and sample 2, the results were the following: sample 1: $\lambda_b = 1000$ $\AA$ and $\lambda_a = 1600$ $\AA$; sample 2: $\lambda_b = 1200$ $\AA$ and $\lambda_a = 1600$ $\AA$.

Using a two-component analysis of the normal state optical conductivity [49], Basov et al. obtained similar anisotropy in the square of the normal state Drude plasma frequency, $\omega_D^2 = 4\pi ne^2/m^*$: $\omega_{Db}^2/\omega_{Da}^2 = [(2.0eV)/(1.3eV)]^2 = 2.2 \pm 0.2$. These results agreed well with the local density approximation band structure calculation [50] that predicted an anisotropy of approximately 2.3 for ω_p^2. The anisotropy in the

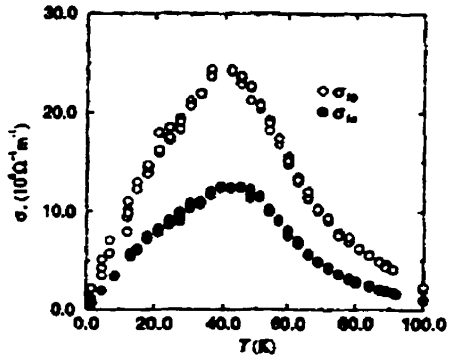

Figure 5.2: The real part of conductivity along a and b directions at 34.8 GHz as a function of the temperature, after[46].

squared london penetration depth $(\lambda_a/\lambda_b)^2 = 2.3$ was very close to the anisotropy in the normal state ω_p^2 [48].

All of the measurements discussed agree with a factor ~ 2.2 anisotropy. There is no indication of anything different occurring in 1-D chains than in the 2-D planes. It appears that all of these anisotropies could be explained by the anisotropy in the mass tensor, n/m^*. But, this turns out to be just a very naive picture that breaks down and cannot fully account for the anisotropy in the transport properties. This is specifically revealed by low temperature $\kappa(T)$ measurements done in our lab and discussed later in this chapter.

5.1.2 *Charge and heat transport: high temperatures*

At a temperature just below T_c, Zhang et al. [46] observed that σ_{1b}, the real part of the conductivity along the b direction, was about 2.4 times as large as σ_{1a}. This anisotropy is of the same magnitude as the one seen in the normal state. At low temperatures, both curves of σ_{1a} and σ_{1b} versus temperature were linear in temperature. σ_{1b} was observed to be about a factor of 2 larger than σ_{1a} throughout the whole temperature range from 1.3 to 100 K. A large peak in σ_1 below T_c in both directions was attributed to the rapid drop in quasiparticle life-time (τ) below T_c. The temperature dependence of the real part of conductivity from Zhang et al. is shown on figure 5.2.

Basov et al.[48] found that the anisotropy of the low frequency limit of σ_1 at 95 Kelvin was $\sigma_b/\sigma_a = 2$. Using a classical skin effect in the normal state, the surface

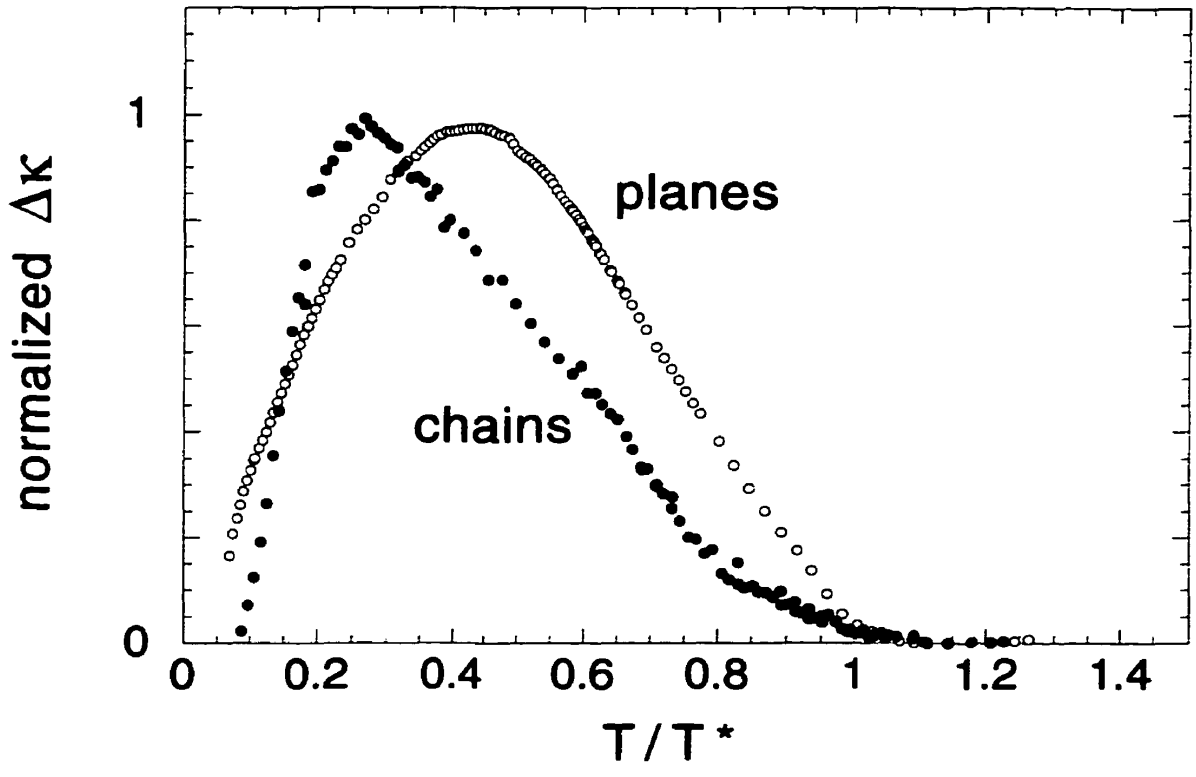

Figure 5.3: Comparison of plane and chain thermal conductivities in $YBa_2Cu_3O_{6.9}$ normalized to 1 after subtracting a constant offset. Normalized $\Delta\kappa$ is plotted as a function of T/T^* where $T^* = T_c$ for planes and T_{onset} for chains after [37].

resistance measurement on a similar crystal yielded a slightly higher anisotropy of 2.3.

Again, as in the case of λ_L measurements, there is no indication of any qualitative difference between the electrical conduction along the two crystalline directions. The only difference found is the quantitative difference between charge transport along the a and b axes.

The high temperature thermal conductivity measurements on $YBa_2Cu_3O_{7-\delta}$ crystals by Gagnon et al. [37] showed a definite difference between transport along the a and b axes. Their study was motivated by two previous findings that were in contradiction with each other. The first set of experimental findings was the previous tunneling data [45]. It was suggestive of independently conducting planes and chains. The second set of experimental evidences were the penetration depth measurements [46]. They were indicative of similar nodal structures in planes and chains; λ_a and λ_b

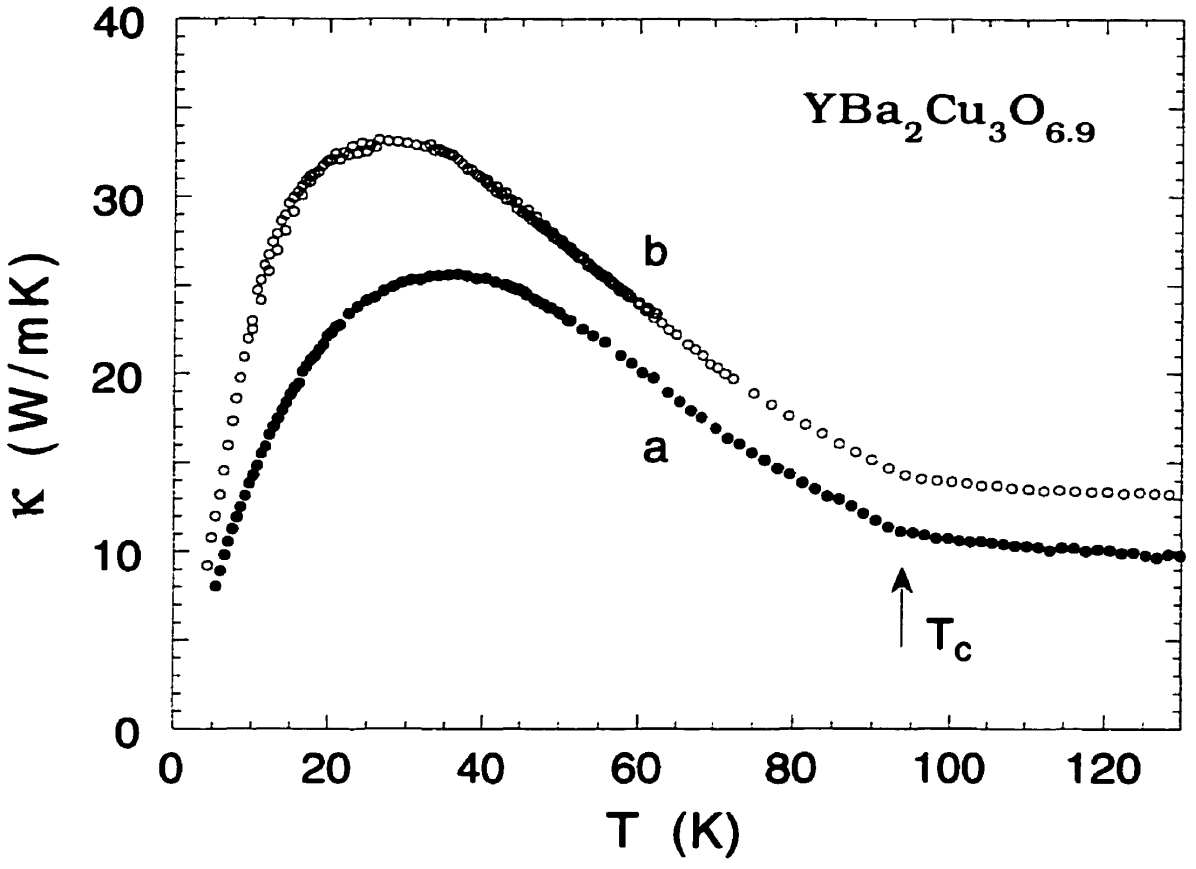

Figure 5.4: The temperature dependence of the thermal conductivity in the a and b directions. The arrow shows the resistively determined T_c after [37].

differed only in magnitude but not in functional form suggesting that one needed to understand the plane-chain coupling below T_c.

Gagnon et al. measured $\kappa(T)$ along two crystalline directions (a and b) of detwinned $YBa_2Cu_3O_{6.9}$ crystals from 5 K up to 150 K thereby using $\kappa(T)$ to probe the behavior of the CuO chains. In the simplest approach, one assumes that the phonon spectrum is roughly isotropic in the a-b plane and attributes most of the anisotropy in κ to chain electrons. The thermal conductivity along the a axis is attributed to the planes κ_a, and the thermal conductivity along the b axis κ_b is viewed as a sum of κ_{chain} and κ_{plane}. Then, κ_{chain} is simply given by the difference in conductivities along the two crystalline directions, $\kappa_{chain} = \kappa_b - \kappa_a$. Figure 5.3 shows the normalized thermal conductivity from the planes compared to the one from the chains.

Conduction along the b axis was higher than along the a axis throughout the whole temperature range, which indicated that the increase was at least partially due to additional electrons in the chains. Gagnon et al. observed that while the normal state anisotropy was roughly constant ($\kappa_b - \kappa_a \sim 3.0$ to $3.5\ W/mK$), the anisotropy ceased to be constant as the temperature was reduced below 60 K and was significantly decreased at lower temperatures. Both κ_a and κ_b showed a clear peak below T_c (where T_c was 93.8 K) but there was a clear addition to $\kappa_b(T)$ below T_c at about $T_{onset} =$ 55 K. The well-known increase in $\kappa(T)$ below the critical temperature is a general characteristic of all high T_c superconductors [25]. This increase is explained by fact that as temperature decreases below the critical temperature, electrons condense into Cooper pairs and there are less normal electrons left to scatter heat carriers; hence, the mean free path of the heat carriers increases and the thermal conductivity increases as well. This is valid as long as the main source of scattering for heat carriers comes from electrons. The threefold increase in $\kappa_b - \kappa_a$, which Gagnon et al. called "chain" conductivity taking place between 55 K and 15 K, resembled the increase in plane thermal conductivity between 90 K and 30 K. The chain carriers experienced a sudden increase in mean free path below $T_{onset} \approx 55\ K$, which pointed to the onset of pair condensation or increase in superfluid density in chains at 55 K. This is shown on figure 5.4. It is clear by now that one can use $\kappa(T)$ to detect changes in superfluid density not only at T_c but also at lower temperatures. This works as long as electrons are the major source of scattering for the carriers of heat.

CONCLUSION on the anisotropy of $\kappa(T)$ at high temperatures:

Gagnon et al. [37] found a qualitatively similar behavior for κ_a and κ_{chain}, as well as the absence of any anomaly in κ_{chain} at T_c (see figure 5.3). These observations suggested a simple scenario where planes and chains were largely decoupled and each electronic system underwent its own superconducting transition. This agreed with the single electron tunneling model's predictions [51, 52]. The proposition of Gagnon et al. at that time was phenomenological. Therefore, there is a clear need for a better understanding of underlying heat carriers and scattering mechanisms. Certainly, their

study shows that a naive treatment of anisotropy in terms of plasma frequency or london penetration depth is inadequate.

The different results from σ and κ measurements call for a closer look at the anisotropy. This is best done at low temperatures as we shell see in the following discussion.

5.2 *Heat conduction: low temperatures*

We have measured the low temperature thermal conductivity in the gapless regime, $T < T_c/100$, of five high quality untwinned single crystals of $YBa_2Cu_3O_{6.9}$ along both high symmetry directions in the basal plane. The temperature range of the experiments was 70 mK to 1 K. For three crystals the current was along the a axis ($J \parallel a$) and for the other two crystals, the current was applied parallel to the b axis ($J \parallel b$).

Since other techniques that aimed at the anisotropy measurements of the transport properties didn't allow for the resolution of the question, we have decided to use a straight forward measurement that probes the anisotropy without much complications in the analysis of the data. The thermal conductivity measurement were done in the limit of low temperatures where neither the phonons nor the inelastic scattering complicated the interpretation of the results and where the impurity scattering dominated. At low temperatures, phonons are easily separated from electrons. The temperature dependence of κ_{ph} is given by well-known asymptotic T^3 behavior. Also at low T, inelastic scattering is negligible [53].

As discussed in the review of thermal conductivity (see section 2.4.2), the phononic term in the thermal conductivity at low temperatures, where scattering of phonons is limited by crystalline boundaries (the mean free path becomes limited by the crystal boundaries), approaches its well defined asymptotic T^3 dependence given by Debye expression:

$$\kappa = \frac{1}{3}\beta < v_{ph} > \Lambda_o T^3. \tag{5.3}$$

Table 5.1: Specifications of the five crystals used for the anisotropy study.

Crystal	T_c K	κ_o/T $\frac{mW}{cmK^2}$
a-1	93.6	0.15 ± 0.01
a-2	93.7	0.14 ± 0.04
a-3	93.3	0.12 ± 0.01
b-1	93.3	0.17 ± 0.03
b-2	93.4	0.18 ± 0.01

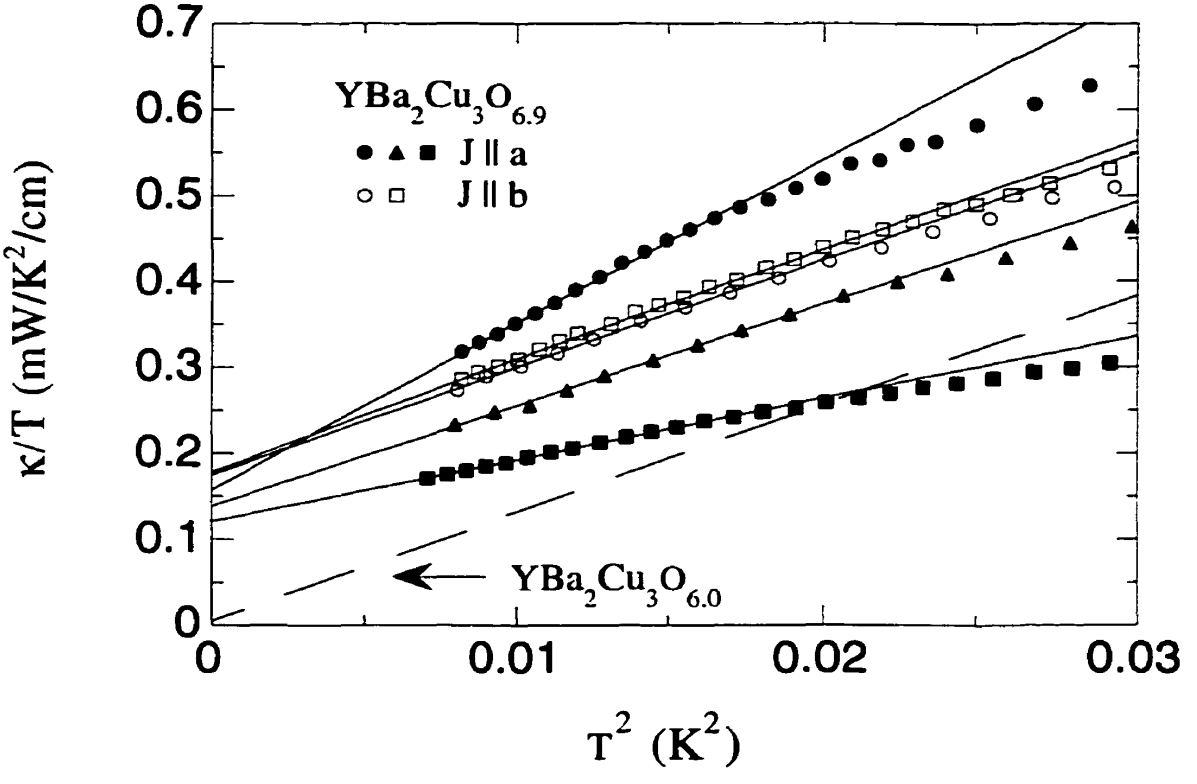

Figure 5.5: Low temperature thermal conductivity, κ/T versus T^2 for five $YBa_2Cu_3O_{6.9}$ crystals used for study of anisotropy: a-1 (solid circles), a-2 (solid triangles), a-3 (solid squares), b-1 (open circles), b-2 (open squares). For three crystals, current was parallel to a axis, $J \parallel a$ and for remaining two, $J \parallel b$. The solid lines are linear fits to the data for $T^2 < 0.015K^2$. The dashed curve shows measurement on deoxygenated $YBa_2Cu_3O_{6.0}$ crystal.

where β is the phonon specific heat coefficient, $< v_{ph} >$ is the average of the acoustic sound velocities, and Λ_o is the maximum mean free path independent of

temperature and limited by the crystal boundaries.

Only by going quite low in temperature, can one extract a meaningful phononic term from the measurements. This is verified by comparing the theoretical Debye prediction using known values for the various parameters in the above Debye expression and the values obtained from the linear fit of the data. It was shown by Taillefer et al. that our data agrees well with the theoretical values [8].

The electronic term is linear in temperature and the phononic term is cubic in temperature at low temperature; therefore the total thermal conductivity can be written as:

$$\kappa = aT + bT^3 \tag{5.4}$$

We plot κ/T versus T^2 such that the fit to the low temperature data ($T < 150\ mK$) is linear and the slope of the fit gives the magnitude of the phononic term while the intercept at $T = 0$ gives the magnitude of the residual normal fluid due to quasiparticles.

5.2.1 Results

The results of our measurements are shown in table 5.1 and in figure 5.5. Firstly, all three curves for the a axis conduction, and both curves for b axis respectively, fall close to each other at the zero temperature limit. The intercept of the lines represents the residual linear term. This clear residual linear term is entirely attributable to quasiparticles at zero temperature [8]. This is confirmed by the fact that fully deoxygenated insulating $YBa_2Cu_3O_{6.0}$ has a zero intercept (represented by the dashed line on figure 5.5).

The slope of the linear fit of $\kappa(T)/T$ versus T^2 is mostly due to phonons. This is supported by the fact that the insulating sample, where there are only phonons as heat carriers, shows a similar increase in conductivity with temperature. The slope could also be in part due to higher temperature corrections to κ as calculated by Graf et al. (see section 2.4.1) [22] but they are probably very small.

The values for the zero temperature $\kappa(T)$ obtained from the linear fit are:

$$\frac{\kappa_{o,a}}{T} = 0.14 \pm 0.03 \; mWK^{-1}cm^{-1} \; for \; J \parallel a \tag{5.5}$$

and

$$\frac{\kappa_{o,b}}{T} = 0.18 \pm 0.03 \; mWK^{-1}cm^{-1} \; for \; J \parallel b \tag{5.6}$$

leading to an anisotropy:

$$\frac{\kappa_{o,b}}{\kappa_{o,a}} = 1.3 \pm 0.3. \tag{5.7}$$

This is *a much weaker* (perhaps *even negligible*) anisotropy than the one found in the normal state resistivity ($\rho_a/\rho_b(250K) = 2.2 \pm 0.2$) [38], the normal state microwave conductivity ($\sigma_{1,b}/\sigma_{1,a}(95K) = 2$) [48] or the square of the london penetration depth ($\lambda_a^2/\lambda_b^2 = 1.7$) [46].

Zhang et al. [46] obtained the residual microwave conductivity by fitting their low temperature data to a straight line: $\sigma_{1,a}(T \rightarrow 0) \approx (0.45 \pm 0.15) \times 10^6 \Omega^{-1}m^{-1}$ and $\sigma_{1,b}(T \rightarrow 0) \approx (0.7 \pm 0.2) \times 10^6 \Omega^{-1}m^{-1}$ giving an anisotropy $\sigma_{1,b}/\sigma_{1,a} = 1.6$. But the uncertainty here is quite large, of the order of 50 %. Our results are consistent with their data. By simply multiplying their values of σ by the Lorenz number L_o, we get values for κ: 0.11 mW/cmK and 0.17 mW/cmK for the a and b axes respectively. They are compatible with our measured values.

The total uncertainty of 20 % on our data comes from two main sources: uncertainty on geometric factors (up to 10%) and uncertainty in linear fits of the data (T=0 extrapolation). The anisotropy ratio bears in itself only the uncertainty due to the fit because it depends directly on our estimate of the resistivity ratio at room temperature which is taken to be 2.3. In this sense, the uncertainty in the geometric factor is minimized and can even be eliminated from the ratio.

5.2.2 Comparison with the theory for a tetragonal superconductor with $d_{x^2-y^2}$ symmetry

It is instructive to make the comparison with the theory for a tetragonal superconductor with $d_{x^2-y^2}$ symmetry. First, we compare our results for properties along the a axis with the theoretical predictions and show that indeed there is agreement with the theory. Then, we argue that taking an anisotropy of 2.2 ± 0.2 in n/m^* (or ω_p^2) as being the only source of anisotropy leads to an inconsistency with the theory for $J \parallel b$. We conclude that the weak anisotropy can not simply be explained in terms of an anisotropy in the ratio of carrier density to effective mass (or in plasma frequency squared). Here, we take the gap function to be: $\Delta = \Delta_o \cos(2\phi)$.

Above the gapless regime, in the clean limit, the temperature dependence of the in-plane London penetration depth is linear and given by [54]:

$$\frac{\Delta\lambda_{\parallel}(T)}{T} = \lambda_{\parallel}(0)\frac{2k_B ln2}{S} \propto \frac{1}{\omega_p S} \tag{5.8}$$

where $S = |d\Delta(\phi)/d\phi|$ is the local slope of the gap at a node. For a d-wave gap, the nodes are at $\phi = 45^o$ and $S = 2\Delta_o$. $\lambda_{\parallel}(0) = c/\omega_p$ is the zero temperature value of the penetration depth; here, c is the speed of light and ω_p is the plasma frequency [54]. Therefore, the temperature dependent London penetration depth is inversely proportional to the product of ω_p and S.

In the T=0 limit, heat transport in the basal plane is expected to be universal as a result of perfect compensation between the increase in density of quasiparticles and the concomitant reduction in the mean free path with increasing impurity scattering [9, 8]. In the zero temperature limit, $\kappa_{\parallel}/T$ is then given by:

$$\frac{\kappa_{oo}}{T} = L_o\sigma_{oo} \rightarrow \frac{L_o ne^2}{m^*}\frac{2\hbar}{\pi S} = \frac{\hbar k_B^2\omega_p^2}{6e^2}\frac{1}{S} \propto \frac{\omega_p^2}{S} \tag{5.9}$$

where σ_{oo} is the charge conductivity in the universal limit and $L_s = (\pi^2/3)(k_B/e)^2$ is the Sommerfeld value of the Lorenz number [22, 8]. Again, as in the case of the penetration depth, the thermal conductivity is related to the same two parameters, ω_p and S.

We use these theoretical expressions and calculate the values for $\Delta\lambda_{||}/T$ and $\kappa_{||}/T$. First, we apply the expressions to the a axis properties.

We obtain a perfect agreement with the experimentally determined values,

$$\frac{\Delta\lambda_a}{T} = 4.7\ \frac{\mathring{A}}{K} \tag{5.10}$$

[46]

and

$$\frac{\kappa_{o,a}}{T} = 0.14\ \frac{mW}{cmK} \tag{5.11}$$

respectively, using $S = 2\Delta_o$ and the weak coupling value for $\Delta_o = 2.15 k_b T_{oc}$ (where T_{oc} is value of T_c in a clean limit) if the plasma frequency is set to 1.5 eV. This value for ω_p is not far from the value 1.3 eV obtained from far infrared reflectance measurements [48]. Not only do we have an excellent theoretical understanding of $\lambda(T)$ and $\kappa(T)$ but we have also established the excellent quantitative agreement for the properties along the a axis in two different regimes (clean and gapless).

If we repeat the same procedure for the b axis properties, we do not obtain the same consistency as for the case of a axis properties. In order to obtain agreement between the theoretical expressions and the experimental values, which are:

$$\frac{\Delta\lambda_b}{T} = 3.6\ \frac{\mathring{A}}{K} \tag{5.12}$$

and

$$\frac{\kappa_{o,b}}{T} = 0.18\ \frac{mW}{cmK} \tag{5.13}$$

we need to use $\omega_p = 2.0eV$ for $\Delta\lambda_b/T$ and $\omega_p = 1.7eV$ for $\kappa_{o,b}/T$. The fact that there is no consistency in the value of ω_p from the two separate estimates is an indication that the anisotropy can not simply be explained by an anisotropy in the plasma frequency. Furthermore, neither estimates obtained for ω_p give an anisotropy as large as 2.2 in ω_p^2.

5.2.3 *Discussion and possible explanations*

In summary, here are the values of the anisotropy obtained from the various experiments:

- The plasma frequency anisotropy from far infrared reflectance measurement [48] was found to be:

$$(\omega_{p,b}/\omega_{p,a})^2 = (2.0/1.3)^2 = 1.54^2 = 2.2. \tag{5.14}$$

- From the temperature dependent London penetration depth measured by Zhang et al. [46], we have an anisotropy of

$$(\Delta\lambda_a/\Delta\lambda_b)^2 = (4.7/3.6)^2 = 1.31^2 = 1.7. \tag{5.15}$$

(In a linear node, one expects $\Delta\lambda \sim \lambda$ and the λ_L and ω_p to be related by $c^2/\lambda_L^2 = \omega_p^2$).

- From the low temperature thermal conductivity, we obtain the much weaker anisotropy of:

$$\kappa_{o,b}/\kappa_{o,a} = 1.3 \pm 0.3 \tag{5.16}$$

which may even be negligible.

It is obvious that there is no general agreement between the values on the anisotropy in the transport properties in the basal plane of $YBa_2Cu_3O_{7-\delta}$. There are some other factors beside n/m^* that contribute to the anisotropy.

W. C. Wu et al. have suggested that small anisotropy could come from the d wave pairing with small s-wave admixture. Could it be that the gap anisotropy is neglected in previous treatments of the anisotropy? For such a pairing $(d_{x^2-y^2} + s)$, they found the anisotropic features in the low-temperature microwave conductivity and thermal conductivity. In this model, the Fermi surface would be distorted from the tetragonality due to the presence of the chains and the nodes would be shifted off the diagonals. But this theory does not provide agreement between the different

experimental results, since the κ fit requires a large s component, while this is in contrast with the λ data [55].

Could it be that the chain gap is nodeless and that the nodes in the chains do not intersect the Fermi surface? There would not be zero energy quasiparticles in the chains since they would be gapped, leading to no transport along the chains at $T \rightarrow 0$. This would bring down the value on the anisotropy ratio to what it is strictly in the CuO_2 planes (slightly orthorhombic) [56].

It is possible that conduction in 1D chains is not universal. Since chains are one dimensional system and the passage of the heat carriers is limited to the one dimensional path, it could be that the scattering rate in chains Γ_{ch} becomes very large for a certain critical impurity concentration such that conduction in chains is greatly diminished or even stops [57].

A last possibility is that localization occurs in the 1D chains, along the lines of Lee's proposal [9].

6

EFFECT OF A MAGNETIC FIELD: RESULTS AND DISCUSSION

As pointed out earlier, one of the main features of superconductors beside their perfect electric conductivity is their distinctive magnetic behavior. When cooled below T_c, a superconductor becomes a perfect diamagnet, meaning it expels the applied magnetic field that was inside the material in its normal state before it became superconducting.

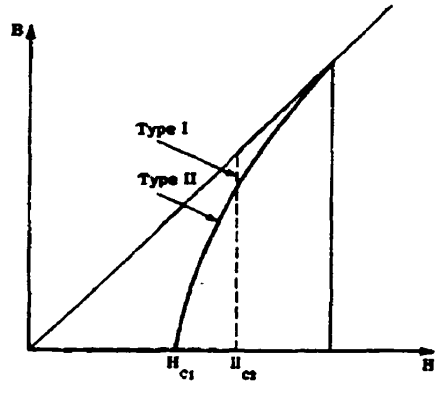

Figure 6.1: The induction as a function of the applied field for Type I and Type II superconductors, after [3].

When high enough fields are applied, the superconductivity starts to break down. In the case of the unconventional superconductors, which are called Type II superconductors, we have two critical fields labeled H_{c1} and H_{c2}. When the first field is reached, the field starts to penetrate inside the material in the form of tubes of flux, known as vortices. Vortices are arranged in an hexagonal lattice and their cores are in the normal state (the gap goes to zero there), while outside the core of the vortex material is still in the superconducting state (with the full gap). When the upper critical field H_{c2} is achieved, superconductivity is completely destroyed and the

material becomes non-superconducting. In between the lower and the upper critical fields, the material is in the mixed state. The mixed state in Type II superconductors was first predicted by Abrikosov in 1957. He showed that the field should penetrate inside the superconductor in the form of vortices each carrying one quantum of flux: $\phi_o = \frac{hc}{2e} = 2.07 \times 10^{-7}\ Gauss\ cm^2$. Figure 6.1 shows the response of the two types of superconductors to an applied magnetic field.

Since YBCO is a Type II superconductor, we will be largely interested in the magnetic properties of these superconductors. However, we will draw some comparison between the conventional and unconventional superconductors. We will compare *s*-wave and *d*-wave superconductors.

6.1 *Type II superconductors*

It has been realized a long time ago, when the superconducting theories started to emerge, that there are two types of superconductors, namely Type I superconductors and Type II or London superconductors. It is important to distinguish between the two because their properties differ. The Ginzburg-Landau theory provides us with the useful ratio labeled κ that gives the criteria for distinguishing between the two.

Ginzburg-Landau theory is the phenomenological theory proposed by Ginzburg and Landau in 1950 before appearance of BCS microscopic theory. It concentrates on superconducting electrons rather than on excitations. The central physical quantity which Ginzburg and Landau proposed was complex pseudowave function ψ; it is an order parameter which describes the superconducting electrons. The biggest success of the theory was the explanation of the intermediate state of superconductor where normal and superconducting states coexist in the presence of a field, $H \approx H_c$. Gor'kov showed that the Ginzburg-Landau theory was a limiting case of the BCS theory valid near T_c in which ψ was directly proportional to the gap parameter, Δ [2].

In Ginzburg-Landau theory, the coherence length is given by:

$$\xi(T) = \frac{\hbar}{|2m^*\alpha(T)|^{1/2}} \tag{6.1}$$

It is the distance over which $\psi(r)$, the order parameter, can vary without significant increase in energy. In the pure superconductor at $T \ll T_c$, $\xi(T) \approx \xi_o$ [2]. Here ξ_o is the Pippard temperature independent coherence length. The free energy is expressed through the dimensionless parameter κ. It is the ratio of two characteristics lengths, penetration depth λ and coherence length ξ.

$$\kappa = \frac{\lambda}{\xi} \tag{6.2}$$

Near T_c, $\xi(T)$ diverges as $(T_c - T)^{-1/2}$ because α vanishes as $(T_c - T)$. Because λ also diverges as $(T_c - T)^{1/2}$ near T_c, ratio κ is approximately independent of temperature. It is convenient to use κ to distinguish between two types of superconductors. When $\kappa < 1/\sqrt{2}$ the material is Type I and when $\kappa > 1/\sqrt{2}$ the material is Type II superconductor.

The characteristic which will be used to discern among the two types of superconductors is the surface energy. It can be both positive and negative, and depending on the sign, it will be favorable to reduce the boundary surface between the normal metal and superconductor or to increase it. In addition, we will use the coherence length, as given by the BCS theory:

$$\xi = \frac{\hbar v_f}{\pi \Delta} \tag{6.3}$$

in the discussion of the two types of superconductors.

If κ is small, meaning that $\xi > \lambda$, then the coherence length is long and the penetration depth is small. These are so called Type I superconductors. For example, for the typical metal superconductor λ_L is small ($\sim$ 300 $\mathring{A}$) and v_f is large ($\sim 10^8$ cm/sec) leading to large coherence length ($\xi_o \sim 10^4$ $\mathring{A}$ for aluminum) [3]. The coherence length, in the G-L theory, is viewed as the distance over which the wave function can vary without a great increase in energy. Since here ξ is large, it means that the order parameter varies slowly from the value 1 in the superconducting region toward the value 0 near the boundary with the normal region. On the other hand, the field drops rapidly inside the superconducting region as λ is short. There will be

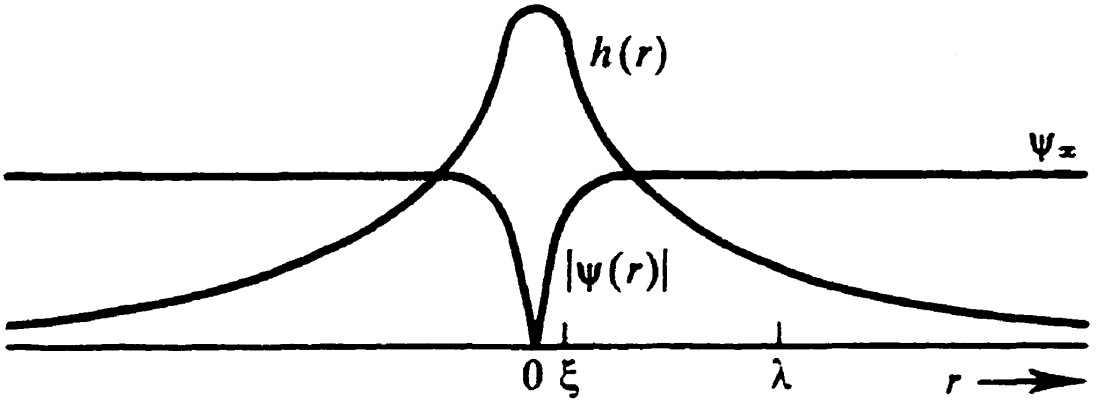

Figure 6.2: Structure of an isolated Abrikosov vortex in a material with $\kappa \approx 8$. The maximum value of $h(r)$ is approximately $2H_{c1}$, after [2].

a region near the interface where both order parameter and field almost vanish. In this region, the pairing (i.e. the condensation energy) vanishes but the field does not penetrate here. There is no compensation of the screening of the field by the gain in energy due to pairing. This scenario leads to a positive surface energy which stabilizes the domain pattern into the intermediate state, where the size of the domain is in between the macroscopic sample size and ξ [2, 12]. When H_c is reached, the sample is not superconducting any more as the field has penetrated uniformly across the sample.

If κ is large, meaning ξ is small and λ is large, the superconductor is a Type II or London superconductor. λ_L is large and typically of the order of 2000 $\mathring{A}$, v_f is small ($\sim 10^6$ cm/sec) and the transition temperature T_c is high, leading to small ξ_o [3]. Here, the surface energy is negative. This means that the energy of the system can be lowered by increasing the boundary surface between superconducting and normal regions. This is effectively done if the field penetrates inside the superconducting region in the form of vortices, which are flux quanta. Inside the vortex, the material is in normal state and these states are bound and quantized. Outside the vortex, the material is in the superconducting state. Figure 6.2 shows the diagram of the variation of the order parameter ψ and the flux density h in a domain wall for a Type II superconductor.

Using expressions for the coherence length, $\xi_o = \hbar v_f/\pi\Delta_o$ and for the zero temperature london penetration depth $\lambda(0) = c/\omega_p$ along with the values for $v_f \sim 10^7\ cm/s$ [9], $\Delta_o = 2.15\ k_B T_c$ [8] and $\hbar\omega_p = 1.3\ eV$ [48], we get the following values for YBCO:

$$\xi_o = 12.2\ \mathring{A} \tag{6.4}$$

and

$$\lambda(0) = 1519\ \mathring{A} \tag{6.5}$$

Clearly, $\lambda \gg \xi_o$ showing that YBCO is a Type II superconductors.

6.2 *Heat transport: conventional superconductors*

In conventional superconductors, the coherence length is a few thousands $\mathring{A}$, contrary to unconventional superconductors where ξ is minute and of the order of 10 $\mathring{A}$. Here, the separation of two vortices is approximately given by: $2R \sim 2\xi_o\sqrt{H_{c2}/H}$. In conventional superconductors, the density of states at low energies is dominated by the contribution from the bound states inside the vortex cores. With the applied magnetic field, vortices are created; but the bound quasiparticle states inside the cores are spatially localized and hence can not easily participate in the low-temperature transport. At the same time, the states outside the cores remain fully gapped, and their contribution to the thermal conductivity is exponentially suppressed. Therefore, while the vortices do not introduce the extra heat carriers, they are effective as scatterers of the carriers. As the vortex density increases with the magnetic field, the scattering of the quasiparticles by vortices increases which shortens the quasiparticle mean free path. This results in the initial suppression of the thermal conductivity $\kappa(T)$ in the magnetic field [23].

We present the findings of Lowell et al. [15] who performed an extensive study of the thermal conductivity of Type II superconductor in the magnetic field. They examined the response of $\kappa(H)$ in pure, i.e clean ($\ell \gg \xi_o$), dilute and dirty limits ($\ell < \xi_o$). The samples were niobium (Nb), NbMo, and NbTa - clean, dilute and dirty

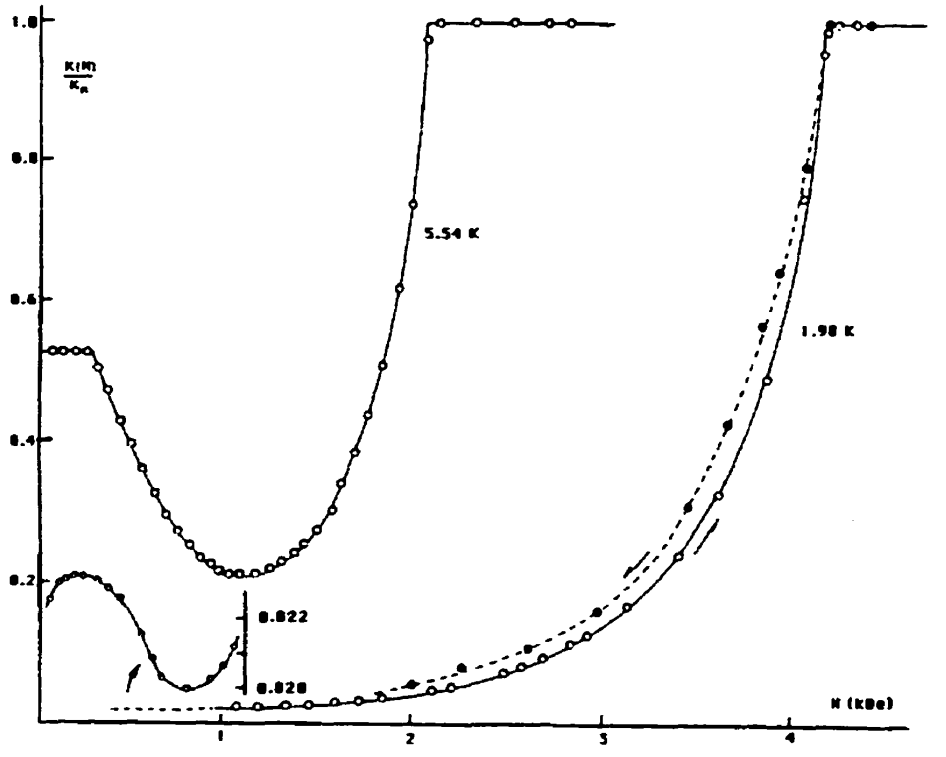

Figure 6.3: Thermal conductivity of niobium as a function of field for two different temperatures. The dotted curve shows data taken in decreasing field. The magnetic field is perpendicular to the sample plane after [15].

superconductors respectively. We focus on their treatment of pure niobium because it serves well for a contrasting comparison with our *d*-wave system.

In a pure limit (Nb) and without the magnetic field, according to Lowell et al. [15], the normal state thermal conductivity varied linearly with temperature suggesting that κ was mostly due to electrons and was limited by impurity scattering. The thermal conductivity in the superconducting state was found to be a monotonically decreasing function of temperature. The thermal conductivity due to electrons in the superconducting state dominated the total thermal conductivity at the temperatures above 2.5 K. At $T < 2.5$ K the thermal conductivity due to phonons became significant. All of these features are very well established by now [15]. For example, see section 2.3.2.

At $H \ll H_{c2}$ (low field) where $\ell_o \gg \xi_o$ (pure limit), κ was rapidly decreasing with the increasing field up to some minimum value, κ_{min}. This was the result of

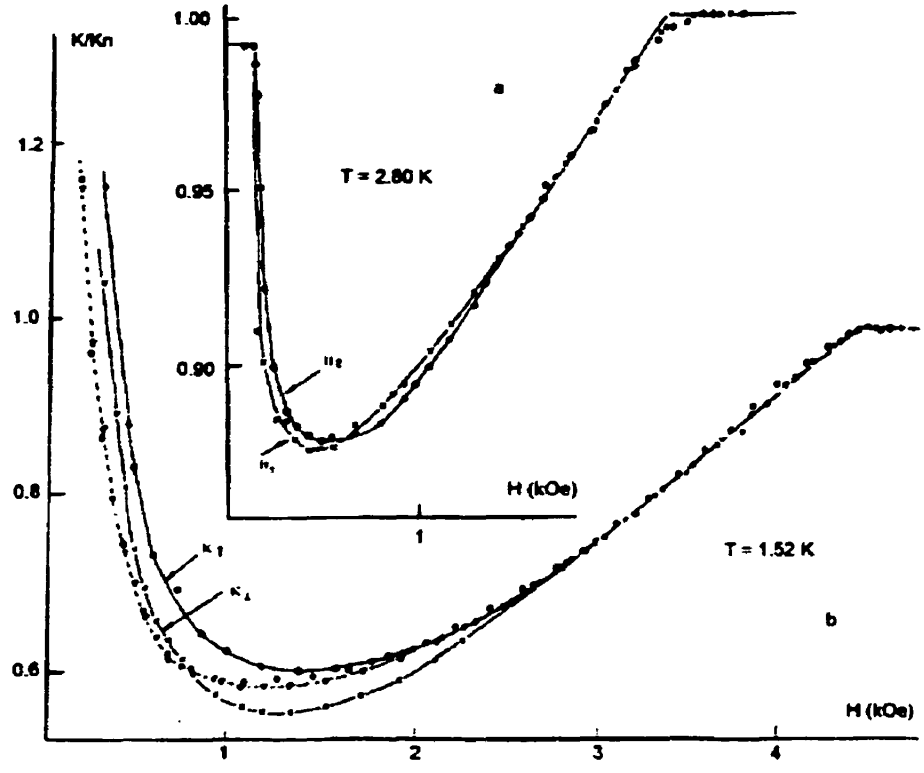

Figure 6.4: Field dependence of the thermal conductivity on $Nb_{80}Mo_{20}$ measured with the field either parallel ($\kappa_{||}$) or perpendicular ($\kappa_{\perp}$) to the heat flow direction (but always parallel to the plane of the sample) at two different temperatures: 2.90 K (a), and 1.52 K (b). The dotted line is the thermal conductivity in the field parallel to the plane of the sample and to the heat-flow direction after [15].

electrons being scattered by vortices (fluxoids). The thermal resistivity ($W \sim 1/\kappa$) in a "dilute" system of fluxoids is given by:

$$W = W_o \left(1 + \frac{B\ell_o a}{\phi_o}\right). \tag{6.6}$$

where W_o is the thermal resistivity in the superconducting state at $B = 0$, ℓ_o is the electronic mean free path, ϕ_o is a flux quantum, and a is the effective diameter of the fluxoids for the scattering of the electrons. Lowell et al. found that in niobium, $a \simeq 5 \times 10^{-6}$ cm and approximately independent of temperature. The electronic mean free path in the pure limit (Nb) was found to be $\ell = 2 \times 10^{-4}$ cm and $\xi/\ell = 25$. Therefore, it was concluded that excitations associated with the fluxoid cores did not contribute appreciably to the heat transport in low fields. It was rather the

scattering of electrons from the vortices that was responsible for the increase in κ. Excitations were bounded to the vortex cores and all H dependence was due to the vortex scattering.

At higher fields and near H_{c2}, κ rapidly increased to its normal state value. In this case, it was not the scattering of the vortices that was important, but it was a pair breaking effect (single particle excitations associated with fluxoids) that were significant in determining the heat transport [15]. Results of Lowell et al. are shown on figure 6.3. Niobium obeyed Maki's prediction for thermal conductivity of a *pure* Type II superconductor in the gapless regime (i.e. in a fields close to H_{c2}) in a magnetic field [58]. That is:

$$\kappa(H) - \kappa_n = (H_{c2} - H)^{1/2}\alpha(T) \tag{6.7}$$

In a pure Type II superconductor, the electronic mean free path is much bigger than the coherence length, $\ell/\xi_o \gg 1$. For such a system, Maki arrived at the following theoretical results. The thermal conductivity $\kappa(T)$ dropped rapidly in the superconducting region as $(H_{c2} - H_o)^{1/2}$, where H_o is the external field. The dynamic properties of a pure Type II superconductor differed considerably from those in a dirty Type II superconductor. The thermal conductivity in field was strongly isotropic. The conduction was maximal when the heat flowed along the fluxoid direction. The angular dependence of the thermal conductivity in a field showed that at $T \ll T_c$, $\kappa_{s\perp} \geq \kappa_{s\|}$; the transport of heat was higher in the transverse than in the direction parallel to the fluxoid. At higher temperatures, $T \sim T_c$ or less than T_c, the conductivity along the fluxoid direction was greater than in the transverse direction. Therefore, at higher temperatures, the anisotropy was inverted from the one at lower temperatures [58].

The early theory for the response of κ to the field in a dirty superconductor was derived by Caroli and Cyrot in 1965 [59]. They found that the thermal conductivity in fields close to H_{c2} varied linearly with H, in contrast to the previous average-gap model by Dubeck et al.[60, 61] that failed to predict such kind of behavior. But

at lower fields, both models were correct in predicting a linear behavior. Results of Lowell et al. [15] for a dirty sample $Nb_{80}Mo_{20}$ are shown on figure 6.4. At higher fields, for a dirty superconductor, Lowell found that $\kappa(T)$ increases linearly with magnetic field. This finding was in agreement with Caroli-Cyrot theory [59]. But, the linear behavior extended well below H_{c2} which couldn't be explained by the Caroli-Cyrot theory. The angular dependence of the thermal conductivity $\kappa(\theta)$ was much weaker than in a pure sample. At lower fields, some anisotropy due to the electronic term was observed, while at very low fields the anisotropy was attributed to the phononic term.

6.3 *Heat transport: unconventional superconductors*

The fact that in the *d*-wave superconductors the density of states and the entropy are dominated by the contribution from the extended quasiparticles states rather than by the bound states associated with the vortex cores was first pointed out by Volovik in 1993 [62]. In a *d*-wave superconductor, the density of states is linear in energy, $N(E) \sim E$. When a magnetic field is applied, it creates vortices with a superfluid flow around them. In this new reference frame, the quasiparticle energy is Doppler shifted on average from energy $E \rightarrow E \pm \frac{h}{e}\vec{v_f} \cdot \vec{A}$. This average shift in energy (so called the field energy) E_H is given by:

$$E_H = \frac{h}{e}\vec{v_f} \cdot \vec{A} \tag{6.8}$$

where $\vec{A}$ is the vector potential. Using the expression for the magnetic flux Φ_o:

$$\phi_o = \oint \vec{A} \cdot d\vec{\ell} \tag{6.9}$$

where the surface integral is taken over one vortex, one obtains that the vector potential $\vec{A}$ can be written as: $\vec{A} = \frac{\Phi_o}{2\pi r}\hat{\theta}$. Then, by calculating the appropriate integrals over the volume and knowing that by definition $H = \frac{\phi_o}{4R^2}$, the average energy E_H can be calculated in terms of the Fermi velocity v_f and the magnetic field H. Here, R is the vortex radius. It turns out that E_H scales with $\sqrt{H}$ (also see

equation 6.10). At $T = 0$, the quasiparticle energy is shifted roughly from $0 \rightarrow E_H$. Therefore, we can write: $N(0) \rightarrow N(E_H)$. Also, because the DOS is linear in energy and because E_H scales as $\sqrt{H}$, it follows that $N(E_H) \sim E_H \sim \sqrt{H}$. This causes the H dependence of all quasiparticle properties (e.g. C/T and κ/T) because all of them are dependent on the DOS. The density of states near the node is increased as more quasiparticles around the nodes are Doppler shifted as field increases; there are more carriers and κ increases as well. Furthermore, each carrier is still subject to the scattering rate from impurities, Γ. As a result, an increase in κ will be the largest in pure samples where scattering rate from impurities is the lowest.

Contrary to conventional superconductor, the coherence length ξ of YBCO is much smaller than the mean free path of the heat carriers. Vortices are far apart from each other and can be treated as a point objects for all practical purposes. Here, the vortex scattering is certainly much less important than in conventional superconductors. Unlike in the *s*-wave superconductors, in the *d*-wave superconductors, there are nodes in the gap that lead to the existence of quasiparticles at zero temperature and at zero field. This residual normal fluid is the result of impurity scattering. At low temperatures, as the field is increased, it is not the scattering of the vortices that is dominant but it is the impurities that still largely determine the scattering rate and thus the mean free path of the heat carriers.

Lately, increasing interest in the studies of the *d*-wave systems in the vortex state by both theoreticians and experimentalists has appeared in order to reconcile some previous findings. For instance, the different results on specific heat need to be resolved. Recent work of Kübert and Hirschfeld [23, 63] has shed more light on the transport properties of *d*-wave superconductors in the vortex state. By definition, the field energy E_H is proportional to the average quasiparticles Doppler shift. The quasiparticle energy, E_H is given by:

$$E_H = a\left(\frac{H}{H_{c2}}\right)^{1/2}\Delta_o \tag{6.10}$$

where H_{c2} is the upper critical field, Δ_o is the gap maximum over the Fermi surface,

and a is a vortex-lattice dependent constant of order unity [23].

They argue that the transport properties in d-wave systems at low temperature and low fields can be described by the model in which quasiparticles are scattered by the same processes as in zero field and can be calculated from the energy dependence of the zero field relaxation time. The dependence of these properties on the magnetic field is a result of the change of the quasiparticle occupation number near the nodes. The extra quasiparticles are created because of the Doppler shift in the presence of the superfluid flow around the vortices. The quasiparticles are Doppler shifted by an energy $\delta\omega_k(R) = \vec{v_s}k$, where $\vec{v_s}$ is the superfluid velocity distribution that depends on the exact form of the vortex lattice, $\vec{v_s} = \phi_o/r\hat{\varphi}$. As the distance from the center of the vortex r increases, the velocity decreases and therefore the energy decreases as well. Authors also point out that in high-T_c superconductors and in UPt_3 systems, ℓ (mean free path) is not significantly determined by the vortex scattering. At low temperatures and fields, the scaling relation as derived by Kübert and Hirschfeld is given through $H^{1/2}/T$ variable.

For the quasiparticle energy that is comparable to the impurity bandwidth, $E_H \sim \gamma$, the breakdown of the scaling occurs [23]. The scaling is not square root in H, but it is rather $H \log H$ scaling as supported by specific heat data by Fisher et al. [64].

It has been theoretically predicted by Simon and Lee [65] that the transport properties in the magnetic field in d-wave superconductors should, in some way, depend on the square root of H. Utilizing the fact that the excitation spectrum of the low energy quasiparticles in two dimensional d-wave superconductors scales as $H^{1/2}$, they were able to calculate the predicted form for the various transport properties expressed through the exact one-parameter scaling. The transport properties they have examined include: specific heat in magnetic field, quasiparticle magnetic susceptibility, optical conductivity tensor and thermal conductivity tensor. They have found that the thermal conductivity tensor is given by the following formula:

$$\kappa_{xy} \sim T^2 F_{kxy}(\alpha T/H^{1/2}). \tag{6.11}$$

where F is some scaling function [65]. This form arises simply from the low-energy Dirac form of the electronic spectrum [63]. The results of Kübert et al. show that the exact one-parameter scaling found by Simon and Lee with $X = T/\sqrt{H}$ is not necessarily obtained but the approximate scaling as predicted by Simon and Lee will be valid in the unitarity limit.

As a result of the density of states being dominated by the extended quasiparticle states, the excitation spectrum of a clean d-wave superconductor in field scales as a function of $\sqrt{H}$. Such a scaling further leads to a specific heat C exhibiting $\sqrt{H}T$ dependence on the field rather than HT dependence as in classical superconductor where localized quasiparticle states inside the cores contribute to the specific heat because the number of vortices scales proportionally to the field. This approach assumes that the coherence length is independent of the field. But some recent μSR work shows that this is not true in systems such as $NbSe_2$ and YBCO [66]. Still, the theoretical predictions for specific heat in field have been supported by the previous experimental work. Moler et al. [67] have found that the specific heat of $YBa_2Cu_3O_{7-\delta}$ crystals in field scaled as $\sqrt{H}$ and could be best described by such a dependence on the field which was in perfect agreement with Volovik's prediction [23, 62]. On the other hand, some other measurements reported a behavior that deviated from such a scaling [64].

The contradictory experimental results were reported on the electronic thermal conductivity in field where $H \perp c$ axis. While Wand et al. [68] didn't find any increase in κ in field, the work by Bredl et al. [69] indicated an increase of thermal conductivity in the field. Therefore, there is a need for resolution of the contradictory experimental results as well as for the theoretical understanding of the problem. We have performed the measurements of thermal conductivity in field, where $H \parallel c$, aiming to help resolve the issue.

6.3.1 *Theory for d-wave superconductor*

Recently, Kübert and Hirschfeld have been involved in theoretical investigation of the behavior of thermal conductivity in d-wave systems in field [23, 63]. They have arrived

at the expression for the magnetic field corrections to the thermal conductivity in the clean limit as $T \rightarrow 0$. For the field applied parallel to the c axis ($H \perp j_Q$), the field dependence of the thermal conductivity for $H << H_{c2}$ at T=0 K is best described by:

$$\frac{\kappa(0;H)}{T} = \frac{\kappa_o}{T}\frac{\rho^2}{\rho\sqrt{1+\rho^2} - sinh^{-1}\rho} \tag{6.12}$$

where $\rho^2 = \frac{8\hbar\Gamma H_{c2}}{\pi^2 a^2 \Delta_o H}$ and κ_o/T is zero temperature and zero field universal value of the thermal conductivity [23].

The central variable in this equation is $\rho^2 = 8\hbar\Gamma H_{c2}/\pi^2 a^2 \Delta_o H$. In d-wave superconductor, in the unitarity limit, $\hbar\gamma \simeq 0.61\sqrt{\Gamma\Delta_o}$. The Doppler shift (field energy) is given by: $E_H = a\left(\frac{H}{H_{c2}}\right)^{1/2}\Delta_o$. Therefore, ρ can be written as:

$$\rho = \frac{2}{0.61}\sqrt{\frac{2}{\pi}}\left(\frac{\hbar\gamma}{E_H}\right). \tag{6.13}$$

It is simply the ratio of the relevant energy scales: the impurity bandwidth γ and the average Doppler shift energy E_H. This ratio comes into the finite field corrections at zero temperature as a squared term thus intensifying the difference in the magnitude of the finite field versus finite temperature corrections. The finite field corrections to κ at zero temperature are promising for investigation of the scattering phase shift because these corrections are sensitive to δ_o; but what is even more promising is the fact that they are not as small as finite temperature corrections in zero field [22]. Contrary to the 0.1% effect of finite T corrections to $\kappa(H = 0)$ at 1 K, the effect of a field can be much bigger, even of the order of 100 % in a few Tesla. For example, in the unitarity limit, which is believed to be the case for YBCO, at $H = 2\ T$, the energy is $E_H \simeq \hbar\gamma$, while in zero field, the energy is $k_B T \simeq \hbar\gamma/10$. Thus, the finite field corrections at zero temperatures are much bigger than the finite T corrections in zero field.

It is important to point out that the thermal conductivity in the field is not expected to be universal any more. Contrary to the thermal conductivity in zero field which is universal [9], the field corrections are not universal. There is an increase

Table 6.1: Residual linear term of thermal conductivity, κ_{oo}/T, obtained from the linear fit to the data below $T^2 < 0.0150$ K in the magnetic fields up to 8 T.

Crystal	κ_{oo}/T in H=0T $\frac{mW}{cmK^2}$	κ_{oo}/T in H=2T $\frac{mW}{cmK^2}$	κ_{oo}/T in H=4T $\frac{mW}{cmK^2}$	κ_{oo}/T in H=8T $\frac{mW}{cmK^2}$
Pure	0.12 ± 0.01	0.16 ± 0.02	0.20 ± 0.025	0.23 ± 0.03
0.6%Zn	0.13 ± 0.01	-	0.167 ± 0.0012	0.18 ± 0.014
3%Zn	0.137 ± 0.004	-	0.14 ± 0.008	0.147 ± 0.005

in thermal conductivity with increasing field as a result of population of extended quasiparticle states that are Doppler shifted in the presence of the vortices. As the concentration of impurities increases, the effect of the field is suppressed. Since the impurities still dominate the heat transport in field in *d*-wave superconductors at low temperatures, the increase in impurities will cause more quasiparticle to be scattered and thus the thermal conductivity in field will not increase as much as in a pure sample.

6.3.2 *Experimental results*

We have measured the thermal conductivity of pure $YBa_2Cu_3O_{6.9}$, $YBa_2(Cu_{0.994}Zn_{0.006})_3O_{6.9}$ (0.6 % doped YBCO) and $YBa_2(Cu_{0.97}Zn_{0.03})_3O_{6.9}$ (3 % doped YBCO), in the gapless regime at low temperatures in fields up to 8T. The field was applied along the c axis ($H \parallel c$).

Our measurements, as in the case of anisotropy studies, have been conducted in a low temperature and gapless regime, $k_BT \ll \hbar\gamma \sim E_H \ll \Delta_o$, where impurity scattering dominates, and where it is possible to separate the phononic from the electronic contribution of the thermal conductivity. We plot κ/T versus T^2 such that the cubic and linear terms can be separated. Since the total thermal conductivity is given by: $\kappa = aT + bT^3$, upon dividing it by the temperature the expression becomes: $\kappa/T = a + bT^2$. Therefore, if the data is fitted to κ/T versus T^2, the intercept will give the linear electronic term and the slope of the fit will give the cubic phononic

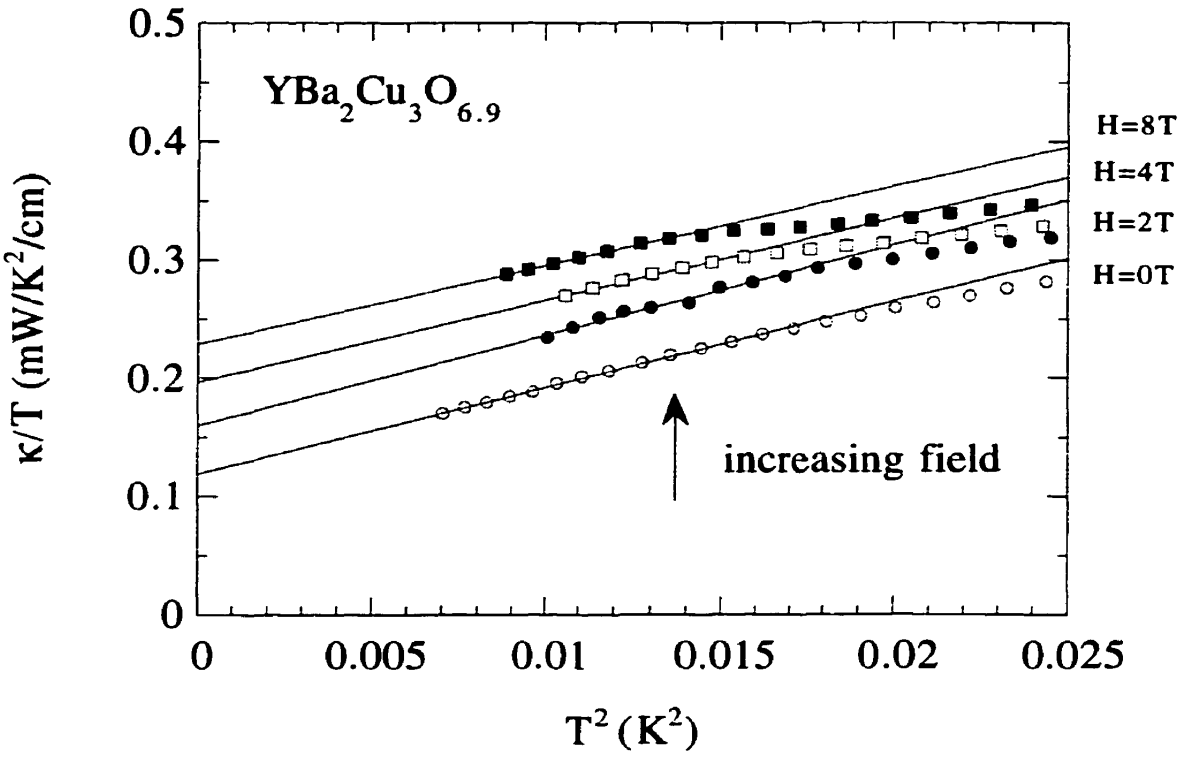

Figure 6.5: Thermal conductivity of the pure $YBa_2Cu_3O_{6.9}$ a axis sample divided by the temperature versus T^2 in the magnetic field up to 8T. The solid lines are linear fits to the data for $T^2 < 0.0150K^2$. The open circles correspond to the data for H=0T, solid circles to H=2T, open squares to H=4T, and solid squares to H=8T.

term.

We have extrapolated the residual linear term in thermal conductivity in all three samples at all fields up to 8 T. Our results are displayed on figures 6.5, 6.6, 6.7 and table 6.1. The uncertainties on our values of κ/T are a combination of the uncertainty in the geometric factor (maximum was 12%) and uncertainty in the linear fits, which is much smaller than the former one. Note, on the other hand, that the normalized field dependence (used in our comparison to theory) is not affected by the geometric factor uncertainty.

Firstly, in zero field, the curves exhibit the well known universal behavior. The intercept of κ/T vs T^2 in zero field is entirely attributable to the zero energy quasi-particles (residual normal fluid). The slope in the $\kappa(T)/T$ versus T^2 is predominantly due to phonons. When the field is applied, there is a definite increase in $\kappa(T)$ in all

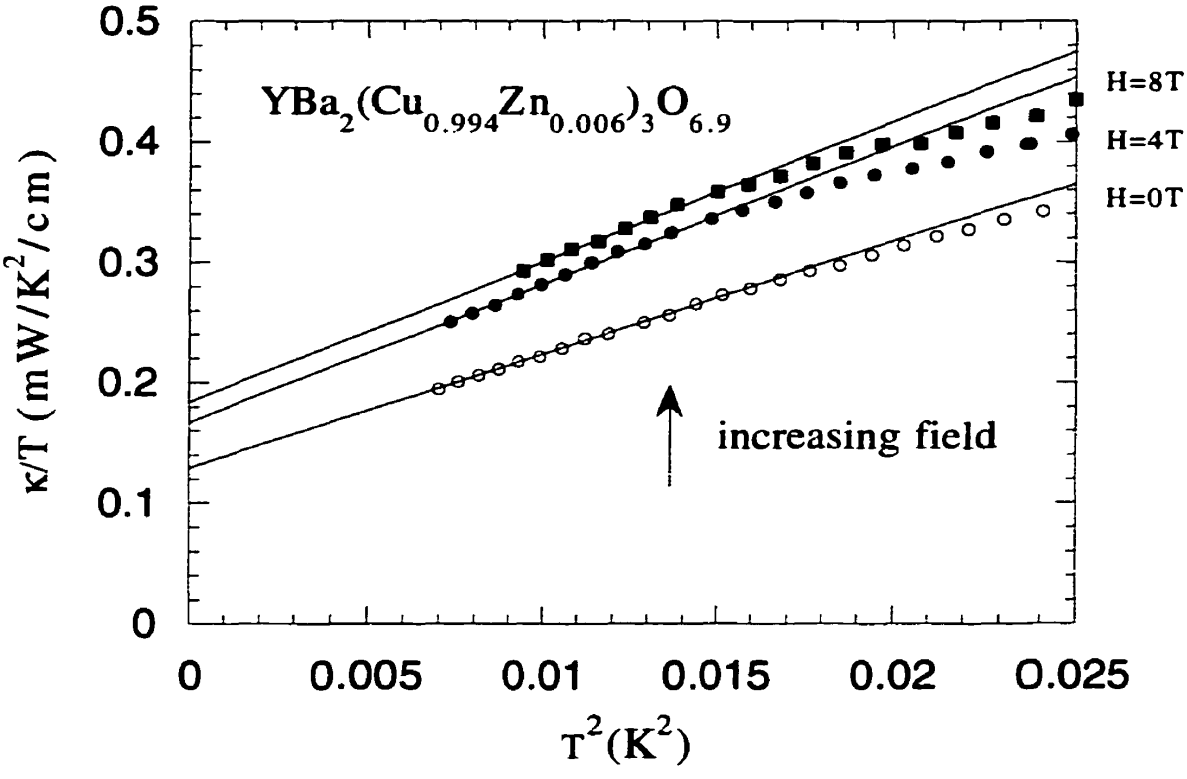

Figure 6.6: Thermal conductivity of 0.6% Zn doped YBCO crystal divided by the temperature κ/T versus T^2 in magnetic field up to 8 T. The solid lines are linear fits to the data below $T^2 < 0.0150K^2$. The open circles represent the data for H=0T, solid circles for H=4T, and solid squares for H=8T.

three samples, and the universal transport is lost. Clearly, the zero intercept (which is due to the electronic linear term) increases with increasing field because the electrons are affected by the magnetic field. On the other hand, we do not expect phonons to be influenced by the field and therefore the slope should remain the same. The increase in $\kappa(T)$ in the field is the result of an increase in the density of states that comes about due to increase in occupation of extended quasiparticles states in the presence of vortices.

It is seen that the pure sample is affected by the field the most while the increase in 3% Zn doped sample is much less pronounced. By introducing up to 3% Zn impurities, we have effectively varied the scattering rate by a factor of 30 [8].

Upon establishing our main experimental findings, we would like to compare our results with the theory for *d*-wave superconductor in the field. Kübert and Hirschfeld have arrived at theoretical expressions for the corrections of the thermal conductiv-

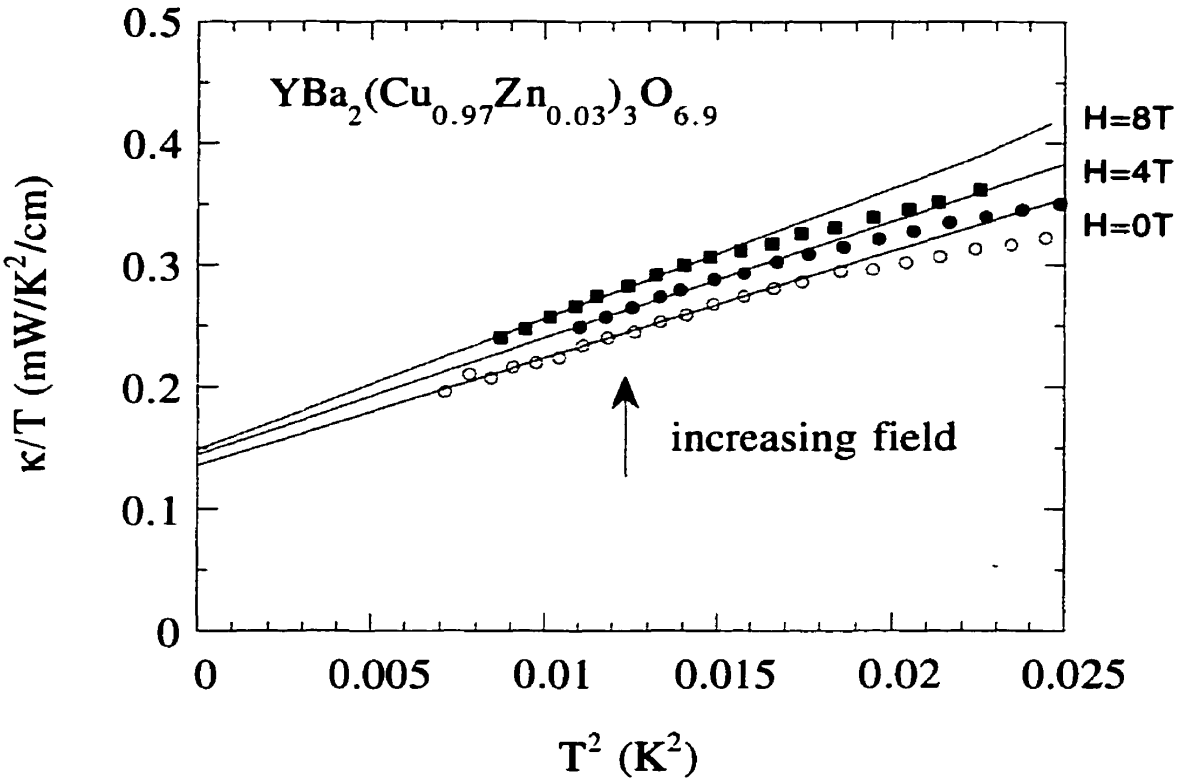

Figure 6.7: Thermal conductivity of 3% Zn doped YBCO crystal divided by the temperature κ/T versus T^2 in magnetic field up to 8 T. The solid lines are linear fits to the data below $T^2 < 0.0150K^2$. The open circles represent the data for H=0T, solid circles for H=4T, and solid squares for H=8T.

ity in the clean limit and zero temperature when the field is applied in a direction perpendicular to the heat current, $H \perp j_Q$ given by equation 6.12 [23].

We have plotted the normalized thermal conductivity for the three samples $\kappa(H)/\kappa_o$ versus the field as given by equation 6.12 along with experimental data collected in our lab. Normalized thermal conductivity in field was calculated from the expression 6.12 using $\Delta_o = 2.15 k_B T_c (1 - 0.8 \times \Gamma/T_c)$ and $H_{c2} = 320\ T$ as determined by the specific heat measurements [70]. This is shown on figure 6.8. The lines represent the calculated fits while the squares represent our data. We see that the theoretical prediction agrees well with our data. Our points, within the uncertainty (error bars), fall on the theoretical curves for all three samples.

For all three fits (pure, 0.6 % Zn, and 3 % Zn) in the field, there is only *one* adjustable parameter, namely v_f. This is true given that the other two parameters

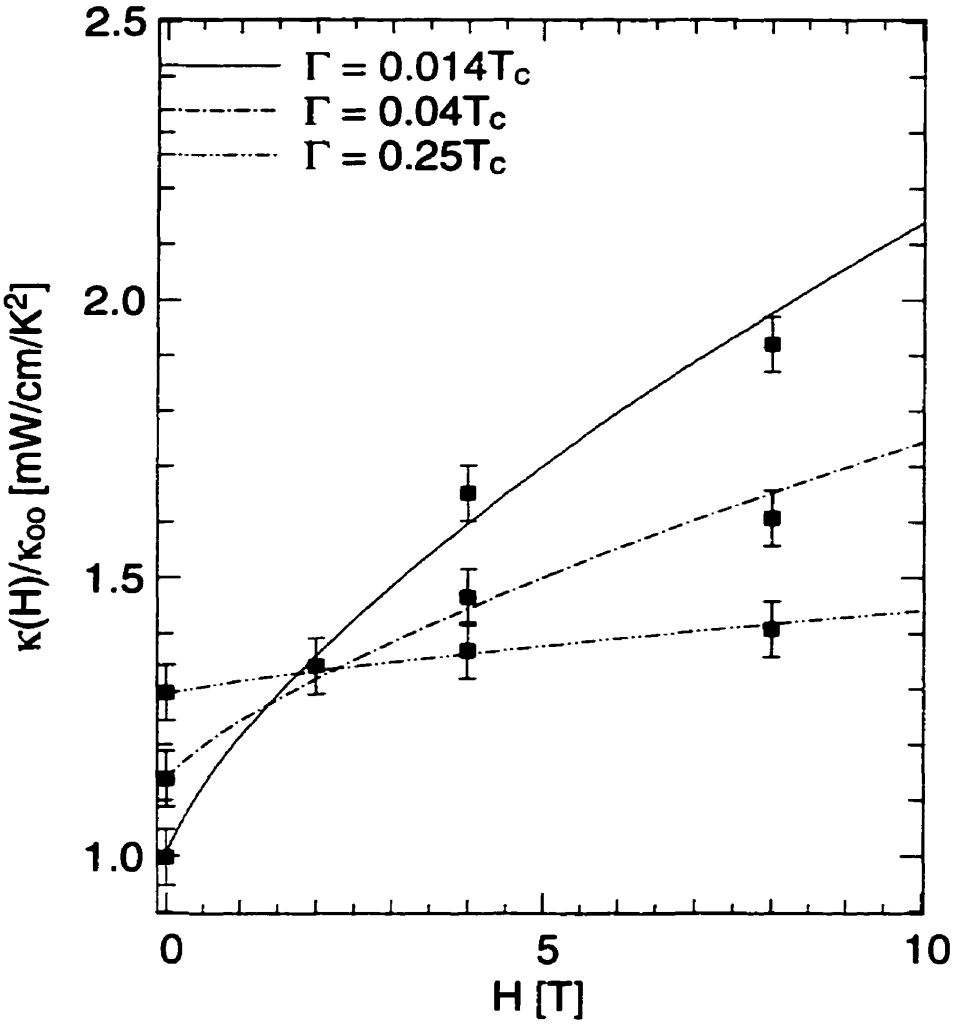

Figure 6.8: Normalized thermal conductivity of YBCO (pure and Zn doped) in a magnetic field ($H \parallel c$). The lines are theoretical fits with $H_{c2} = 320$ T to the equation 6.12 while squares correspond to our data.

in the expression for $\kappa(T, H)$, a and Γ are well known and understood. The constant a is of the order unity and depends on the particular lattice structure. It can vary at the most from 1 to 1/2. The scattering rate Γ can be obtained for each fit from the separate measurements. The one parameter self-consistent calculation agrees well with the value for Γ obtained from separate measurements, as we shell see in the continuation of the discussion. Therefore, we have a good understanding of both a and Γ which leaves us with v_f as the only adjustable variable.

We have used the known relations for $\xi_o = \frac{\hbar v_f}{\pi \Delta_o}$, $H_{c2} = \frac{\phi_o}{2\pi \xi_o^2}$ to calculate the

adjustable parameter v_f. Here, $\phi_o = \frac{hc}{2e} = 2.07 \times 10^{-15}\ Tm^2$. For YBCO, $H_{c2} = 320\ T$ as determined from specific heat data [67] and $\Delta_o = 2.15 k_B T_c$ as given by the weak coupling limit [53]. From the above expressions and given values, the Fermi velocity is calculated to be $v_f = 8.5 \times 10^6\ m/s$. This is in a good quantitative agreement with the Fermi velocity obtained by Lee $v_f = 1.18 \times 10^7\ cm/sec$ [71] based on photoemission data.

As a check on the extent of the agreement between the theory by Kübert and Hirschfeld which we used and other works, we calculated the scattering rate Γ from the theoretical fit using $\Delta_o = 2.15 k_B T_c (1 - 0.8 \times \Gamma/T_c)$, $a = 1/2$ and $H_{c2} = 320T$ and compared it with other estimates for Γ. The calculated values are shown in table 6.2. There are a couple of other ways that can be used for the estimation of Γ:

1. Γ can be calculated from the residual resistivity obtained from the microwave conductivity measurements. Under the assumption that the inelastic scattering term in the resistivity is independent of the concentration of element used for doping, which in our case is Zn, the scattering rate $\Gamma = 1/2\tau_o$ can be estimated via $\rho_o = m^*/ne^2\tau_o$ by the following expression:

$$\Gamma_\rho = \left(\frac{\omega_p^2}{8\pi}\right)[\rho_o(x=0) + A(x) - A(0)] \tag{6.14}$$

where $\omega_p = \sqrt{4\pi ne^2/m^*}$ is the Drude plasma frequency and $\rho_o(x=0)$ is the resistivity of the pure crystal at T=0 estimated from the microwave conductivity. Taillefer et al. [8] have calculated Γ for crystals with various Zn concentrations using $\omega_p = 1.3\ eV$ and $\rho_o(x=0) = 1\ \mu\Omega cm$. Their findings are summarized in table 6.2.

2. The other estimate is based on the suppression of the critical temperature upon doping given by Sun and Maki [72]. They plotted κ/κ_o vs Γ/Γ_c where $\Gamma_c = 0.88T_c$ is a critical scattering rate and κ_o is the universal value of thermal conductivity at T=0 in the pure limit ($\Gamma \to 0$). The values for 0.6% Zn, and 3% Zn doped crystals obtained from fit of Sun and Maki are also summarized in the table 6.2.

The separate estimates of the scattering rates are in a good agreement, specifically the estimates from 2. and from equation 6.12. The observation regarding the effect

Table 6.2: Various estimates of the scattering rate Γ in units of $\hbar/k_B$ for Zn doped YBCO crystals.

Source	Pure	0.6%Zn	3%Zn
from 1.	0.014	0.13	0.54
from 2.	ref.	0.06	0.25
from 6.12	0.014	0.04	0.25

of the different levels of impurities agrees well with the theoretical prediction that the increase in impurity concentration leads to a lesser effect of the field due to an increase in the scattering rate; as the concentration of impurities is increased, the scattering of the quasiparticles by impurities increases as well.

In conclusion, our experimental results of $\kappa(T)$ in the magnetic field are in a good agreement with a *d*-wave theory. In the absence of a field, the zero temperature limit of thermal conductivity κ_{oo}/T exhibits a well known universal behavior. Our measurements confirm the existence of the residual normal fluid at zero temperature. Furthermore, at the low temperature and in the magnetic field, we observe the predicted increase in thermal conductivity as a result of the population of the extended quasiparticle states in the presence of the vortices. In the low temperature regime, $\kappa(T = 0; H)/T$ is governed by the impurities, and as the concentration of the impurities increases the effect of the field is suppressed. The fitted values of Γ agree with the 1-parameter self-consistent calculation. The calculated value for the Fermi velocity from our data agrees well with the one predicted by the theory.

In order to shed more light and to understand even better the behavior of thermal conductivity in the field, the best approach would be to look at the behavior of other superconducting compounds.

7

CONCLUSION

The thermal conductivity at low temperatures has been used as a probe of the quasiparticle behavior in the high-T_c superconductor $YBa_2Cu_3O_{7-\delta}$. Both the effects of anisotropy and of magnetic field were examined.

The experimental results revealed a very weak (perhaps negligible) anisotropy in the low temperature thermal conductivity in the basal plane contrary to the much higher anisotropy of 2.2 ± 0.2 found in other transport properties such as the normal state resistivity, the normal state microwave conductivity, the plasma frequency (squared) and the London penetration depth (squared). Our results for a current along the a axis, agreed well with the predictions of the theory for the d-wave superconductors. We have also attained great qualitative understanding of properties in both gapless and clean regimes. Such a weak anisotropy in transport calls for a more detailed examination of the role of the chains in $YBa_2Cu_3O_{7-\delta}$.

The magnetic field studies also agreed well with the theory for d-wave superconductors. We found that the thermal conductivity at $T \rightarrow 0$ increased in field, in the expected way. The growth in κ/T with field is the result of an increase in the density of state due to the population of extended quasiparticle states in the presence of vortices. This is in contrast to the classical superconductors where the field causes an initial decrease in thermal conductivity, as a result of vortex scattering. The introduction of a varying impurity concentration suppressed the effects of the magnetic field. The growth in κ_{oo}/T was much less pronounced for the Zn doped crystals. This finding was in a good quantitative and qualitative agreement with the theory.

Now that the behavior of the thermal conductivity in field has been established,

more studies should be undertaken in order to explain some new puzzling data observed recently. Particularly, one would be interested in field induced phase transition ($\sim$ 1% effect) in d-wave superconductors as observed in BSCCO compound. An abrupt kink followed by a plateau in field dependence of thermal conductivity has been observed and was attributed to the new phase transition into the gapped state for a certain critical field which is dependent on temperature. The quasiparticles in such a state would have an exponentially activated behavior. Krishana et al. proposed that the new state above the kink is one in which order parameter changes from $d_{x^2-y^2}$ to $d_{x^2-y^2} + id_{xy}$, where d_{xy} is the term that breaks the time reversal symmetry.

We measured the thermal conductivity of YBCO crystal in the magnetic field and observed a clear increase in residual linear term; but we did not detect an effect similar to the one in BSCCO. Because we found the excellent agreement between our experimental results and the theory for the pure $d_{x^2-y^2}$ pairing states, it is very likely that the gap Δ_{xy} that develops in the phase transition is much smaller than our energy scale. It could be that the effect of the field is observed for very low fields (of the order of milli Tesla) since the critical field for the transition is temperature dependent. If the field at which the phase transition occurs is indeed in the milli Tesla range, then our measurements of low temperature $\kappa(T)$ in field for YBCO could certainly put the upper bound on the value of the gap, Δ_{xy}.

BIBLIOGRAPHY

[1] M. Brian Maple. High temperature superconductivity. *cond-mat/9802202.* February 1998.

[2] Michael Tinkham. *Introduction to Superconductivity.* McGraw-Hill, Inc., New York, second edition, 1996.

[3] P. G. de Gennes. *Superconductivity of Metals and Alloys.* Addison-Wesley Publishing Company, New York, second edition, 1989.

[4] R. Berman. *Thermal conduction in solids.* Oxford University Press, Oxford, 1976.

[5] J. Bardeen, L. N. Cooper, and J. R. Schrieffer. Theory of superconductivity. *Physical Review*, 108(5):1175–1204, December 1957.

[6] J. M. Ziman. *Principles of the Theory of Solids.* Cambridge University Press, New York, 1964.

[7] Benoit Lussier. *Heat Conduction in $YBa_2Cu_3O_{7-\delta}$; Ph.D. Thesis.* McGill University, 1996.

[8] Louis Taillefer, Benoit Lussier, Robert Gagnon, Kamran Behnia, and Hervé Aubin. Universal heat conduction in $YBa_2Cu_3O_{6.9}$. *Physical Review Letters*, 71(3), July 1997.

[9] Patrik A. Lee. Localized states in a d-wave superconductor. *Physical Review Letters*, 71(12):1887–1890, September 1993.

[10] J. Bardeen, G. Rickayzen, and L. Tewordt. Theory of the thermal conductivity of superconductors. *Physical Review*, 113(4):982–994, February 1959.

[11] Neil W. Ashcroft and N. David Mermin. *Solid State Physics.* Sanders College Publishing, New York, 1976.

[12] Vladimir Z. Kresin and Stuart A. Wolf. *Fundamentals of Superconductivity.* Plenum Press, New York, 1990.

[13] K. Mendelssohn. *Physica*, 19, 1953.

[14] Olsen and Rosenberg. *Phil. Mag.*, 43, 1952.

[15] J. Lowell and J. B. Sousa. *Journal of Low Temperature Physics*, 3(1), 1970.

[16] C. B. Satterthwaite. Thermal conductivity of normal and superconducting aluminum. *Physical Review*, 125(3), February 1962.

[17] N. V. Zavaritskii. *J. Exptl. Theoret. Phys.*, 34, 1958.

[18] P. H. Kess, J. G. A. Rolfes, and D. de Klerk. Thermal conductivity of niobuim in the purely superconducting and normal states. *Journal of Low Temperature Physics*, 17, 1974.

[19] J. Dominec. Review article: Ultrasonic and related experiments in high-t_c superconductors. *Supercond. Sci. Technol.*, 5, 1993.

[20] L. Coffey, T. M. Rice, and K. Ueda. *J. Phys. C*, 18:L813, 1985.

[21] C. J. Pethick and D. Pines. Transport processes in heavy-fermion superconductors. *Physical Review Letters*, 57:118–121, 1986.

[22] M. J. Graf, S-K. Yip, and J. A. Sauls. Electronic thermal conductivity and the wiedemann-franz law for unconventional superconductors. *Physical Review B*, 53:15147–15159, June 1996.

[23] C. Kübert and P. J. Hirschfeld. Quasiparticle transport properties of d-wave superconductors in the vortex state. *Physical Review Letters*, 80(22), June 1998.

[24] Philip D. Thacher. Effect of boundaries and isotopes on the thermal conductivity of lif. *Physical Review*, 156(3), April 1967.

[25] C. Uher. *Physical Properties of High Temperature Superconductors*, volume 3. World Scientific, Singapore, 1992.

[26] Thomas P. Sheahen. *Introduction to High-Temperature Superconductivity.* Plenum Press, New York, 1994.

[27] *Kelvinox 300 Dilution Refrigerator: Operator's handbook.* Oxford Instruments, Scientific Research Division, Old Staton Way, Eynsham, Witney, Oxon, England, 2.1 edition, September 1992.

[28] Frank Pobell. *Matter and Methods at low Temperatures.* Springer-Verlag, Berlin, second edition, 1996.

[29] O. V. Lounasmaa. *Experimental Principles and Methods Below 1K.* Academic Press, London, 1974.

[30] unknown, editor. *Research Chemicals, Metals and Materials.* A Johnson Matthey Company, 1997-98.

[31] G. Burns. *High temperature superconductivity.* Academic Press, New York, 1992.

[32] Shou-Cheng Zhang. Research article: A unified theory based on SO(5) symmetry of superconductivity and antiferromagnetism. *Science*, 275, February 1997.

[33] R. Liang et al. *Physica C*, 195, 1992.

[34] T. A. Vanderah et al. *J. Cryst. Growth*, 118, 1992.

[35] P. Schleger et al. *Physica C*, 176, 1991.

[36] J. R. LaGraff and D. A. Payne. *ibid.*, 212, 1993.

[37] Robert Gagnon, Song Pu, Brett Ellman, and Louis Taillefer. Anisotropy of heat conduction in $YBa_2Cu_3O_{6.9}$: A probe of chain superconductivity. *Physical Review Letters*, 78(10):1976–1979, March 1997.

[38] Robert Gagnon, Christian Lupien, and Louis Taillefer. T^2 dependence of the resistivity in the Cu-O chains of $YBa_2Cu_3O_{6.9}$. *Physical Review B*, 50(5):3458–3461, August 1994.

[39] Y. Iye. *Physical Properties of High Temperature Superconductors*, volume 3. World Scientific, Singapore, 1992.

[40] D. Goldschmidt and Y. Eckstein. *Physica C*, 200, 1992.

[41] U. Poppe et al. *Journal of Applied Physics*, 71, 1991.

[42] M. J. V. Menken et al. *Journal of Crystal Growth*, 96, 1989.

[43] T. A. Friedemann, M. W. Rabin, J. Giapintzakis, J. P. Rice, and D. M. Ginsberg. Direct measurement of the anisotropy of the resistivity in the a-b plane of twin-free, single crystal, superconducting $YBa_2Cu_3O_{7-\delta}$. *Physical Review B*, 42(10), October 1990.

[44] U. Welp, S. Fleshler, W. K. Kwok, J. Downey, Y. Fang, G. W. Crabtree, and J. Z. Lui. a-b anisotropy of the normal-state resistivity of untwinned $YBa_2Cu_3O_{7-\delta}$. *Physical Review B*, 42(16), December 1990.

[45] R. Combescot and X. Leyronas. Coupling between planes and chains in $YBa_2Cu_3O_7$: A possible solution for the order parameter controversy. *Physical Review Letters*, 75(20):3732–3735, November 1995.

[46] Kuan Zhang, D. A. Bonn, S. Kamal, Ruixing Liang, D. J. Baar, W. N. Hardy, D. Basov, and T. Timusk. Measurement of the ab plane anisotropy of microwave surface impedance of untwinned $YBa_2Cu_3O_{6.95}$ single crystals. *Physical Review Letters*, 73(18), October 1994.

[47] W. N. Hardy, D. A. Bonn, D. C. Morgan, Ruixing Liang, and Kuan Zhang. *Physical Review Letters*, 70, 1993.

[48] D. N. Basov, R. Liang, D. A. Bonn, W. N. Hardy, B. Dabrowski, M. Quijada, D. B. Tanner, J. P. Rice, D. M. Ginsberg, and T. Timusk. In-plane anisotropy of the penetration depth in $YBa_2Cu_3O_{7-x}$ and $YBa_2Cu_4O_8$ superconductors. *Physical Review Letters*, 74(4), January 1995.

[49] D. B. Tanner and T. Timusk. *Physical Properties of High Temperature Superconductors III.* World Scientific, Singapore, 1992.

[50] Philip B. Allen, Warren E. Pickett, and Henry Krakauer. Anisotropic normal-state transport properties predicted and analyzed for high-t_c oxide superconductors. *Physical Review B*, 37(13), May 1988.

[51] T. Xiang and J. M Wheatley. Superfluid anisotropy in ybco: Evidence of pair tunneling superconductivity. *Physical Review Letters*, 76(1), January 1996.

[52] W. A. Atkinson and J. P. Carbotte. *Physical Review B*, 52, 1995.

[53] May Chiao, Brett Ellman, Robert Gagnon, and Louis Taillefer. Anisotropy of heat conduction by the residual normal fluid in $YBa_2Cu_3O_{6.9}$. *preprint, to be published*, 1998.

[54] D. Xu, S. K. Yip, and J. A. Sauls. Nonlinear meissner effect in unconventional superconductors. *Physical Review B*, 51(22), June 1995.

[55] W. C. Wu, D. Branch, and J. P. Carbotte. Effect of anisotropy on universal transport in unconventional superconductors. *to be published*, 1998.

[56] Chris O'Donovan and J. P. Carbotte. *Physical Review B*, 1997.

[57] A. V. Balatsky, A. Rosengren, and B. L. Altshuler. *Physical Review Letters*, 73, 1994.

[58] Kazumi Maki. Thermal conductivity of pure type-ii superconductors in high magnetic fields. *Physical Review*, 158(2), June 1967.

[59] C. Caroli and M. Cyrot. *Phys. Kondensierten Materie*, 4, 1965.

[60] L. Dubeck, P. Lidenfeld, E. A. Lynton, and H. Rohrer. *Physical Review Letters*, 10, 1963.

[61] L. Dubeck, P. Lidenfeld, E. A. Lynton, and H. Rohrer. *Rev. Mod. Phys.*, 36, 1964.

[62] G. E. Volovik. J. exptl. theoret. phys. lett. 58, 1993.

[63] C. Kübert and P. J. Hirschfeld. Vortex contribution to specific heat of dirty d-wave superconductors: Breakdown of scaling. 1998.

[64] R. A. Fisher, J. E. Gordon, S. F. Reklis, D. A. Wright, J. P. Emerson, B. F. Woodfield, E. M. McCarron III, and N. E. Phillips. Magnetic-field dependence of the low-temperature specific heat of some high-t_c copper-oxide superconductors. evidence for an $h^{1/2}t$ contribution in the mixed state. *Physica C*, 252, 1995.

[65] Steven H. Simon and Patrik A. Lee. Scaling of the quasiparticle spectrum for d-wave superconductor. *Physical Review Letters*, 78(8), February 1997.

[66] Jeff Sonier. *Private communication*, August 1998.

[67] Kathryn A. Moler, David L. Sisson, Jeffrey S. Urbach, Malcolm R. Beasley, Aharon Kapitulnik, David J. Baar, Ruixing Liang, and Walter N. Hardy. Specific heat of $YBa_2Cu_3O_{7-\delta}$. *Physical Review B*, 55(6), February 1997.

[68] B. Wand et al. *Journal of Low Temperature Physics*, 105, 1996.

[69] C. D. Bredl et al. *Z. Phys. B*, 86, 1992.

[70] B. Revaz et al. *Czech. J. Phys.*, 46, 1996.

[71] Patrick A. Lee and Xiao-Gang Wen. Unusual superconducting state of underdoped cuprates. *Physical Review Letters*, 78(21), May 1997.

[72] Y Sun and K. Maki. Transport properties of d-wave superconductors with impurities. *Europhysics Letters*, 34(4), November 1995.